

# Antibody Engineering for Cancer Therapy

By  
Yik Andy Yeung

B.S., University of Wisconsin-Madison, 1999  
M.S.CEP., Massachusetts Institute Technology 2002

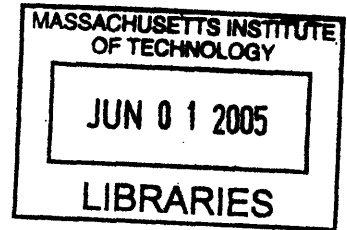
Submitted to the Department of Chemical Engineering  
in Partial Fulfillment of the Requirements for the Degree of

DOCTOR OF PHILOSOPHY  
in Chemical Engineering

at the

Massachusetts Institute of Technology  
May, 2005 [June 2005]

© 2005 Massachusetts Institute of Technology  
All rights reserved



Signature of Author Yik Andy Yeung  
Department of Chemical Engineering  
May 2005

Certified by K. Dane Wittrup  
J.R. Mares Professor of Chemical Engineering and Bioengineering  
Thesis Supervisor

Accepted by Daniel Blankschtein  
Professor of Chemical Engineering  
Chairman, Committee for Graduate Students

**ARCHIVES**

# Antibody Engineering for Cancer Therapy

By  
Yik Andy Yeung

Submitted to the Department of Chemical Engineering on  
May, 2005 in Partial Fulfillment of the Requirements for the  
Degree of Doctor of Philosophy in Chemical Engineering

## ABSTRACT

Antibodies targeting various tumor-associated antigens have been developed successfully to treat cancer. In this Thesis, novel antibodies and antibody-conjugate against two tumor antigens, AF-20 antigen and human aspartyl (asparaginyl)  $\beta$ -hydroxylase (HAAH), were developed. Previously, these two tumor antigens have been shown to be present on a variety of tumor cells, while they have minimal expression on normal tissues, rendering them excellent targets for antibody therapy.

For the AF-20 work, the variable region (V) gene of a previously isolated mouse monoclonal antibody (mAb) AF-20 was cloned from hybridoma mRNA and used to construct an AF-20 single-chain Fv (scFv). The AF-20 scFv was shown to bind specifically to the same epitope as mAb AF-20 with a binding affinity of 4nM. The AF-20 scFv was also internalized into tumor cells in a manner identical to that of the original mAb AF-20. The scFv was later employed for cellular internalization of virus-sized fluorescent quantum dots. In addition, to demonstrate the versatility of this antibody, an immunotoxin composed of AF-20 scFv fused to the highly cytotoxic recombinant toxin gelonin was constructed, and its *in-vitro* efficacy against three different tumor cell lines were evaluated. The  $IC_{50}$  of the AF-20 scFv-gelonin fusion was consistently one to two logs lower than the  $IC_{50}$  of free gelonin on FOCUS (liver), L3.6pl (pancreas) and PC3 (prostate) cells, further demonstrating the capability of the AF-20 scFv as a targeting module. Therefore, this AF-20 scFv is a potential internalization vector for toxins, enzymes, radionuclides and virus for targeted therapy of AF-20-antigen expressing tumor cells.

For the HAAH study, twelve novel human scFv against HAAH were isolated from a human non-immune scFv library displayed on the surface of yeast. Five of the twelve scFv were reformatted as human IgG1. One of the reformatted IgG, 6-22, showed significant binding to recombinant HAAH protein in ELISA, tumor cell lines, and tumor tissues. 6-22 IgG was also shown to target the catalytic domain of HAAH, and its apparent dissociation constant was determined to be 1.0nM. 6-22 IgG alone does not exhibit significant cytotoxicity toward the tumor cells. However, 6-22 IgG internalizes into tumor cells and can therefore be employed to deliver cytotoxic moieties into tumor cells. A goat anti-human IgG-saporin conjugate was delivered into tumor cells by 6-22 IgG and hence elicited cytotoxicity toward the tumor cells *in vitro*. Meanwhile, the monovalent affinity of 6-22 scFv was too low for therapeutic or diagnostic application, so 6-22 scFv was affinity matured using directed evolution and yeast surface display. After

two rounds of mutagenesis, a mutant, C4-18, with an affinity of 0.6nM was isolated. Overall, these human  $\alpha$ -HAAH scFv and IgG can potentially be used in the diagnosis and therapeutic treatment of HAAH-expressing tumor cells.

Thesis Supervisor: K. Dane Wittrup

Title: J.R. Mares Professor of Chemical Engineering and Bioengineering

Dedicated to my parents Biao and Yuk-yin.  
Thanks for your unconditional support.

## Acknowledgements

I would like to thank my thesis advisor, Dane Wittrup, for his advice, encouragement and support over the course of my research study. I am very thankful for having such a wonderful experience working with him. I would like to appreciate him for providing exceptional insights on my research, and a great working environment where I can share openly, try freely, and learn greatly

I would also like to thank Jack Wands, my thesis committee member and collaborator, with numerous advice, discussions and reagents. I would not be able to work on this project without him starting the groundwork. In addition, I want to give thanks to the other member of my committee, Linda Griffith, for her advice. I am grateful for the financial support from the Biotechnology Process Engineering Center (BPEC) and Panacea Pharmaceuticals. Many thanks to Michael Lebowitz and Angela Finney of Panacea for all the discussions, ideas and reagents they have provided.

I would like to express gratitude to the past and present members of the Wittrup Lab for being my terrific colleagues and making the lab such a pleasant place to work. I truly enjoy all the scientific and non-scientific discussions with them. And I especially appreciate all the help and encouragements from them. They are Brenda Kellogg, Katarina Midelfort, Jason Burbank, Christilyn Graff, Sarah Bannister, Jeffrey Swers, Balaji Rao, Jennifer Cochran, Mark Olsen, Yongsung Kim, Andy Rakestraw, David Colby, Stefan Zajic, Shaun Lippow, Ginger Chao, Stephen Sazinsky, Wai Lau, Dasa Lipovsek, Andrea Piatesi, Shanshan Howland, and Greg Thurber. Thanks to my undergraduate assistants, Terence Dobrowsky and Inna Koyrakh, for providing help on my research.

I would also like to acknowledge and thank the people who have made my stay in MIT and Boston so wonderful. I first want to thank brothers and sisters from MIT Hong Kong Students Bible Study Group, they have been tremendous in encouraging, learning, playing, praying and sharing with me. I especially thank the pastors, brothers and sisters from Boston Chinese Evangelical Church for their constant support and nurturing.

Most importantly, I want to give the biggest thanks to my parents, Biao and Yuk-yin. Without their unconditional support and love, I would not be able to achieve this degree. It was their influence for having the initiative and plan that I should study in the United States. To this end, they have made huge sacrifice and I am forever grateful to them. I am extremely thankful for their care, love, teaching, and for bringing me up in a warm and harmonize family.

# Table of Contents

<b>Chapter 1: Introduction and Background.....</b>	<b>8</b>
1.1 Antibody Structure and Function.....	8
1.2 Antibody Engineering.....	10
1.2.1 Yeast Surface Display.....	10
1.2.2 Mutagenesis and Library Screening.....	13
1.3 Antibody Therapeutics for Cancer Therapy .....	16
1.3.1 Tumor Antigens .....	16
1.3.2 Mechanism of Tumor Killing .....	17
1.3.3 Current Antibody Therapeutics.....	18
1.4 Thesis Overview .....	19
<b>Chapter 2: Characterization of a Single-chain Fv for Delivery of Cytotoxic Moieties to Hepatocellular Carcinoma Cells .....</b>	<b>21</b>
2.1 Introduction.....	21
2.2 Materials and Methods.....	23
2.2.1 Cloning of the AF-20 V Genes .....	23
2.2.2 Construction of the AF-20 scFv.....	24
2.2.3 Soluble Expression of AF-20 scFv .....	25
2.2.4 Coomassie Gel Analysis and Western Blot .....	25
2.2.5 Binding of the scFv to FOCUS Cells.....	26
2.2.6 Internalization of the AF-20 scFv into FOCUS Cells.....	27
2.2.7 Construction of AF-20 scFv-Gelolin Immunotoxin.....	27
2.2.8 <i>In-vitro</i> Cytotoxicity of the Immunotoxin .....	28
2.2.9 Display of AF-20 scFv and Binding of AF-20 scFv Displaying Yeasts ..	28
2.3 Results.....	29
2.3.1 Construction of AF-20 scFv.....	29
2.3.2 Expression of the AF-20 scFv in <i>Saccharomyces Cerevisiae</i> .....	29
2.3.3 Binding Epitope and Affinity of the AF-20 scFv against FOCUS Cells..	34
2.3.4 Internalization of the AF-20 scFv into Tumor Cells.....	36
2.3.5 Facilitated Internalization of Nano-scale Particles .....	39
2.3.6 <i>In-vitro</i> Cytotoxicity of AF-20 Gelolin Fusion Construct .....	40
2.3.7 Display of AF-20 scFv on the Yeast Surface.....	42
2.3.8 Binding of AF-20 Displaying Yeasts against FOCUS Cells .....	42
2.4 Discussion .....	46
<b>Chapter 3: Isolation and Engineering of Human Antibodies against Human Aspartyl (Asparaginy) <math>\beta</math>-Hydroxylase .....</b>	<b>54</b>
3.1 Introduction.....	54
3.2 Materials and Methods.....	56
3.2.1 Cell Lines and Materials .....	56
3.2.2 Isolation of Anti-HAAH Leads.....	57
3.2.3 Conversion of scFv to IgG.....	58
3.2.4 ELISA .....	59

3.2.5	Binding of the IgGs to Tumor Cells .....	60
3.2.6	Immunohistochemistry .....	60
3.2.7	Internalization Studies of 6-22 IgG.....	61
3.2.8	Cytotoxicity of 6-22 Immunotoxins.....	61
3.2.9	Construction of Random Mutagenesis Library.....	62
3.2.10	Construction of CDR Domain Shuffling Library of 6-22 scFv .....	63
3.2.11	Construction of Heavy Chain Shuffling Library of 6-22 scFv .....	64
3.2.12	Fluorescence Activated Cell Sorting of Mutant Library.....	64
3.3	Results.....	65
3.3.1	Isolation of Human Antibody Fragments against HAAH.....	65
3.3.2	Conversion of scFv to IgG and ELISA.....	66
3.3.3	IgG Binding against Tumor Cell Lines.....	69
3.3.4	Domain Mapping of Clone 6-22 and 6-23 .....	72
3.3.5	Immunohistochemistry using 6-22 IgG .....	74
3.3.6	Internalization of 6-22 IgG into the Tumor Cells .....	74
3.3.7	Cytotoxicity of 6-22 IgG Immunotoxin on Tumor Cell Lines .....	79
3.3.8	Random Mutagenesis of 6-22 scFv.....	81
3.3.9	CDR Domain Shuffling of 6-22 scFv .....	83
3.3.10	Heavy Chain Shuffling of 6-22 scFv .....	83
3.3.11	Conversion of C4 scFv to C4 IgG.....	85
3.3.12	Random Mutagenesis of C4 scFv .....	85
3.4	Discussion .....	88

## **Chapter 4: Quantitative Screening of Yeast Surface-Displayed Polypeptide**

<b>Libraries by Magnetic Bead Capture .....</b>	<b>95</b>	
4.1	Introduction.....	95
4.2	Materials and Methods.....	97
4.2.1	Yeast Strains and Plasmids .....	97
4.2.2	Materials and Media .....	98
4.2.3	Growth and Induction .....	99
4.2.4	Fluorescence Labeling and Measurements .....	99
4.2.5	Binder Identification from Magnetic Bead Capture .....	100
4.2.6	Dissociation Kinetics by Fluorescent Measurement and Magnetic Bead.....	101
4.2.7	Kinetic Screening by Magnetic Bead Capture.....	102
4.3	Results.....	103
4.3.1	Model System Validation .....	103
4.3.2	Isolation of binders from nonbinders.....	106
4.3.3	Affinity Maturation.....	111
4.4	Discussion .....	118
4.5	Conclusion .....	123

<b>Appendix.....</b>	<b>125</b>
----------------------	------------

<b>References.....</b>	<b>131</b>
------------------------	------------

<b>Curriculum Vitae.....</b>	<b>142</b>
------------------------------	------------

# Chapter 1: Introduction and Background

## 1.1 Antibody Structure and Function

Antibody is involved in the humoral branch of the adaptive immunity. Antibodies, produced by B cells, recognize pathogens or foreign molecules through specific binding to the antigen. This specific interaction can neutralize the antigen or trigger effector functions of the immune system to eliminate the antigen. Examples of the effector functions are opsonization, activation of complement and antibody-dependent cell-mediated cytotoxicity (ADCC).

Antibody consists of two identical light (L) chains and two identical heavy (H) chains, as shown in Figure 1.1. The molecular weight of the light and heavy chain are about 25 and 50kDa respectively. Each light chain is bound to a heavy chain by a disulfide bond and a combination of noncovalent interactions such as salt bridges, hydrogen bonds and hydrophobic interaction. The amino-terminal regions of light and heavy chains, which vary greatly among antibodies with different specificities, are called variable (V) regions,  $V_L$  for light chain and  $V_H$  for heavy chain. The regions of relatively constant sequences beyond the variable regions are called constant (C) regions,  $C_L$  for light chain and  $C_H$  for heavy chain. Within the V regions, sequence variability is concentrated in several hypervariable regions. These hypervariable regions, which constitute the antigen-binding site of an antibody, are called complementarity-determining regions (CDRs). The remaining domains of  $V_L$  and  $V_H$ , which exhibit far less variation, are called the framework regions (FW).



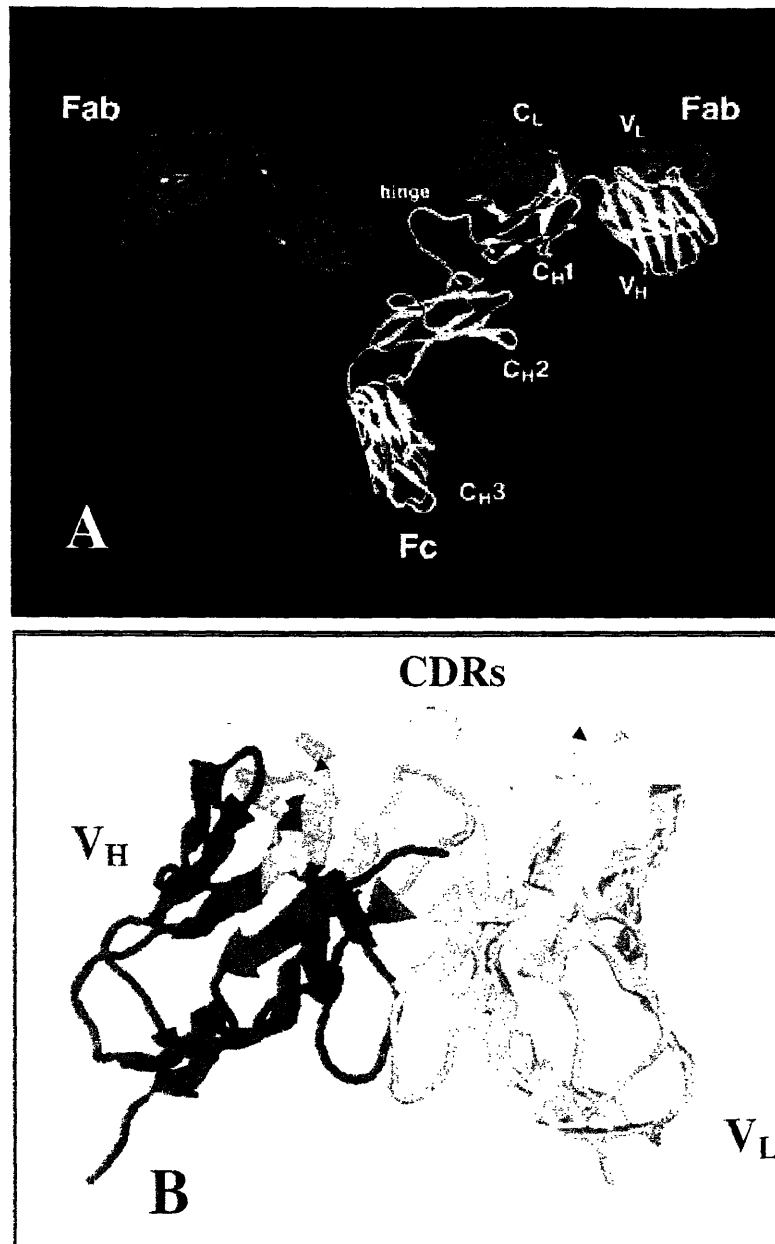


**Figure 1.1 Schematics of Antibody Structure.** (A) Antibody consists of two identical light (red) and heavy (blue & yellow) chains. The amino-terminal regions of the light and heavy chain, which are responsible for antigen binding, are called V<sub>H</sub> and V<sub>L</sub>. The Fc region is involved in activating the effector function of immune system. The IgG picture is adapted from [www.antibodyresource.com/intactab.html](http://www.antibodyresource.com/intactab.html). (B) Antibody mediates specific interaction with its antigen through the CDRs of the V<sub>H</sub> (blue and green) and V<sub>L</sub> (red and yellow). The CDRs of V<sub>H</sub> and V<sub>L</sub> are shown in green and yellow respectively, whereas the framework regions are shown in blue and red colors respectively for V<sub>H</sub> and V<sub>L</sub>.

## **1.2 Antibody Engineering**

Protein engineering has been employed extensively to modify the functions and properties of antibodies (Hudson and Souriau, 2001). Examples of protein engineering include reducing the size of an antibody from IgG format to single-chain Fv (scFv), modifying the valency of an antibody, changing the affinity of Fc receptors, and more frequently, improving the affinity and stability of an antibody. To date, given the inconsistent results from rational protein design, directed evolution is still the most effective method available for exploration and engineering of antibodies. Directed evolution involves displaying a diverse array of antibody mutants on a genetic package (Shusta, et al., 1999), and then selecting favorable mutants from the pool. Such packages, which link the phenotype to its genotype, include ribosome (Hanes, et al., 1998; He and Taussig, 1997; Mattheakis, et al., 1994), bacteriophage (Griffiths and Duncan, 1998; McCafferty, et al., 1990; Smith, 1985), bacteria (Francisco, et al., 1992; Georgiou, et al., 1997) and yeast (Boder and Wittrup, 1997; Boder and Wittrup, 2000).

### **1.2.1 Yeast Surface Display**

Yeast surface display was previously developed in our lab for directed evolution of protein. One of the advantages of using yeast for displaying protein is that as a eukaryote, yeast contains similar protein-processing machinery to a mammalian cell. Thus yeast is more likely than prokaryotes to correctly express and display mammalian surface or secreted proteins, in this case antibodies. Yeast surface display involves displaying the antibody of interest through fusion with a two-unit cell wall glycoprotein called  $\alpha$ -agglutinin, whose original function is to mediate cell-cell adhesion between a-

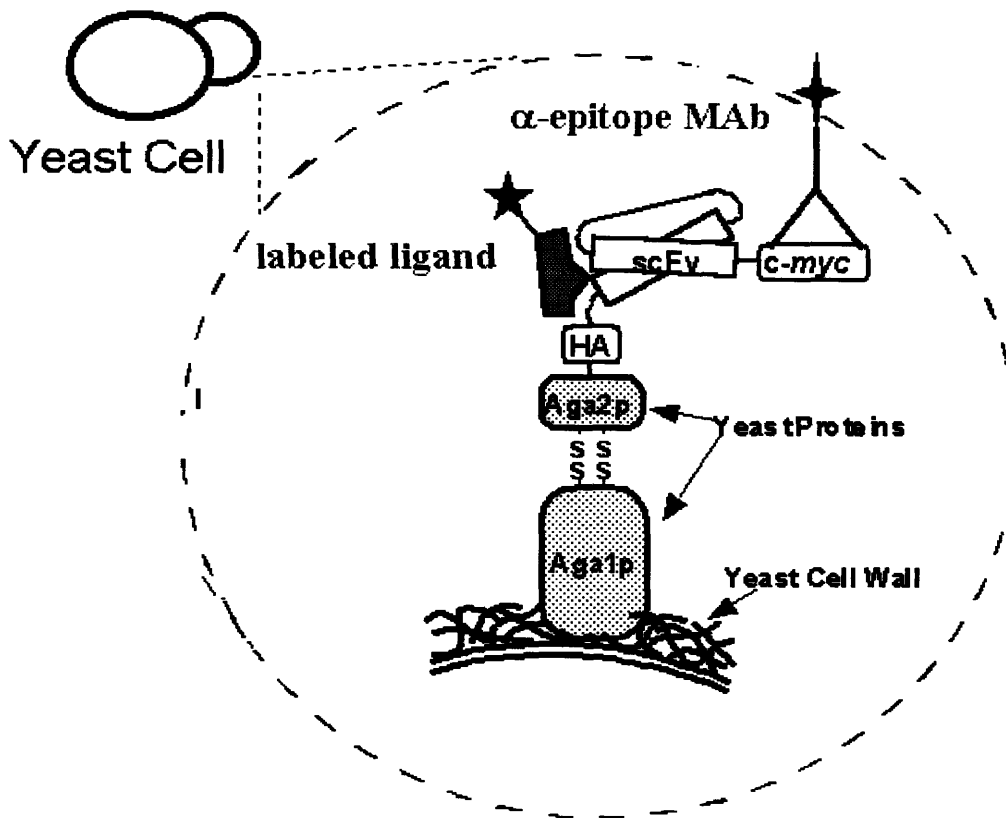


**Figure 1.2 Schematic of Yeast Surface Display.** The antibody of interest (scFv) is displayed on the yeast surface through fusion to Aga1-Aga2 protein. Two epitopes tags, HA and c-myc, are fused to the N-terminus and C-terminus of the antibody respectively. The displayed antibody is able to bind ligands on the yeast surface, and the presence of epitope tags can be detected using commercially available antibodies.

type and  $\alpha$ -type haploid cells (Boder and Wittrup, 1997) (Figure 1.2). A-agglutinin consists of two distinct domains, Aga1p and Aga2p, connected by two disulfide bonds. Aga1p subunit anchors the assembly to the cell wall via a  $\beta$ -glucan covalent linkage. The antibody is fused to the C-terminus of Aga2p, where the native a-agglutinin binding activity localizes. The antibody in the display construct is flanked by two epitope tags, with hemagglutinin (HA) and c-myc on the N- and C-terminus of the antibody respectively. Expression of the full-length antibody on the cell surface can be simply confirmed by detecting the presence of c-myc tag on the cell surface using commercially available antibodies. Additionally, due to the intrinsic quality control of the endoplasmic reticulum (ER), the presence of c-myc tag on the cell surface strongly implies that the surface displayed antibody is folded properly (Hammond and Helenius, 1995).

The number of displayed antibodies is on the order of  $10^4$  copies per cell. The displayed antibody is able to bind ligands on the yeast surface. Specifically, surface-displayed antibodies are incubated with soluble fluorophore-conjugated ligands. The presence of fluorescence on the yeast cells, which indicates the binding of ligands, is detected using a flow cytometer. The fluorescence from surface-displayed antibody binding can be normalized with the simultaneous labeling of the epitope tags (HA or c-myc), preventing any expression bias on the antibody binding fluorescence level. Previously, yeast displaying anti-FITC scFv has been shown to bind simultaneously two macromolecules, a 200kDa-size FITC-dextran and a 150kDa-size mouse antibody 9e10 (anti-c-myc IgG) (Boder and Wittrup, 1997). This demonstrates that the surface-displayed antibodies are readily accessible to their antigens and there is minimal steric hindrance from any cell wall components on the binding of the displayed antibody. In

addition, the dissociation constant of the antibody-antigen interaction can be measured directly on the yeast surface by labeling the antibody-displaying yeast with different concentrations of the antigen, eliminating the need for soluble antibody expression. The dissociation constants measured from yeast surface were shown to be highly similar to the ones measured using soluble antibodies (Boder, et al., 2000).

### **1.2.2 Mutagenesis and Library Screening**

Antibody engineering using yeast surface display involves mutagenizing the antibody gene, displaying the library of mutant antibodies on the yeast surface and subsequently screening for the desired mutants. Multiple methods have been used to mutagenize an antibody gene: random mutagenesis (Boder, et al., 2000; Daugherty, et al., 2000a; Graff, et al., 2004; Leung, 1989), hot-spot site directed mutagenesis (Chowdhury and Pastan, 1999; Goyenechea and Milstein, 1996), targeted mutagenesis of complementary determined region (CDR) residues (Schier, et al., 1996b; Wu, et al., 1998; Yang, et al., 1995), DNA shuffling (Cramer, et al., 1996; Graff, et al., 2004; van den Beucken, et al., 2001; Zhao, et al., 1998), CDR shuffling (Ellmark, et al., 2002; Jirholt, et al., 1998; Marks, et al., 1992; Schier, et al., 1996a), and chain shuffling (Marks, et al., 1992; Schier, et al., 1996a).

Random mutagenesis introduces amino acid changes throughout the entire antibody sequence. One of the most frequently used random mutagenesis techniques is error-prone PCR. In error-prone PCR, mutations are intentionally introduced during PCR through the use of error-prone DNA polymerases and reaction conditions (Cadwell and Joyce, 1992; Leung, 1989). Taq DNA polymerase, which lacks proofreading ability, is commonly employed in error-prone PCR and introduces on average  $10^{-4}$  error per base

pair. To attain practical mutation frequencies, the error rate of Taq DNA polymerase is further increased by altering PCR reaction buffers, such as by using unbalanced dNTP concentrations (Cadwell and Joyce, 1992) during the reaction, by addition of manganese (Leung, 1989), or by addition of nucleoside analogues (Zaccolo and Gherardi, 1999; Zaccolo, et al., 1996). The desired range of mutation frequencies is usually achieved by controlling the amount of the different reagents added and the number of PCR cycles. For example, in the case of random mutagenesis using nucleoside analogues, concentration of the nucleoside analogues and number of PCR cycles can both be used to control mutation rate. Typical mutation frequency for an antibody in random mutagenesis is from 0.5% to 3%.

On the other hand, other mutagenesis techniques, which target particular regions of an antibody, have also been used to improve the affinity of an antibody. One of the most commonly targeted regions is the CDRs of an antibody, as the CDRs are responsible for the direct interaction with the antigen. Mutagenesis targeting antibody CDRs would minimize the structural change in the antibody framework, as mutations are being concentrated in the CDRs only. Minimal framework residue alteration is particularly important in the engineering of human antibodies, since changes in the framework residues may affect the immunogenicity of an antibody.

Overall, different mutagenesis methods have different advantages and each one achieves a different objective. Considerations such as ease and rate of mutagenesis, extent of affinity improvement per round of mutagenesis, and immunogenicity of the mutants, should be taken into account when choosing an appropriate mutagenesis

method. However, these mutagenesis methods can also be applied in a sequential manner to affinity mature an antibody over several rounds of mutagenesis.

After mutagenesis, improved mutants are screened using yeast surface display. These mutant genes, along with the restriction enzyme-digested display plasmid backbone, are co-transformed into yeast. Through homologous recombination in yeast, full-length plasmids containing the mutant genes are created (Gunyuzlu, et al., 2001). A typical number of transformants in a random mutagenesis library is approximately  $10^7$  per 10  $\mu\text{g}$  of mutant DNA. In general, if the antigen is available in soluble form, fluorescence-activated cell sorting (FACS) can be employed to isolate the improved mutants from the library. The mutant library is first labeled at the desired equilibrium or kinetic binding conditions to provide maximum fluorescence differentiation between the improved mutants and the wild-type scFvs (Boder and Wittrup, 1998). Then FACS is used to isolate the improved mutants, which have higher fluorescence intensity. Optimal equilibrium and kinetic binding conditions for the cell labeling have been calculated from mathematical models (Boder and Wittrup, 1998). Screening using optimal labeling and FACS allow for separation of mutants based on a specified quantitative improvement in affinity. With optimal labeling, FACS has been shown to be capable of discriminating with precision and reproducibility minimally-improved mutant over wild type yeast (VanAntwerp and Wittrup, 2000). Current FACS instrumentation is capable of sorting up to  $10^8$  cells per hour. With a library of  $10^7$  yeast transformants, a ten-fold over-sampling of the library requires about 1 hour to sort. Typically, four to five rounds of screening will be performed to enrich the library to a panel of improved clones. If library size is in

excess of  $10^8$ , magnetic beads can be used to enrich the populations, so that the library size can be manageable by FACS (Siegel, et al., 2004).

Previously, yeast surface display has been used to affinity mature an anti-fluorescein antibody from 1nM to 50fM in 4 rounds of mutagenesis and screening (Boder, et al., 2000). In addition, the dissociation rate of an anti-carcinoembryonic antigen (CEA) antibody has also been improved over 1000 fold (from a half-life of 10 minutes to 4-7 days at 37°C) after 2 rounds of mutagenesis and screening using yeast surface display (Graff, et al., 2004). Therefore, yeast surface display has been shown to be a robust screening method, and is used in this study to isolate novel binder and to engineer antibodies.

### **1.3 Antibody Therapeutics for Cancer Therapy**

#### **1.3.1 Tumor Antigens**

Malignant transformation of the cell is usually associated with alteration in the surface antigenic composition. Tumor antigens can result from genetic mutation in tumor cells that generate altered cellular proteins; these kinds of antigens are unique to the tumor cells. These genetic mutations can be induced chemically, physically or virally (i.e. Epstein-Barr virus and Human Papilloma virus). In addition, tumor cell surface antigens can also be aberrantly glycosylated (Tag-72 and Mucins), rendering them different from those on the normal cells (Urban and Schreiber, 1992). However, there are also tumor antigens that are not unique to the cancer cells; these tumor antigens are normally present on healthy cells. When the cells become malignant, the expression profile or level of these antigens change dramatically. One example of aberrant expression profiles is carcinoembryonic antigen (CEA). Tumor cells express CEA over the entire surface of the



cells, while in normal cells, CEA is only present on the apical surface of the cells (Hammarstrom, 1999). Meanwhile, tumor antigens can also be over-expressed when cells become cancerous. Examples are CD20 overexpression in non-Hodgkin lymphoma and CD44 overexpression in lung cancer. When these tumor-associated antigens are expressed at a level (higher density) that can significantly distinguish their malignant phenotypes from the normal healthy phenotypes, this makes them (antigens) excellent targets for antibody-targeted therapy.

### **1.3.2 Mechanism of Tumor Killing**

Antibody can block tumor growth or mediate the killing of tumor cell by several different mechanisms (Houghton and Scheinberg, 2000). First, antibody can bind to the growth factor receptors or other signaling molecules on the cancer cells, leading to apoptosis or inhibition of the cell growth (Groner, et al., 2004). Examples are Bevacizumab, which binds vascular endothelial growth factor (VEGF), and Cetuximab, which block the binding of EGF or TGF- $\alpha$  against EGFR. Another way to mediate killing is to recruit the natural immune system to kill tumor cells. Antibody bound to the cancer antigen can activate the complement components, leading to opsonization of cancer cells by complement receptors-expressing phagocytic cells, direct lysis of tumor cells and inflammation with recruitment of inflammatory cells. In addition, the bound antibody can bind to the activating Fc receptors on the effector cells like macrophages and NK cells, leading to antibody-dependent cellular cytotoxicity (ADCC) or release of cytokines. Examples are Rituxan® in the treatment of non-Hodgkin's lymphoma and Herceptin® in the treatment of metastatic breast cancer. Besides using naked antibody to cure cancer, antibodies or antibody fragments can be conjugated with different cytotoxic moieties to

kill the tumor cells. These cytotoxic moieties include a variety of entities, ranging from radionuclide molecules to a virus carrying therapeutic genes or a liposome carrying loads of drugs, toxins, or enzymes (Trail and Bianchi, 1999). For example, antibody BR96-doxorubicin conjugate was used to target Le<sup>y</sup>-related tumor-associated antigen expressed on most human carcinoma (Trail, et al., 1993). Antibody-directed drug delivery can improve the therapeutic efficacy of cytotoxic moieties by targeting tumor cells specifically while reducing the potential systemic toxicities of the drugs. However, the success of a targeted cell-killing function is predicated on the existence of tumor-associated antigens.

### **1.3.3 Current Antibody Therapeutics**

Antibodies targeting various tumor-associated antigens have been developed successfully to treat cancer. Currently, there are eight monoclonal antibodies approved by the Food and Drug Administration (FDA) for cancer therapy. Table 1.1 summarizes these FDA-approved antibodies and their targets. These approved antibodies can be divided into two types, naked and conjugated. Naked antibodies are those without any moiety attached to it; while conjugated antibodies have either toxin, radioactive material or cytotoxic drug attached to them. Most of the approved antibodies, except Bexxar, are either chimaeric or humanized, minimizing the neutralization effect of HAMA (human anti-murine antibody). In addition to these approved antibodies, there are hundreds of clinical trials worldwide involving the use of antibodies to treat cancer ([www.clinicaltrials.gov](http://www.clinicaltrials.gov)). In general, antibody has been proven to be a successful molecule for targeted cancer therapy.

**Table 1.1 FDA Approved Antibodies for Cancer Therapy**

<b>Antibody</b>	<b>Type</b>	<b>Target</b>	<b>Condition</b>	<b>Approved</b>
Rituxan	Chimaeric	CD20	Non-Hodgkin's Lymphoma	Nov, 1997
Herceptin	Humanized	HER2	Metastatic Breast Cancer	Sept, 1998
Mylotarg	Humanized (Toxin: calicheamicin)	CD33	Acute Myelogenous Leukemia	May, 2000
Campath	Humanized	CD52	Chronic Lymphocytic Leukemia	May, 2001
Zevalin	Chimaeric (In-111 or Y-90 linked)	CD20	Non-Hodgkin's Lymphoma	Feb, 2002
Bexxar	Murine (I-131 linked)	CD20	Non-Hodgkin's Lymphoma	Jun, 2003
Erbix	Chimaeric	EGFR	Metastatic Colorectal Cancer	Feb, 2004
Avastin	Humanized	VEGF	Metastatic Colorectal Cancer	Feb, 2004

#### 1.4 Thesis Overview

In this work, antibodies and antibody-conjugates against two tumor antigens, AF-20 antigen and human aspartyl (asparaginy)  $\beta$ -hydroxylase (HAAH), were developed. These two antigens have been previously shown to be present on a variety of tumor cells; while they have minimal expression on normal tissues, rendering them good targets for antibody therapy.

Chapter 2 of this thesis describes the development of an antibody fragment and an antibody toxin conjugate against AF-20 antigen. Previously, a mouse monoclonal antibody (AF-20) was raised against this antigen; however, the gene of this antibody was not available. In this work, the gene of AF-20 antibody was cloned and used to construct an antibody fragment (scFv). The antibody fragment was characterized and shown to function similarly as its parental IgG counterpart. Antibody-toxin conjugate was also

constructed to illustrate that the antibody fragment can be a targeting domain for immunotoxin to treat a variety of cancers.

Chapter 3 of the thesis gives details about the isolation and engineering of novel human antibodies against HAAH using yeast surface display. Novel human antibody fragments (scFv) were isolated against HAAH, and then converted into IgG formats. These human IgGs were shown to bind specifically to the tumor cells, illustrating the potential use of them in cancer diagnosis and therapy. One of the antibodies was also affinity matured using directed evolution and yeast surface display.

Chapter 4 focuses on the development of a quantitative screening tool, magnetic bead capture, for cell-based polypeptide library screening. Magnetic bead capture was used as an alternative tool to the flow cytometric sorting for screening of favorable mutants from a library. Results showed that magnetic bead capture probability of labeled cells correlated closely with the surface ligand density, and magnetic beads capture was capable of quantitatively screening for both novel binders from an excess of non-binders and high-affinity binders from an excess of low-affinity binders.

## **Chapter 2: Characterization of a Single-chain Fv for Delivery of Cytotoxic Moieties to Hepatocellular Carcinoma Cells**

### **2.1 Introduction**

Antibodies have been employed extensively in recent years for the treatment of various diseases, in particular cancer (Carter, 2001; Gura, 2002). Tumor cell killing can be achieved by blocking the biological function of the antigen, through recruitment of immune effector functions or through delivery of attached toxins or radionuclides. Previously, monoclonal antibody (Mab) AF-20 was obtained by immunizing BALB/c mice with the FOCUS cell line, isolated from a poorly differentiated hepatitis B virus positive hepatocellular carcinoma (HCC) (He, et al., 1984; Wilson, et al., 1988). The antigen to which AF-20 IgG binds has been partially characterized (Moradpour, et al., 1995). The antigen is a 180kDa homodimeric glycoprotein found on a variety of cancers including liver, pancreatic, prostate, colon and breast tumor cell lines, while it has minimal expression on normal tissues. However, full identification of this antigen is still in progress.

AF-20 antigen expression is particularly prevalent in hepatocellular carcinoma, where it is expressed on 75 of 75 primary HCC tumors and on distant metastases. HCC comprises about 90% of the primary liver cancer in the United States, and the incidence for this tumor type has increased recently (El-Serag, et al., 2003; El-Serag and Mason, 1999). Common cancer therapies like chemotherapy and radiotherapy are relatively ineffective in treating HCC and prognosis remains poor despite a variety of other treatment options including surgical resection, chemoembolization, and percutaneous

injection of ethanol. Immunotherapy using AF-20 IgG would present an attractive alternative option for the treatment of HCC.

Previously, an iodinated form of AF-20 IgG showed excellent localization toward target tumor cells *in vivo*, and the highly specific and sensitive interaction rendered this antigen to be a potential target for immunotherapy (Takahashi, et al., 1989). One interesting property of this antigen is that once AF-20 IgG is bound, the complex is rapidly internalized at 37°C (Moradpour, et al., 1995). Utilizing this internalization property of the antigen, AF-20 IgG has been conjugated chemically to different moieties to specifically deliver both detection and therapeutic DNA to tumor cells. Examples of the moieties conjugated include liposomes (Moradpour, et al., 1995), DNA-binding cholesteryl-spermine (Mohr, et al., 1999) and adenovirus (Mohr, et al., 2000; Yoon, et al., 2000). Overall, AF-20 IgG has been proven to be an effective antibody for targeting tumor cells in mice. However for targeting solid tumors, whole intact IgG has poor tumor penetration properties (Jain and Baxter, 1988). One possible way to improve the tumor targeting properties of AF-20 IgG is to reduce its size. Fragments of antibodies like single-chain Fv (scFv) have better penetration abilities and faster whole body clearances than the intact IgG (Adams, et al., 1993; Yokota, et al., 1992; Yokota, et al., 1993), exhibiting potentially better pharmacokinetics for tumor targeting. Genetic fusion of AF-20 antibody fragments with protein toxins or enzymes or conjugates with virus particles or toxins are also of interest for targeted therapy of cancer.

In this study, we have cloned the V gene of AF-20 IgG and use it to construct a scFv. The scFv was displayed on the yeast surface and secreted as soluble form from yeast. The soluble AF-20 scFv was shown to bind to the same epitope as AF-20 IgG with

a binding affinity of 4nM. The AF-20 scFv also retained the internalization ability of the AF-20 IgG, and was shown to facilitate the internalization of virus-sized particles, Quantum Dots, into the tumor cells. These studies demonstrate the potential of using the AF20 scFv to target virus particles or liposome vehicles to HCC and other tumor cells expressing AF-20 antigen. Also, the potential of immunotherapy using AF-20 scFv as the targeting domain of an immunotoxin was explored. The toxin used in this study was the recombinant plant toxin gelonin (Falasca, et al., 1982). Our results show that AF-20 scFv–gelonin fusions consistently gave higher cytotoxicities than native gelonin on different tumor cell lines. Overall, this study demonstrates the promise of using engineered antibody fragments derived from Mab AF-20 for targeted therapy of HCC and other cancers.

## **2.2 Materials and Methods**

### **2.2.1 Cloning of the AF-20 V Genes**

Hybridoma cells expressing AF-20 IgG were cultured in media consisting of Dulbecco's modified eagle media (Sigma, St Louis, MO), 20% fetal calf serum (Hyclone, Logan, UT), 2% glutamine, 100U/ml penicillin and 0.1mg/ml streptomycin (Sigma). Cells were grown in T-flasks at 37°C in a 5% CO<sub>2</sub> atmosphere. About 10<sup>8</sup> cells were grown up for RNA isolation, and total RNA was isolated using guanidinium thiocyanate precipitation as described in the Ig Prime Kit protocol (Novagen, Madison, WI). First strand cDNA synthesis was carried out as described in the Ig Prime Kit protocol. The PCR amplification reactions were then setup respectively for the heavy and light chains using the mouse IgG and kappa light chain primer sets provided by the kit. PCR products

were run on a 1% agarose gel and stained. DNA bands in the region of 400 to 500 bp were excised, purified and ligated into pSTBlue1 using the Perfectly Blunt Cloning Kit (Novagen). The ligated products were transformed into Nova Blue *E. coli* cells (Novagen), and the resulting plasmids were isolated from the *E. coli* and sequenced to determine the identity of the AF-20 heavy and light chain variable regions.

### 2.2.2 Construction of the AF-20 scFv

The scFv was constructed in the configuration of V<sub>H</sub>-Linker-V<sub>L</sub> using the splicing by overlap extension (SOE) PCR method (Horton, et al., 1989; Krebber, et al., 1997). A 20-amino acid linker with four repeats of (Gly)<sub>4</sub>-Ser was used. The V<sub>H</sub> chains were amplified using V<sub>H</sub> 5' primer: gatc gatc gagctagc-caggtccaactgcagcagtc, and V<sub>H</sub> 3' primer: ccactctcacagtctcctcaggtggtgg-tggttctggtggtggtggttctggcggcggcggctcc. The V<sub>L</sub> chains were amplified using V<sub>L</sub> 5' primer: ggcggcggcggctccggaggaggaggatcggacatcttgctgactcag and V<sub>L</sub> 3' primer: gggacaaagttggaaataaaaaatgctgatgctggtggatccatcatcatcatcattgataactcaggctc gatc gatc. The V<sub>L</sub> 3' primer incorporated an arginine to asparagine mutation at a lysine-arginine site near the c-terminus in order to remove a potential Kex2 cleavage site. PCR reactions were carried out on a Perkin Elmer DNA Thermal Cycler 480 in a 100 µL volume using 100 ng of template, 1 µM of primers, 0.2 mM of dNTP, 5 U *Pfu* Polymerase (Invitrogen, Carlsbad, CA). The cycling conditions used were 1 cycle of 96°C for 2 minute followed by 30 cycles of 96°C for 1 minute, 53°C for 1 minute and 72°C for 2 minutes, and finally 1 cycle of 72°C for 10 minutes. The V<sub>H</sub> and V<sub>L</sub> PCR fragments were separately gel-purified. The SOE reaction contained 400µM of each dNTP, 2µg each of the V<sub>H</sub> and V<sub>L</sub> PCR products and 5U of *Pfu* Polymerase in 100 µL volume. The reaction was run for 5 cycles with no primers at cycling conditions of 96°C



for 1 minute, 53°C for 1 minute, 72°C for 2 minutes and then followed by 1 cycle of 72°C for 10 minutes. Outside primers ( $V_H$  5' primer and  $V_L$  3' primer) were then added to the reaction for a further 15 cycles. The PCR product was gel purified, restriction-digested with *NheI* and *XhoI*, and ligated into the corresponding sites in the pRS based secretion vector. The ligated product was then transformed into XL1-Blue *E. coli* cells (Stratagene, La Jolla, CA) for amplification and sequencing.

### **2.2.3 Soluble Expression of AF-20 scFv**

The AF-20 scFv secretion plasmid along with a plasmid contain a Trp marker were co-transformed into yeast strain YVH10 using lithium acetate method (Gietz and Schiestl, 1991). The pRS based yeast secretion vector and the yeast strain have been previously described (Parekh, et al., 1995; Robinson, et al., 1994). Yeast culturing and induction of scFv secretion were performed as previously described (Shusta, et al., 1998). The yeast supernatant containing soluble scFv was concentrated using stirred cell protein concentrator series 8000 from Millipore (Billerica, MA). The concentrated protein solution was then purified using Nickel-NTA resin according to the manufacturing protocol from Qiagen (Valencia, CA). Nickel-column-purified AF-20 scFv was dialyzed in PBS (pH 7.4) for later experiments.

### **2.2.4 Coomassie Gel Analysis and Western Blot**

Various amount of protein samples were resolved by SDS-PAGE gel electrophoresis using a 4% stacking and 12.5% resolving gel. For Coomassie analysis, the gel was stained with Coomassie staining solution (0.4g/L stain, 7% acetic acid, 35% methanol) for 1 hour and destained overnight in destain buffer (7% acetic acid, 35% methanol). Images of the bands were taken with Fluor-S imager (Bio-Rad, Hercules,

CA). For western blot, after electrophoresis, protein was transferred to a nitrocellulose membrane using an Xcell II transfer apparatus (Invitrogen, Carlsbad, CA). The membrane was then probed with 0.5 $\mu$ g/ml of tetra-HIS antibody (Qiagen) in Tris-buffered saline with 0.1% Tween-20 and followed by 1:2000 dilution of goat anti-mouse IgG horseradish peroxidase conjugate (Sigma). Detection was performed with SuperSignal® substrate from Pierce (Rockford, IL) and Fluor-S imager. In this work, purified proteins were de-glycosylated with N-glycosidase Endo H<sub>f</sub> and PNGase F according to the manufacturing protocol from New England Biolabs (Beverly, MA)

### **2.2.5 Binding of the scFv to FOCUS Cells**

FOCUS cells were cultured as previously described (Yoon, et al., 2000). FOCUS cells were detached from the culture plates using versene solution (Gibco, Carlsbad, CA), and then resuspended in PBS supplemented with 1g/L bovine serum albumin (BSA). ScFv was allowed to bind to the FOCUS cells at 4°C for 4 to 6 hours. The cells were then washed with PBS/BSA and stained with 1:50 dilution of anti-FLAG-IgG-FITC conjugate (Sigma) at 4°C for 30min. Stained cells were then analyzed by flow cytometry. The scFv epitope mapping experiment was similarly performed with the exception that excess amount (10 fold) of AF-20 IgG was added to the initial scFv incubation step. The titration of AF-20 scFv against FOCUS cells was also performed similarly but with different secondary detection antibodies. Different concentrations of scFv were incubated with FOCUS cells at 4°C for 4 to 6 hours, and then the cells were stained with 100nM of mouse anti-FLAG IgG (Sigma) and followed by 1:50 dilution of goat anti-mouse IgG-phycoerythrin conjugate (Sigma) for 20min at 4°C. Cell fluorescence was then detected using a flow cytometer.

### **2.2.6 Internalization of the AF-20 scFv into FOCUS Cells**

Vitrogen from Cohesion Technologies (Palo Alto, CA) was added to a clean coverslip and subsequently FOCUS cells were cultured on these collagen-coated coverslips. 200nM of AF-20 scFv or control scFv was pre-incubated with 50nM of mouse anti-FLAG IgG. After overnight culturing, FOCUS cells were washed, and allowed to bind the pre-incubated materials in serum-free media at 37°C for 1 hour. After the incubation, cells were fixed with 4% cold formaldehyde (Sigma) for 20min and then permeabilized with 0.1% saponin (Sigma). The permeabilized cells were labeled with 1:100 dilution of goat anti-mouse IgG-FITC conjugate (Sigma) and 1:10000 dilution of Hoechst dye (Molecular Probe) at room temperature for 30min. Fluorescence inside the cells was detected using a confocal microscope. For the internalization study of Quantum dot, 250nM of AF-20 scFv or control scFv was pre-incubated with 75nM of biotinylated mouse anti-FLAG IgG and 2 $\mu$ L of Qdot 565-streptavidin conjugate (Quantum Dot, Hayward, CA) in a total volume of 50 $\mu$ L of serum-free media. After 1 hr of pre-incubation, the pre-incubated mixture were diluted with 300 $\mu$ L of serum-free media and presented to the cells grown on coverslip at 37°C for 3hour. Cells were then analyzed directly using a confocal microscope.

### **2.2.7 Construction of AF-20 scFv-Gelonin Immunotoxin**

AF-20 scFv was fused to the amino terminus of the gelonin to construct the AF-20 scFv-gelonin immunotoxin. The immunotoxin was constructed and expressed according to the previous report (Rosenblum, et al., 2003). Briefly, overlapping PCR products containing the AF-20 scFv/rGel gene were cloned into the bacterial expression plasmid pET-32a(Novagen). An epitope tag, FLAG, was inserted at the amino terminus

of the immunotoxin for detection. The AF-20scFv/rGel protein was expressed using the *E. coli* strain AD494(DE3)pLysS by induction with 100  $\mu$ M IPTG at 23°C for 16 hrs. Soluble protein was purified using Blue Sepharose 6 Fast Flow and stored in PBD at 4°C.

### **2.2.8 *In-vitro* Cytotoxicity of the Immunotoxin**

A 72-hr cell proliferation assay with log-phase (5000 to 10000 cells/well) AF-20 antigen-positive cells were performed as described previously (Nishikawa, et al., 1992). The cells used in this studied were FOCUS cells (HCC), L3.6pl cells (pancreatic tumor) and PC3 cells (prostate tumor). Cell viability was assessed using either alamarBlue™ (Biosource, Camarillo, CA) or the previously described crystal violet staining procedures (Nishikawa, et al., 1992). Cell viability detection using alamarBlue™ was performed according to the manufacturing protocol.

### **2.2.9 Display of AF-20 scFv and Binding of AF-20 scFv Displaying Yeasts**

For yeast surface display, AF-20 scFv was restriction digested and ligated into pCTCON vector. The vector was then transformed into EBY100. EBY100 cells carrying the plasmid was grown in SD-CAA for 24hr and then induced in SG-CAA+0.2% glucose media for another 24hr. The display level was detected with mouse monoclonal antibody 9e10 (Covance, Berkeley, CA) and goat anti mouse-phycoerythrin conjugates (Sigma).

FOCUS cells were grown as a monolayer on a coverslip-bottom petri dish (Mattek, Ashland, MA).  $10^7$  yeast cells displaying either no scFv, control scFv or AF-20 scFv were allowed to roll and bind to the monolayer of FOCUS cells respectively at room temperature for 1hr in Dulbecco's PBS (Gibco). Four washes with Dulbecco's PBS were performed to remove the yeast cells that non-specifically stick to the FOCUS cells. Then the yeast-FOCUS cells complex were fixed in ice cold 4% formaldehyde for 20min, and

then washed four times with room temperature PBS. The complex was later imaged using a light microscope and the number of yeast cells on the FOCUS cells was counted.

## **2.3 Results**

### **2.3.1 Construction of AF-20 scFv**

The variable region genes of the mouse AF-20 IgG were cloned from AF-20 hybridoma cDNA with degenerate PCR primers from the Ig Prime kit (Novagen), and were sequenced separately. The translated amino acid sequences of the variable regions of both heavy and light chains are shown in Figure 2.1. The AF-20 scFv was constructed in the configuration of  $V_H$ -linker- $V_L$  using the splicing by overlap extension (SOE) PCR method (Horton, et al., 1989; Krebber, et al., 1997), with four repeats of (Gly<sub>4</sub>-Ser) as the linker. Two epitope tags were added to the flanking regions of the scFv, a FLAG tag on the N-terminus and a 6xHis tag at the C-terminus. The epitope tags were later used for both scFv detection and purification. DNA sequencing of the whole AF-20 scFv gene construct confirmed that the scFv gene sequence containing both epitope tags was in frame and contained no mutations. A schematic of the AF-20 scFv is shown in the top panel of Figure 2.2.

### **2.3.2 Expression of the AF-20 scFv in *Saccharomyces Cerevisiae***

The AF-20 scFv gene was subcloned into the pRS based secretion vector (Parekh, et al., 1995), and the AF-20 scFv was expressed in *Saccharomyces cerevisiae* strain YVH10 (Robinson, et al., 1994). Supernatant from the AF-20 scFv secreting yeast was concentrated and purified using Nickel-NTA resin. The purified AF-20 scFv was then

```

A S Q V Q L Q Q S G P D L V K P G A S V
1 gctagccaggtccaactgcagcagctctggacctgacctggtgaagcctggggcttcagtg 60
R I S C K A S G Y T F A G H Y V H W V K
61 aggatatcctgcaaggttctggctacaccttcgcaggccactatgtacactgggtgaag 120
Q R P G R G L E W I G W I F P G K V N T
121 cagaggcctggacggggacttgagtggattggatggattttccctggaaaggtaaatact 180
K Y N E K F K G K A T L T A D K S S S T
181 aagtacaatgagaagttcaagggcaaggccacattgactgcagacaaatcctccagcaca 240
A Y M Q L S S L T S E D S A V Y F C A R
241 gcctacatgcagctcagcagcctgacctctgaggactctgcggtctatctgtgcaaga 300
V G Y D Y P Y Y F D Y W G Q G T T L T V
301 gttggatatgattacccgtactactttgactactggggccaaggcaccactctcacagtc 360
S S G G G G S G G G G S G G G S G G G
361 tcctcaggtggtggtggttctgggtggtggttctggcggcggcggctccggaggagga 420
G S D I L L T Q S P A I L S V S P G D R
421 ggatcggacatcctgctgactcagtcctccagccatcctgtctgtgagtcaggagacaga 480
V S F S C R A S Q S I G T S I H W Y Q Q
481 gtcagtttctcctgcagggccagtcagagcattggcacaagcatacactggtatcagcaa 540
R T N G S P R L L I K Y A S E S I S G I
541 agaacaaatggttctccaaggcttctcataaagtatgcttctgagtctatctctggatc 600
P S R F S G S G S G T D F T L S I N S V
601 ccttccaggttttagtggcagtgatcagggacagattttactcttagcattaacagtggtg 660
E S E D V A D Y Y C Q Q S S S W P F T F
661 gagtctgaagatgttgcagattactgtcaacaaagtagtagctggccattcacgttc 720
G S G T K L E I K N A D A G G S
721 ggctcggggacaaaagttggaataaaaaatgctgatgctggtggatcc

```

**Protein Sequence: variable domain of heavy chain**

QVQLQQSGPDLVKPGASVRISCKASGYTFAGHYVHWVKQRPGRGLEWIGWIFP  
GKVNTKYNEKFKGKATLTADKSSSTAYMQLSSLTSEDSAVYFCARVGYDYPY  
FDYWGQGTTLTVSS

**Protein Sequence: variable domain of light chain**

DILLTQSPAILSVSPGDRVSFSCRASQSIGTSIHWYQQRTNGSPRLLIKYASESISGI  
PSRFSGSGSGTDFTLSINSVESEDVADYYCQQSSWPFTFGSGTKLEIKNA

**Figure 2.1** The nucleic acid and amino acid sequences of the variable domains of AF-20 IgG. Genes of the variable domains were cloned from the AF-20 IgG secreting hybridoma cells and sequenced. Underlined regions are the corresponding complementarity-determining regions (CDRs) of the variable domains. N-Glycosylation occurred on the italic/red asparagine residue during the expression of antibody fragment in *Saccharomyces cerevisiae*.

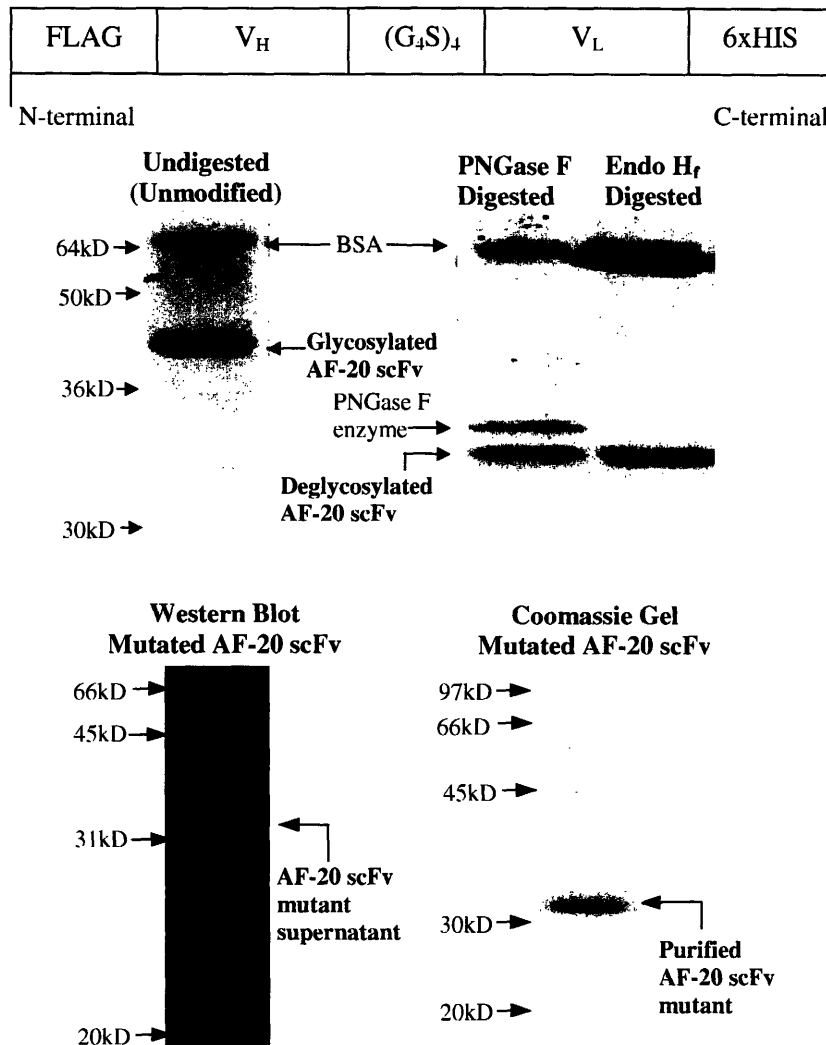


**Figure 2.2 Secretion and Purification of AF-20 scFv.** The top panel illustrated the schematic of the secreted AF-20scFv. Variable domains of heavy chain and light chain were connected through a (Gly)<sub>4</sub>-Ser linker, forming a single-chain Fv. Two epitope tags, n-terminal FLAG and c-terminal 6xHis, were inserted for detection and purification. Soluble AF-20 scFv was purified using Nickel-NTA resin. Native AF-20 scFv was glycosylated in *Saccharomyces cerevisiae* as shown in the middle panel. Purified proteins were run on SDS-PAGE gel and stained with Coomassie Blue-stain. Unmodified AF-20scFv migrated at about 40 to 45kDa, which was much higher than the expected size of 30kDa (middle left panel). After being digested in N-glycosidase (PNGase F and Endo H<sub>f</sub>), AF-20 scFv migrated at a smaller size (about 33kDa), which was closer to the expected size (middle right panel). The asparagine on light chain, where N-glycosylation occurred (Figure 1), was mutated to aspartic acid. Western blot of the asn-to-asp mutant supernatant using mouse anti-FLAG IgG-HRP conjugate showed that the AF-20scFv mutant migrated at about 30kDa (lower left panel). The Coomassie Blue-stained gel on the lower right panel showed that purified AF-20 scFv mutant (N→D) also migrated at about 30kDa and was without any significant contamination from yeast proteins.

analyzed by SDS-PAGE. The middle left panel of Figure 2.2 shows that purified AF-20 scFv migrated at a size about 40 to 45kDa, which was larger than the expected size of 30kDa. Western blot analysis of the 40kDa band using tetra-HIS antibody (Qiagen) revealed that the band contained a 6xHis tag (data not shown). The reason for the aberrant size of the AF-20 scFv was determined to be due to glycosylation in *S. cerevisiae*. A consensus N-glycosylation site (asn-gly-ser) is present on the light chain sequence, and this particular region of the antibody was predicted to be surface exposed by homology modeling. To investigate the glycosylation status of the scFv, the purified antibody fragment was incubated with two different N-glycosidases (PNGase F and Endo H<sub>f</sub>) and then examined by SDS-PAGE (Bretthauer and Castellino, 1999). The middle right panel of Figure 2.2 showed that the N-glycosidase-digested scFv bands migrated at about 33kDa, which was smaller than the undigested band and closer to the theoretical size (30kDa). This confirmed that the AF-20 scFv was N-glycosylated during secretion in *Saccharomyces cerevisiae*. The Fv model in Figure 2.3 also indicated that the glycosylation site was close to the junction between variable and constant domains of the light chain, and on the opposite side from the CDRs. Coomassie gel analysis of the purified AF-20 IgG showed that the light chain migrated at slightly less than 30kDa, thus free of glycosylation (data not shown). Therefore, this glycosylation site is likely unique to the scFv format of the antibody, due to the exposure of this interfacial site upon construction of the scFv format. This would suggest that removing the glycosylation site should not significantly alter the binding affinity of AF-20 scFv. In order to prevent the potential interference of glycosylation on protein expression in *Saccharomyces cerevisiae*



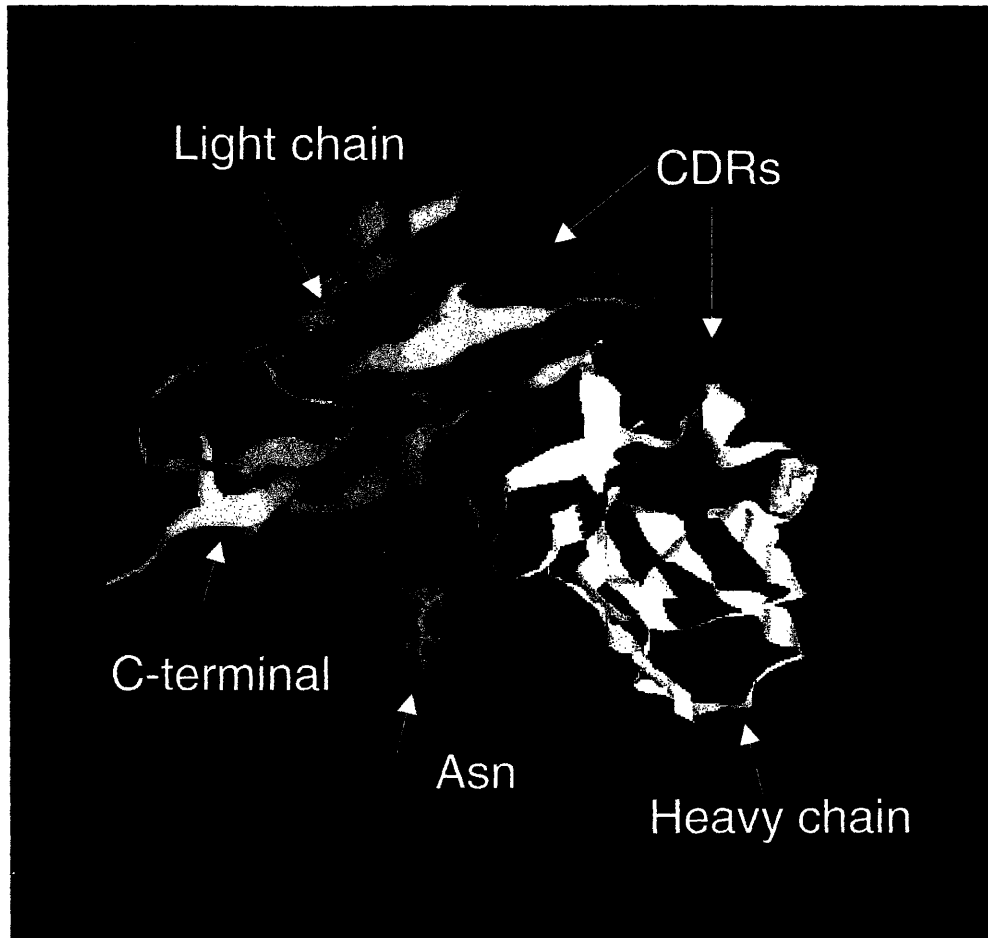


**Figure 2.3 Homology Model of AF-20 Fv.** The AF-20 Fv model was computed using web antibody modeling (<http://antibody.bath.ac.uk>). The red and white ribbons are the framework regions of the light and heavy chains respectively. The CDRs of the light and heavy chains are shown in blue. The asparagine residue where N-glycosylation occurs is shown in green, and it is located far away from the CDRs.

and downstream purification, the asparagine of the Asn-Gly-Ser consensus sequence (Figure 2.1), was changed to an aspartic acid by site directed mutagenesis. Western blot analysis of the supernatant of mutated AF-20 scFv (N41D) showed that the scFv migrated at the expected size of 30kDa (bottom left panel of Figure 2.2). This was further confirmed by SDS-PAGE of the purified, mutant AF-20 scFv (bottom right panel of Figure 2.2). In addition, purified AF-20 scFv was free of any major contaminants from yeast native proteins. This N41D non-glycosylated mutant was used in subsequent studies.

### **2.3.3 Binding Epitope and Affinity of the AF-20 scFv against FOCUS Cells**

FOCUS cells which overexpress AF-20 antigen were used as a model system to determine the specificity of the AF20 scFv (Wands, et al., 1997). FOCUS cells were detached from culture plates using versene solution to protect the integrity of the cell membrane antigens. FOCUS cells were incubated with buffer alone, nonspecific control scFv (anti-fluorescein scFv) or AF-20 scFv at 4°C. Then the cells were stained with mouse anti-FLAG IgG-FITC conjugate and analyzed by flow cytometry (FACS). The top panels of Figure 2.4 showed that the FACS histograms of control (anti-fluorescein) scFv and no scFv (background) were virtually identical. The bottom left panel of Figure 2.4 shows that AF-20 scFv binds to FOCUS cells. To demonstrate that this binding is specific, AF-20 scFv was incubated with FOCUS cells in the presence of an excess AF-20 IgG. Cells were then stained with mouse anti-FLAG IgG-FITC conjugate, which only recognizes the AF-20 scFv. Figure 2.4 bottom right panel showed that the binding of AF-20 scFv to FOCUS cells is completely abolished by the addition of AF-20 IgG. This

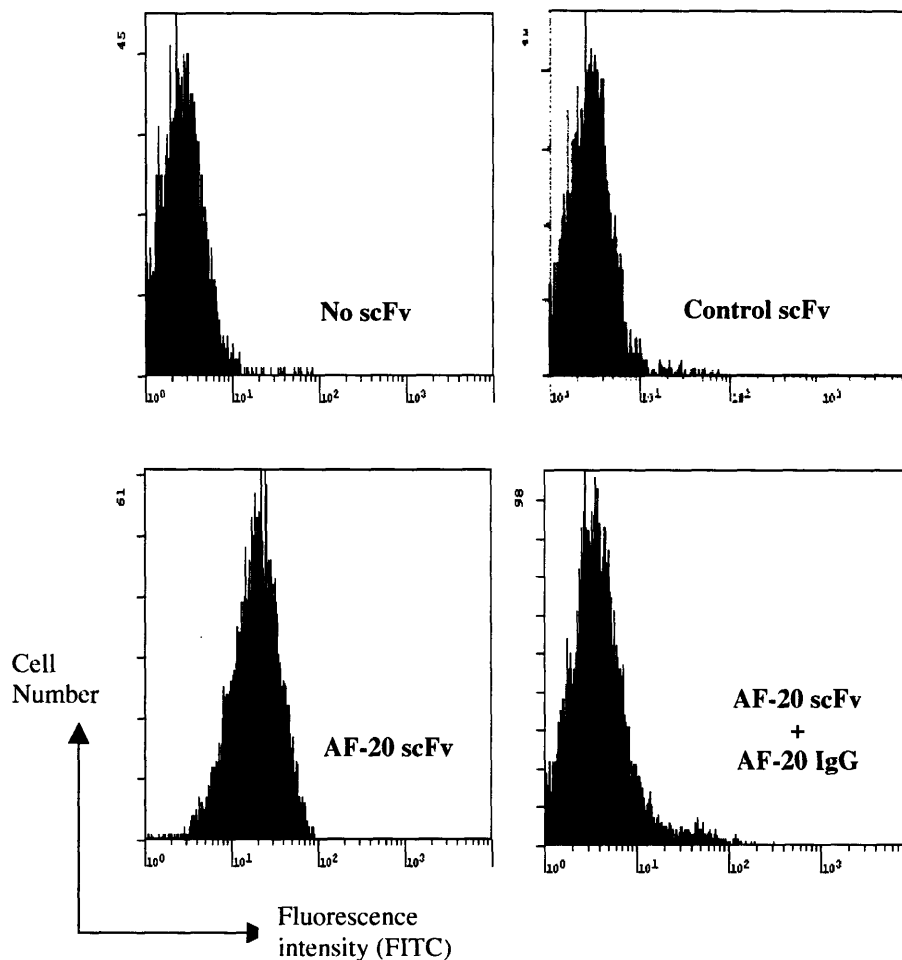


**Figure 2.4 *In-vitro* Specific Binding of AF-20 scFv on the Surfaces of FOCUS Cells.** FOCUS cells were detached from the plates and were allowed to bind buffer, control scFv (anti-fluorescein scFv) or AF-20scFv at 4°C. The cells were then stained with mouse anti-FLAG IgG-FITC conjugate, which only recognized the FLAG tag on control and AF-20 scFv, and stained cell were analyzed using FACS. The top left and right panels showed that control scFv did not bind FOCUS cells, whereas the AF-20 scFv showed binding against FOCUS cells (lower left panels). With the addition of AF-20 IgG, the binding of AF-20scFv on the surface of FOCUS cells were significantly lowered (lower right panel). This indicated that the AF-20 scFv bind to the same epitope as the AF-20 IgG.

illustrates that AF-20 scFv binds specifically to FOCUS cells, with a binding epitope competitive with and likely identical to AF-20 IgG. The dissociation constant of AF-20 scFv against AF-20 antigen at 4°C was determined. FOCUS cells were allowed to bind to different concentrations of AF-20 scFv solubly at 4°C. The scFv bound cells were then incubated with mouse anti-FLAG IgG, and followed by staining with goat anti-mouse IgG-phycoerythrin conjugate. The cell surface fluorescence was analyzed using FACS. Figure 2.5 shows the titration curves of AF-20 scFv against FOCUS cells at 4°C. The dissociation constant was determined to be  $3.8 \pm 0.7 \text{ nM}$  at 4°C.

#### **2.3.4 Internalization of the AF-20 scFv into Tumor Cells**

One of the salient properties of AF-20 antigen is that once AF-20 IgG binds, the complex is internalized readily (Moradpour, et al., 1995). The ability of the AF-20 scFv to internalize similarly was studied. FOCUS cells were seeded on collagen plated coverslips overnight. Control (nonspecific) scFv or AF-20 scFv were pre-incubated with mouse anti-FLAG IgG, so that the scFv would be presented in a bivalent form to the FOCUS cells, similar to the AF-20 IgG. Conjugated bivalent scFv were then incubated with the adhered FOCUS cells for 1 hr at 37°C in serum free media. The cells were then washed, fixed and permeablized. The presence of mouse antibodies inside the cells, which implied the internalization of scFv, was detected with goat anti-mouse IgG-FITC conjugate. Cells were also co-stained with Hoechst, a nuclear dye. Stained cells were then analyzed using a confocal microscope. Figure 2.6 top, left panel showed negligible internalized green fluorescence signal (FITC) for the control scFv, indicating the absence of any substantial internalization of control scFv into the FOCUS cells. On the other hand, the top, right panel of Figure 2.6 showed intense FITC fluorescence surrounding

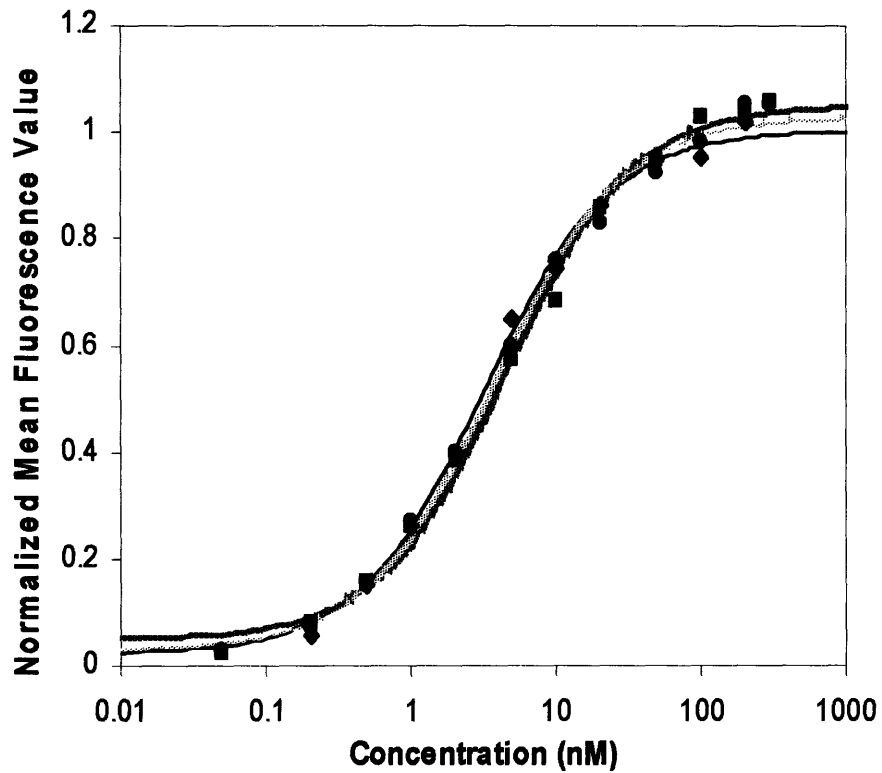


**Figure 2.5 Titration Curve of AF-20 scFv against FOCUS Cells.** FOCUS cells were first resuspended in solution, and incubated with various concentrations of AF-20 scFv at 4°C. AF-20 scFv bound cells were then stained with mouse anti-FLAG IgG and followed by goat anti-mouse IgG-PE conjugate. Cell fluorescence was detected with FACS. Triplicate trials were performed. The data was fit respectively for each trial and the average dissociation constant of the AF-20 scFv against FOCUS cell at 4°C was determined to be  $3.8 \pm 0.7$ nM.

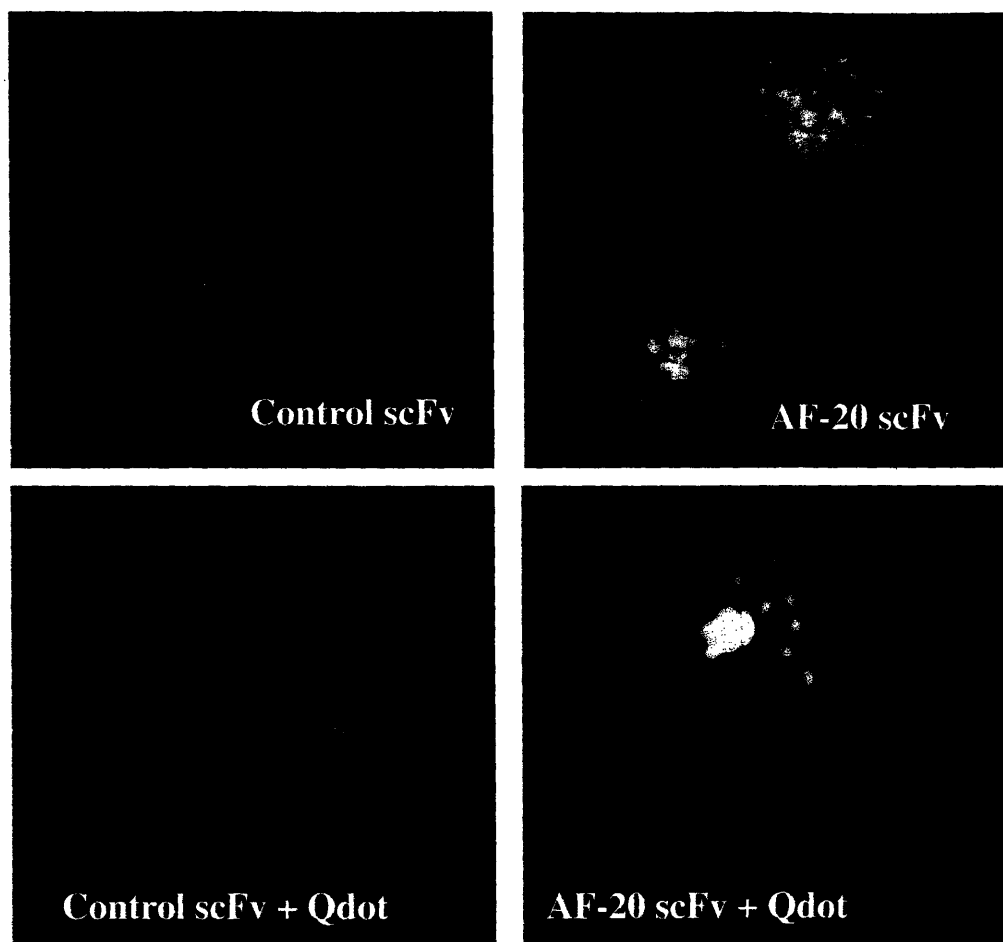


**Figure 2.6 *In-vitro* Internalization Study of AF-20 scFv into FOCUS Cells.** The abilities of the AF-20scFv to internalize by itself and to facilitate the internalization of other particles into the tumors cells were studied. FOCUS cells were used in both studies. For the self-internalization study, mouse anti FLAG IgG conjugated AF-20 scFv or control scFv were incubated with the FOCUS cells at 37°C in serum-free media for 1 hr. Cells were then fixed, permeabilized, and stained with goat anti-mouse IgG-FITC conjugate and Hoechst dye. The green fluorescence beside the nuclei in the top right panel showed that conjugated AF-20 scFv internalized readily into the FOCUS cells *in vitro*. There was no significant green fluorescence signal in the control scFv experiment (top left panel), indicating the lack of internalization of control scFv. For the facilitated internalization study, quantum dot Qdot565 was used as the model particle. The AF-20 scFv or control scFv was pre-incubated with biotinylated mouse anti-FLAG IgG and Qdot 565-streptavidin conjugate. Adhered FOCUS cells were then incubated with the pre-incubated materials and Hoechst dye at 37°C in serum-free media for 1 hr. The absence of red fluorescence in the control scFv experiment (bottom left panel) indicated that there was no facilitated internalization of quantum dot into the FOCUS cells by control scFv. Whereas the red fluorescence in the bottom right panel showed that AF-20 scFv was able to facilitate the internalization of nano-scale particles, quantum dots, into FOCUS cells. The blue fluorescence was from the Hoechst staining of the nuclei.

the nuclei of the cells, suggesting that the bivalent AF-20 scFv internalized readily into the FOCUS cells, just as AF-20 IgG did. However, when AF-20 scFv was presented monovalently to the FOCUS cells, the extent of internalization was significantly reduced, signifying the importance of bivalency in the rapid internalization of the antibody.

### **2.3.5 Facilitated Internalization of Nano-scale Particles**

The ability of the AF-20 scFv to internalize into the tumor cells could be employed to deliver virus or liposome particles carrying suicide gene into tumor cells for gene therapy (Haisma, et al., 2000; Kashentseva, et al., 2002; Mohr, et al., 2000; Nettelbeck, et al., 2004; Yoon, et al., 2000). Virus or liposome particles in this case are considerably larger than the AF-20 scFv protein. The ability of the AF-20 scFv to facilitate internalization of much larger particles into tumor cells was examined. Quantum dots conjugated to streptavidin (Qdot 565) were used as model particles in this study. This particle is about 30nm in diameter and comparable in size to a viral particle. AF-20 scFv or control scFv (anti-fluorescein) was pre-incubated with biotinylated mouse anti-FLAG IgG and Qdot 565-streptavidin conjugate. The pre-incubated materials were then incubated with FOCUS cells at 37°C in serum free media for 3 hr. Cells were also co-incubated with the Hoechst dye. Internalized quantum dots, which emit red fluorescence upon excitation at 565nm, were detected by confocal microscopy. The control scFv did not facilitate the internalization of quantum dots (bottom left panel of Figure 2.6), as there was negligible red fluorescence inside the cells. However in the AF20 treated samples there was considerable red fluorescence inside the cells (bottom right panel Figure 2.6). These results indicate that the AF-20 scFv is able to facilitate internalization of a nano-scale particle.

### 2.3.6 *In-vitro* Cytotoxicity of AF-20 Gelonin Fusion Construct

The capability of AF-20 scFv to serve as the targeting domain in an immunotoxin construct was studied. The toxin used in this study was recombinant gelonin, a highly cytotoxic ribosome-inactivating protein (Falasca, et al., 1982). It was previously shown that fusing a targeting scFv or a growth factor to gelonin greatly improved the cell-killing efficacy of gelonin both *in vivo* and *in vitro* (Rosenblum, et al., 2003). Therefore, AF-20 scFv-gelonin fusion were constructed as previously reported to determine if the addition of AF-20 scFv to gelonin would similarly improve the efficacy of gelonin (Rosenblum, et al., 2003). The AF-20 scFv/rGel purified protein was confirmed to have the same binding affinity as AF-20 scFv at 4°C, indicating that the AF-20 scFv domain was properly folded and fully functional (data not shown). The *in vitro* cytotoxic effects of the AF-20 scFv/rGel fusion toxin and free rGel were assessed and compared on three different tumor cell line. The tumor cells lines employed in this study were FOCUS cells, L3.6pl cells and PC3 cells, which are liver, pancreatic and prostate cancer cell lines respectively. Log-phase cells (5000 to 10000 cells per well) were seeded in 96-well plates overnight, and then exposed to various concentrations of AF-20 scFv/rGel fusion and free rGel respectively. After the treatment, cell viabilities of the treated cells and the untreated positive control cells were determined either using Alamar Blue stain or crystal violet stain. Figure 2.7 showed that in the case of FOCUS cells, the IC<sub>50</sub> value for AF-20 scFv/rGel was approximately 100 to 200nM; whereas the IC<sub>50</sub> value for free rGel was about 2μM, one log higher than the IC<sub>50</sub> of AF-20 scFv-gelonin fusion. As for the L3.6pl cells, the IC<sub>50</sub> value for AF-20 scFv-gelonin was approximately 35nM; meanwhile the IC<sub>50</sub> value for the free gelonin was about 1μM. For the PC3 cells, the IC<sub>50</sub> value for AF-



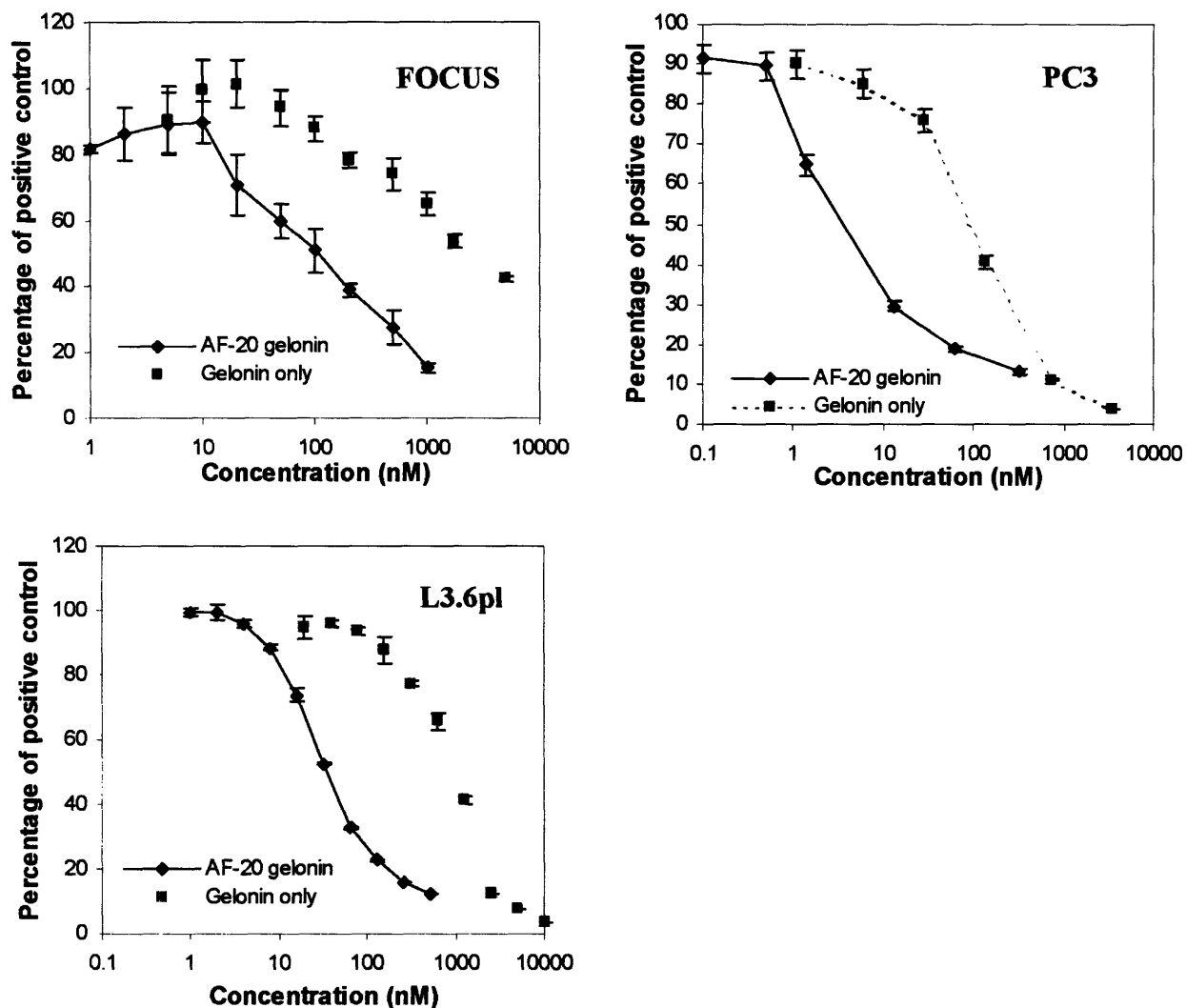


**Figure 2.7 Comparative *In-vitro* Cytotoxicity of the Free Gelonin and AF-20 scFv/rGel Fusion Construct on FOCUS, L3.6pl and PC3 Cells.** Different tumor cell lines (FOCUS, L3.6pl and PC3) were plated and treated with various concentrations of free rGel or AF-20 scFv/rGel fusion construct respectively. Cell viabilities were detected using Alamar blue stain (FOCUS) or using crystal violet dye (L3.6pl and PC3). For the FOCUS cells, the  $IC_{50}$  values for AF-20 scFv/rGel and free rGel were about 100nM and 2 $\mu$ M respectively. For the L3.6pl cells, the  $IC_{50}$  values for AF-20 scFv/rGel and free rGel were about 35nM and 1 $\mu$ M respectively. As for the PC3 cells, the  $IC_{50}$  values for AF-20 scFv/rGel and free rGel were about 3.5nM and 100nM respectively. The  $IC_{50}$  value for AF-20 scFv/rGel was consistently shown to be one to two logs lower than the  $IC_{50}$  value for free rGel on three different cell lines.

20 scFv-gelolin was approximately 3.5nM, while the IC<sub>50</sub> value for free gelolin was about 100nM. The IC<sub>50</sub> value for AF-20 scFv-gelolin was consistently one to two logs lower than the IC<sub>50</sub> value for free gelolin. This illustrates that the AF-20 scFv can function as a targeting module in the construction of immunotoxins.

### **2.3.7 Display of AF-20 scFv on the Yeast Surface**

The AF-20 scFv was ligated into the display plasmid, which contained both the HA and the c-myc tags, and subsequently, the plasmid was transformed into yeast. The transformed yeast cells were then induced to display the AF-20 scFv on the cell surface. The expression of the AF-20 scFv was detected by first labeling the induced yeast cells with mouse antibody 9e10, followed by staining the yeast cells with goat anti-mouse IgG-phycoerythrin (PE) conjugate. Figure 2.8 showed the histograms of the PE fluorescence level for both induced and non-induced yeast populations. The non-induced yeast population, which did not display any AF-20 scFv, has negligible level of PE signal; whereas the yeast population displaying the AF-20 scFv showed a high level of PE intensity. The high level of PE signal implied the expression of AF-20 scFv on the yeast surface. It is common for induced yeast cultures to contain a negative population due to loss of the display plasmids during growth and induction. However, in general, this negative population is only a minor portion of the total population and does not interfere with the detection and screening processes. The expression of AF-20 scFv on the yeast surface also suggests that the scFv is well folded on the yeast surface.

### **2.3.8 Binding of AF-20 Displaying Yeasts against FOCUS Cells**

After confirming the AF-20 scFv is well expressed on yeast surfaces, binding of these AF-20 scFv-displaying yeast cells to the FOCUS cells were evaluated. As soluble

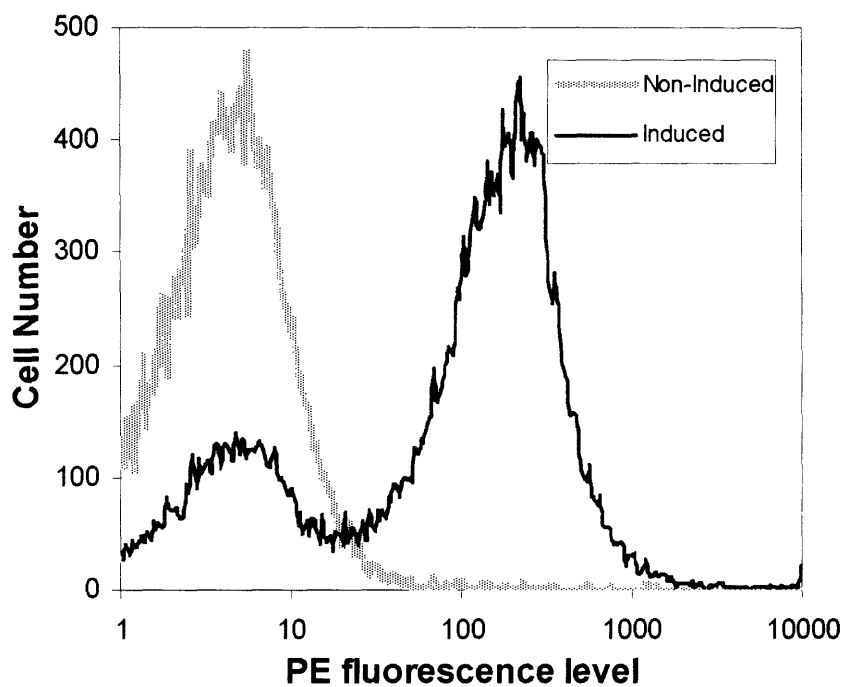


**Figure 2.8 FACS Histogram of the AF-20 scFv Expression on Yeast Surface.** The c-myc tag of the non-induced and induced yeast populations was labeled and stained with PE-conjugated antibody. The high level of PE signal for the induced yeasts indicated that the AF-20 scFv was expressed and folded properly on the surface of yeast. Meanwhile, the non-induced (control) yeast population, which did not display the AF-20 scFv, had negligible level of PE signal.

AF-20 antigen is not available yet, the formation of the yeast-FOCUS cell complex was used to determine the binding of AF-20 scFv to its antigen. FOCUS cells were grown as a monolayer on a coverslip. A non-displaying yeast population and yeast populations displaying either AF-20 scFv or a control scFv were allowed to roll and bind to the monolayer of FOCUS cells respectively at room temperature. Several washes were performed to remove the yeast cells that non-specifically stick to the FOCUS cells. Then the yeast-FOCUS cells complex were fixed and imaged using a light microscope. Figure 2.9 showed the images of the yeast-FOCUS cells complexes with both the AF-20 scFv-displaying yeast population and non-displaying yeast population. The top right panel of Figure 2.9 showed that there are high levels of yeast-FOCUS cell complex formation with the AF-20 scFv-displaying yeast population, whereas a minimal amount of complexes was detected in the case of the non-displaying yeast population. Similarly, minimal amount of complexes were formed with cells that displaying the control scFv (data not shown). Quantitative measurements of the number of yeast cells on the FOCUS cell surface at multiple areas of the coverslip showed that yeast-FOCUS cells complex formation was significantly higher for the AF-20 scFv displaying yeast population than for the non-displaying yeast population or the yeast population displaying the control scFv. This indicated that the AF-20 scFv displaying on the yeast surface was functional and responsible for the binding of the yeast cells to the FOCUS cells.

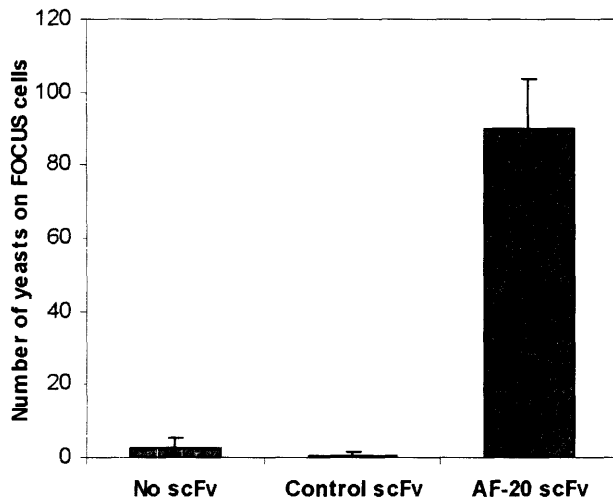
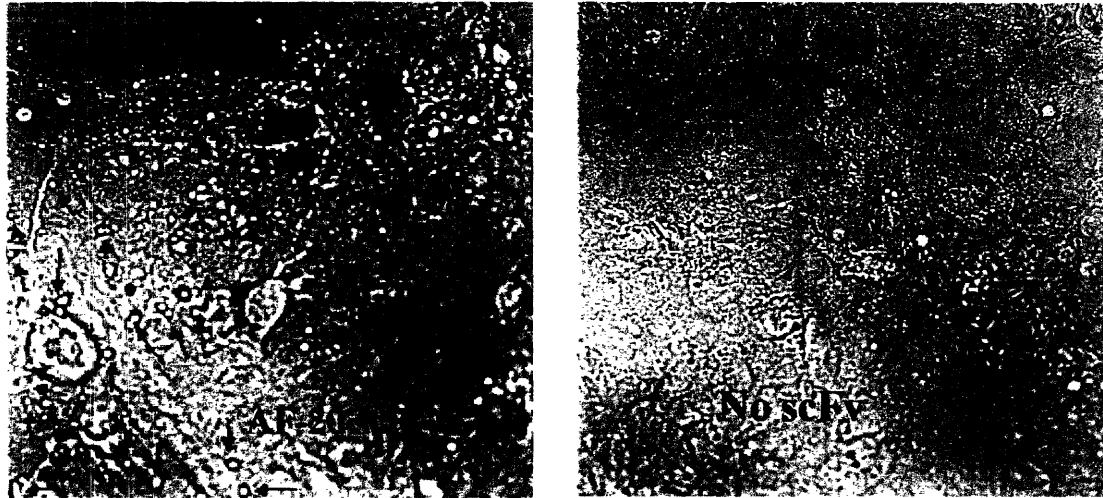


**Figure 2.9 Formations of Yeast-FOCUS Cells Complexes.** Yeast cells that did not display any scFv and yeast cells displaying either control scFv or AF-20 scFv were allowed to bind respectively to a monolayer of FOCUS cells. After several washes, amount of yeast cells that were retained on the FOCUS cells were imaged and counted. The top left image showed that high numbers of AF-20 scFv displaying yeast cells were retained on the FOCUS cells surface, whereas as shown in the top right figure, negligible amount of the non-displaying yeast cells were captured on the FOCUS cells surface. Three images were taken at different regions of coverslip for each case. The number of retained yeast cells on each image was counted. Quantitative measurements showed that AF-20 scFv displaying yeast cells is retained at a significantly higher level than those of non-displaying yeast cells and control scFv displaying yeast cells on the surfaces of FOCUS cells.

## 2.4 Discussion

In this study, we cloned the variable region genes of the AF-20 IgG and used the genes to construct a scFv. The AF-20 scFv was shown to retain the same binding and internalization ability as the IgG format, and also shown to facilitate the internalization of virus-scale particles into tumor cells. In addition, the AF-20 scFv was demonstrated to be an effective targeting domain for the construction of immunotoxin. This AF-20 scFv is a candidate for targeting toxins, enzymes, radionuclides, liposomes or virus for targeted therapy.

One of the tumors AF-20 IgG has been shown to target is HCC, for which common cancer therapies are ineffective. Immunotherapy using AF-20 antibody would present an alternative option for the treatment of HCC. Targeting internalization epitopes has been previously shown to improve the targeted delivery of liposome into lymphoma cells over targeting non-internalization epitope (Sapra and Allen, 2002). Prior experiments using AF-20 IgG as the targeting molecule have been performed and shown to be successful. Different AF-20 conjugated moieties like liposome and virus carrying therapeutic genes has been delivered to the liver tumor cells *in vitro*. Since, as shown in this study, the AF-20 scFv binds to the same epitope as the AF-20 IgG and internalized similarly as AF-20 IgG, it is expected that the AF-20 scFv could substitute in the previous applications involving AF-20 IgG, specifically targeting viral or other particles to the liver tumor cells. This is further confirmed by our result that AF-20 scFv was able to facilitate internalization of nano-scale particle into the tumor cells. Thus, this AF-20 scFv has the potential to deliver to the cytoplasm of target cells various cytotoxic payloads.

We found that the monovalent format of AF-20 scFv did not internalize as readily as the bivalent format of AF-20 scFv *in vitro*. The identity of the AF-20 antigen is as yet unknown. Perhaps dimerization of the receptor by the bivalent format of antibody is required for rapid internalization of the complexes. One example of this type of bivalent-activated internalization is an antibody, MGR2, targeting the extracellular domain of p185HER2, a transmembrane glycoprotein coded by the HER2/neu oncogene (Srinivas, et al., 1993). Srinivas and co-workers showed that MGR2 IgG induced internalization in two cell lines overexpressing the p185HER2 receptor; whereas the MGR2 Fab targeting the same epitope was not internalized. However, when MGR2 Fab fragment was conjugated using a rabbit anti-mouse IgG to give a bivalent format, internalization was observed. This is similar to our previous observations in the case of AF-20 scFv, illustrating that bivalency is important for the rapid internalization of the antibody.

Immunotoxins have been used in both laboratory and clinical settings to kill cancer cells. Different protein toxins including *Pseudomonas* exotoxin, *Diphtheria* toxin, gelonin, ricin A chain, as well as small molecule toxins such as maytansinoids and calicheamycins have been either chemically conjugated or genetically fused to different antibodies to construct immunotoxins and immunochemotherapeutics (Bera, et al., 1999; Hexham, et al., 2001; Ma, et al., 2001; Rosenblum, et al., 2003; Safavy, et al., 2003; Thompson, et al., 2001). In this work, we have constructed an immunotoxin consisting of AF-20 scFv and rGel, and demonstrated the improved efficacy of AF-20 scFv immunotoxin over free rGel on three different tumor cell lines. The IC<sub>50</sub> of the AF-20 immunotoxin was about 3.5nM and 35nM for L3.6pl and PC3 cells respectively. Previously, a similar scFv-gelonin immunotoxin was constructed to treat melanoma cells,

and the  $IC_{50}$  for that particular immunotoxin is about 8nM *in vitro* (Rosenblum, et al., 2003). Meanwhile, the  $IC_{50}$  of AF-20 gelonin for FOCUS cells is on the order of 100nM, which is significantly higher than the  $IC_{50}$  of other cell lines. One potential reason could be the differences in gelonin responses among the cell lines used. There were previous reports showing that tumor cells could develop resistance to gelonin (McGrath, et al., 2003; Rosenblum, et al., 1996). One distinct feature of these gelonin-resistance cells is that these cells specifically shuttle the internalized toxin into the lysosome (McGrath, et al., 2003). To this end, we investigated whether disrupting the lysosome would improve the efficacy of the immunotoxin on FOCUS cells. We incubated the FOCUS cells simultaneously with the toxins and 100 $\mu$ M chloroquine, a lysosomotropic agent, for four hours, and the cell viabilities of the treated cells and untreated positive control cells were recorded. The  $IC_{50}$  of the AF-20 scFv-gelonin was enhanced to about 0.4nM, while the  $IC_{50}$  of the gelonin was also lowered to about 40nM (bottom panel of Figure 2.10). Under the influence of chloroquine, the extent of improvement for free gelonin was 10 fold less than the extent of improvement for AF-20 scFv-gelonin. Meanwhile, there was no observable change in the viability of the chloroquine-exposed control cells, compared to the non-exposed control cells (top panel of Figure 2.10).

Microscopic studies also confirmed that the internalized bivalent AF-20 scFv co-localized with the lysosome, indicating that AF-20 scFv was transported into lysosome (Figure 2.11). The efficacy improvement by disrupting lysosome has also been observed with an immunotoxin directed against murine B cells. May et al. showed that in the presence of chloroquine, the less potent immunotoxin became 100 fold more potent, concluding that intracellular routing is important in determining the efficacy of the



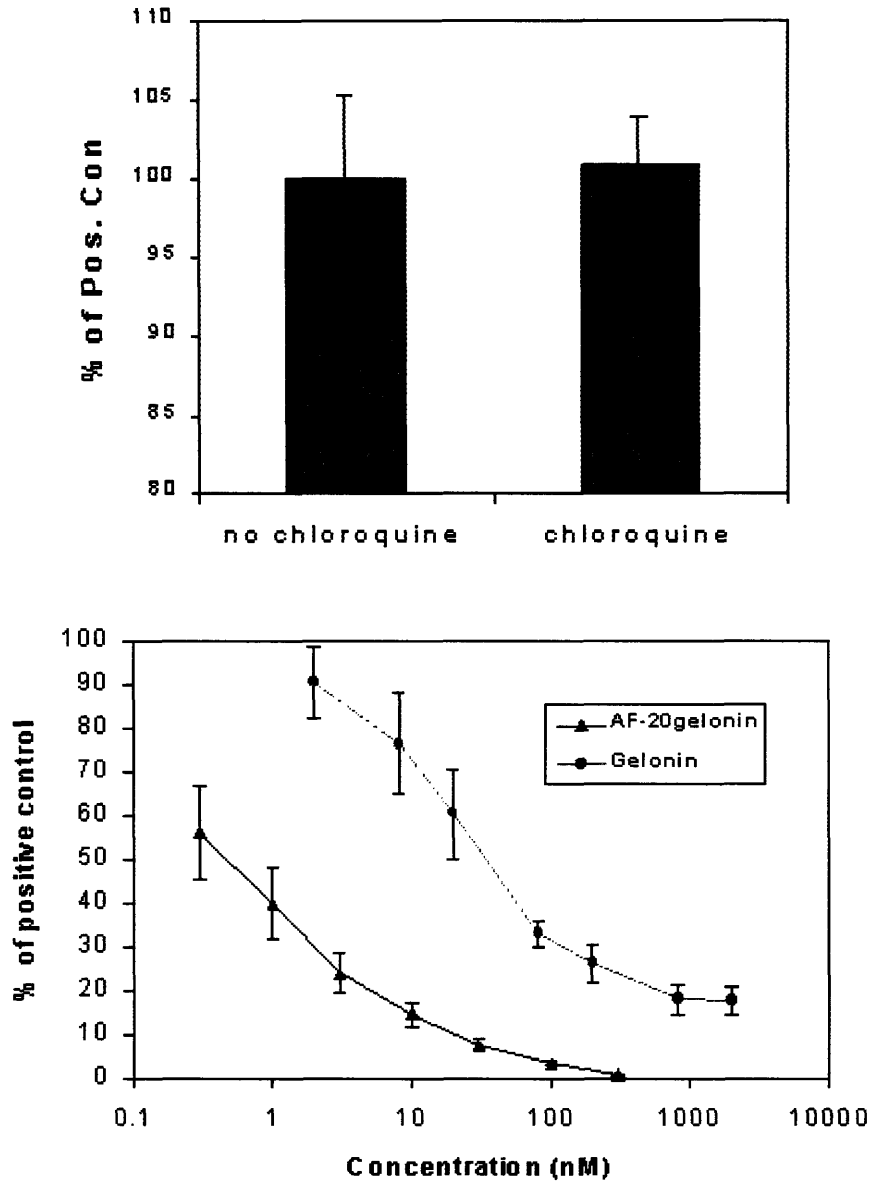


**Figure 2.10 *In-vitro* Cytotoxicity of AF-20/rGel under the Influence of Chloroquine.** FOCUS cells were simultaneously incubated with the AF-20-gelonin toxin and chloroquine, and cell viabilities of the treated cells and untreated positive control cells were recorded. The top panel shows that there is no observable change in the viability of the chloroquine-exposed control cells, compared to the non-exposed control cells, thus the chloroquine treatment under the experimental conditions were not toxic to the cells. The bottom panel shows that the  $IC_{50}$  of the AF-20 scFv-gelonin is enhanced to about 0.4nM, while the  $IC_{50}$  of the gelonin is also lowered to about 40nM. Under the influence of chloroquine, the extent of improvement for free gelonin (2 $\mu$ M to 40nM) was about 10 fold less than the extent of improvement for AF-20 scFv-gelonin (200nM to 0.4nM), indicating that the efficacy of AF-20/rGel can be improved if lysosomal trafficking is avoided.

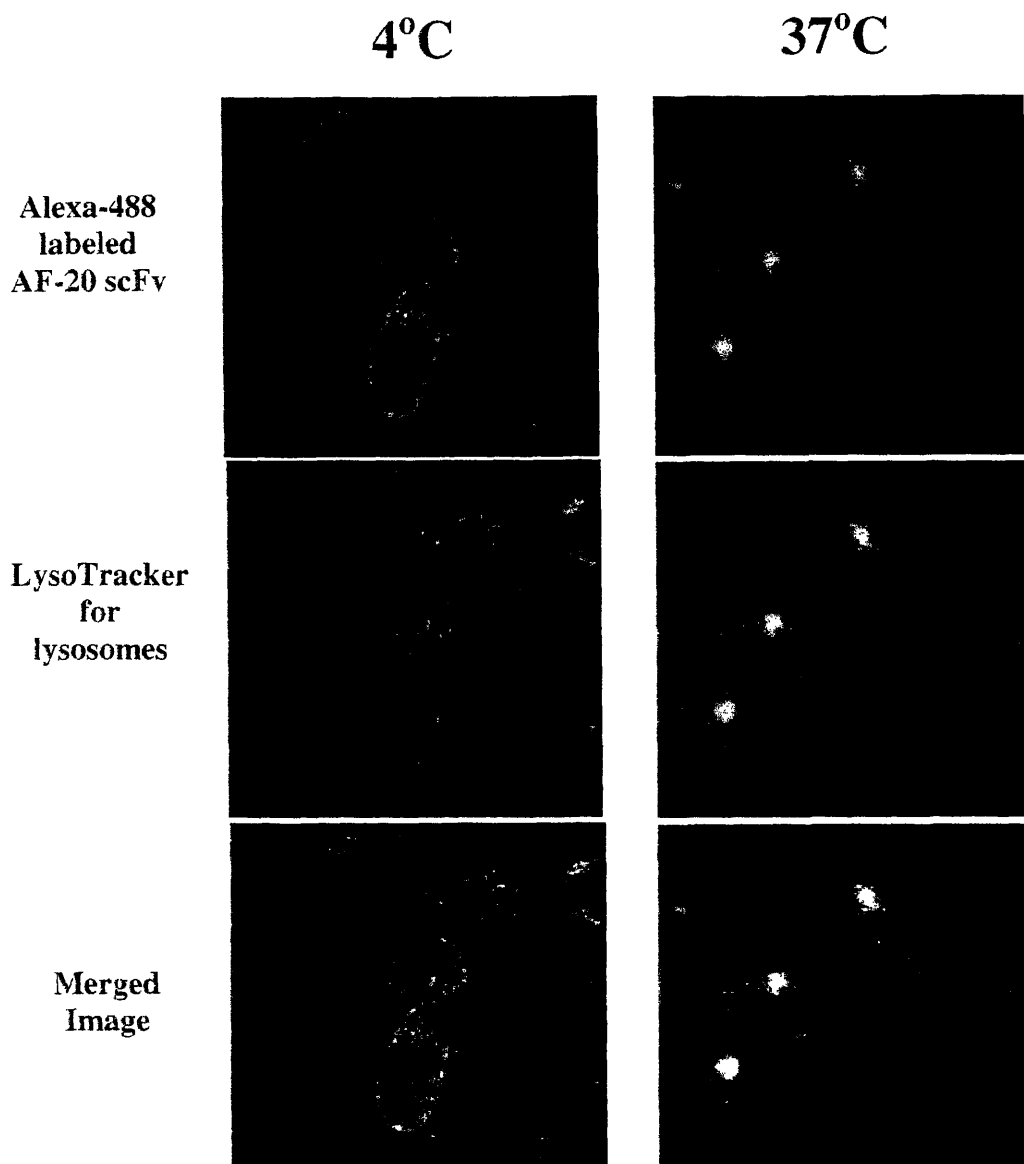


**Figure 2.11 Co-localization of AF-20 scFv and Lysosome.** Alexa-488 labeled AF-20 scFv was conjugated using mouse anti-FLAG IgG. The conjugated antibodies along with the red LysoTracker dye (Molecular Probe) were incubated with the FOCUS cells at 4°C or 37°C in serum-free media. Images were taken with a deconvolution microscope. At 4°C, the scFv (green) primarily resides on the outside of the cells, and does not co-localize with the lysosome (red dots inside the cells). However, at 37°C, the AF-20 scFv is internalized and co-localized with the lysosome (yellow), indicating that the AF-20 scFv is shuttled into the lysosome.

immunotoxin (May, et al., 1991). Their results were similar to the results of the AF-20 scFv-gelonin on FOCUS cells. However, in a clinical setting, it is difficult to pre-treat the tumors with any lysosomotropic agent. A potential remedy may be to incorporate into the immunotoxin a peptide or polymer that is capable of inducing endosomal escape. These endosomal escape entities will enable more efficient delivery of the toxin into the cytosol, potentially improving the efficacy of the immunotoxin on HCC and other gelonin-resistant tumor cells (Akinc and Langer, 2002; Panyam, et al., 2002; Van Rossenberg, et al., 2002; Wadia, et al., 2004).

Another potential way to improve the efficacy of the AF-20 immunotoxin would be to increase the avidity of the AF-20 targeting module, hence the affinity of AF-20 immunotoxin toward tumor cells (Thompson, et al., 2001). In addition, our internalization study showed that the divalent AF-20scFv internalized much faster than monovalent AF-20 scFv. We would expect higher amount of immunotoxin delivered to the cells by using the divalent immunotoxin, thereby exhibiting higher efficacy. Surprisingly, this was not the case. Instead of presenting the immunotoxin to the tumor cells in a monovalent format, AF-20 immunotoxin, which contained an FLAG tag, was artificially conjugated using a mouse anti-FLAG IgG to form a bivalent immunotoxin. However, our study showed that the conjugated immunotoxin did not demonstrate any significant efficacy improvement over the monovalent fusion toxin as assessed on two different cell lines (data not shown). One reason for the lack of efficacy improvement could be due to high antigen density. Bera and co-workers showed that the bivalent e23 dsFv immunotoxin, targeting erbB3, was 9–29-fold more cytotoxic than the corresponding monovalent dsFv immunotoxin on cells expressing relatively low amounts of erbB2 (A431, MCF7, HepG2,

and LNCP) (Bera, et al., 1998). However, improved cytotoxicity of the bivalent immunotoxin was not evident on cells overexpressing erbB2 antigen, such as SK-BR-3 and N87 cells, although the bivalent immunotoxin did bind to both A431 and N87 cells with higher affinity than the monovalent immunotoxin (Bera, et al., 1998). Therefore, antigen density could be one of the factors affecting the difference between monovalent and divalent immunotoxins. Another possible factor is the trafficking properties of the monovalent and divalent immunotoxin, which were described in the previous paragraph. Other studies have also shown that trafficking properties played an important role on determining the efficacy of the immunotoxin (Yazdi, et al., 1995). Further study is needed to determine the trafficking properties of the monovalent and bivalent immunotoxin.

The AF-20 V gene can be fused to various moieties to develop alternative applications. One potential application is in tumor imaging. Different antibody fragments like scFv, diabody, and minibody can be constructed for targeting tumors and have been shown to perform better than its IgG counterpart (Adams, et al., 1993; Bera, et al., 1998; Hu, et al., 1996; Kikuchi, et al., 2004; Wu and Yazaki, 2000). Specifically, due to its small size (around 30kDa), scFv has been shown to penetrate tumors rapidly and have rapid clearance from serum and normal tissue, leading to excellent tumors to normal organs ratios (Kuan, et al., 1999). However, the rapid clearance also renders the absolute quantity of scFv retained on the tumor to be low. Diabody or minibody, that is significantly larger than scFv, has higher tumor uptake by avoiding the rapid first-pass clearance from the circulation. Compensating poor penetration with slower clearance and potential avidity effect, diabody has also been shown to be as successful a molecule, if

not better, as scFv targeting cells *in vivo* (Adams, et al., 1993; Adams and Schier, 1999; Adams, et al., 1998; Nielsen, et al., 2000; Viti, et al., 1999). In the future, different AF-20 fragment like AF-20 diabody or AF-20 minibody could be constructed for tumor imaging.

Overall, this study showed that AF-20 scFv is an effective module to target a variety of AF-20 antigen-expressing tumor cells. Potentially, AF-20 scFv could be humanized in the future if immunogenicity is a concern for long-term therapeutic applications (Kettleborough, et al., 1991; Roguska, et al., 1994). With the V gene of the AF-20 antibody, other tumor targeting or killing modules could be easily constructed.

# Chapter 3: Isolation and Engineering of Human Antibodies against Human Aspartyl (Asparaginy) $\beta$ -Hydroxylase

## 3.1 Introduction

Over-expression of the enzyme human aspartyl (asparaginy)  $\beta$ -hydroxylase (HAAH) has been detected in a variety of cancers including lung, liver, colon, pancreas, prostate, ovary, bile duct and breast (Lavaissiere, et al., 1996; Palumbo, et al., 2002; Sepe, et al., 2002). It is proposed that upon cellular transformation, HAAH is overexpressed and translocated to the cell surface (Lavaissiere, et al., 1996). HAAH belongs to the  $\alpha$ -keto-glutarate-dependent dioxygenase family of prolyl and lysyl hydroxylase (Gronke, et al., 1989; Hanauske-Abel and Popowicz, 2003). In normal cells, HAAH primarily resides in the endoplasmic reticulum and is involved in post-translational modification of specific proteins via hydroxylation of specific aspartate or asparagine residues in EGF-like domains (Gronke, et al., 1989; Przysiecki, et al., 1987). Consensus hydroxylation sequence contains the amino acids Asp, Asp/Asn, Asp/Asn, and Tyr/Phe at defined positions, and hydroxylation occurs at the third Asn/Asp in the consensus sequence. Examples of proteins that contain this consensus sequence are clotting factor (Gronke, et al., 1989), Notch receptor and ligands (Rebay, et al., 1991), and extracellular matrix proteins (Downing, et al., 1996). The HAAH protein can be divided into four distinct domains: a cytoplasmic amino terminal domain, a transmembrane domain, a highly negative charged domain that projects into the lumen of the endoplasmic reticulum, and a catalytic carboxyl terminal domain which is responsible for the enzymatic activity of HAAH (Jia, et al., 1994; McGinnis, et al., 1996). Another

protein, Humbug (Junctate), is also produced from the same HAAH locus through alternative splicing of the mRNA transcript (Dinchuk, et al., 2002). Humbug is a truncated form HAAH, lacking only the HAAH catalytic domain. Humbug, which cannot hydroxylase protein, is proposed to be involved in cellular calcium homeostasis (Treves, et al., 2000).

The detailed biological role of HAAH in tumor formation *in vivo* is still under investigation. Previous *in vitro* and *in vivo* studies have been performed to shed light on the biology of HAAH in malignant transformation. Ince and co-workers showed that *in vitro* overexpression of enzymatically active HAAH in NIH-3T3 cells was able to induce malignant transformation in cell culture, increase cellular motility and invasiveness, and establish tumor formation *in vivo* (Ince, et al., 2000). In addition, increased HAAH expression also led to enhanced cell motility and proliferation in neuroblastoma cell lines *in vitro* (Sepe, et al., 2002). It was also shown that the expression level of HAAH correlated with the migratory potential of the cells. High HAAH expression was observed in proliferating term placental trophoblasts (Lavaissiere, et al., 1996) and in the tumor infiltrating margins that interfaced with uninvolved tissue (Maeda, et al., 2004). HAAH expression was also demonstrated to correlate with tumor size, vascular invasion and poor prognosis (Maeda, et al., 2004). Therefore, HAAH was proposed to play a direct, activating role in malignant transformation and tumor aggressiveness (Ince, et al., 2000). A striking observation is that a variety of tumor cells express this particular protein on their surface. This enzyme is highly specific for cancer and has been detected by immunohistochemistry in more than 99% of 1000 tumor specimens (*unpublished data*), and has minimal expression on the surfaces of normal tissues (Lavaissiere, et al., 1996).

Due to the highly specific nature of HAAH expression on tumor cell surfaces, it is an attractive target for cancer immunotherapy.

Previously, several mouse monoclonal antibodies targeting HAAH have been isolated (Dinchuk, et al., 2002; Wilson, et al., 1988), however murine antibodies are undesirable for therapeutic use in human due to immunogenicity. Therefore, human antibodies targeting HAAH are desired for anti-HAAH immunotherapy. In this work, fully human single-chain Fv fragments (scFv) against HAAH were isolated using a human non-immune antibody fragment library displayed on yeast surface. Five of these isolated scFv were reformatted into human IgG. Two of the IgGs, 6-22 and 6-23, were shown to have significant binding to tumor cell lines. In addition, 6-22 IgG, targeting the catalytic domain of HAAH, was also shown to internalize into tumor cells and facilitate the internalization of toxin into the tumor cells. Furthermore, 6-22 scFv was affinity matured to become a sub-nanomolar HAAH binder using different mutagenesis methods. Overall, these human anti-HAAH antibodies can potentially be useful for immunotherapy targeting HAAH-expressing tumor cells.

## **3.2 Materials and Methods**

### **3.2.1 Cell Lines and Materials**

The non-immune human scFv library used to isolate anti-HAAH binders has been previously described (Feldhaus, et al., 2003). Cell lines COS-7L and H460 were purchased from Invitrogen (Carlsbad, CA) and American Type Culture Collection (ATCC) respectively. Liver tumor cell line, FOCUS, was previously isolated (He, et al., 1984). Magnetic colloid used for library screening was acquired from Miltenyi Biotec (Auburn, CA). Mouse antibodies FB-50 and 15c7 were purified from previously isolated



hybridoma cells (Wilson, et al., 1988). Mouse anti-c-myc antibody 9e10 was obtained from Covance (Princeton, NJ). Fluorophores streptavidin-phycoerythrin, goat anti-mouse IgG-Alexa 488 and goat anti-mouse IgG-phycoerythrin, and also rabbit anti-Alexa 488 IgG were purchased from Molecular Probe (Eugene, OR). Meanwhile, goat anti-human IgG-phycoerythrin conjugate was obtained from Rockland (Gibbertsville, PA). The IgG1 plasmid was a kind gift from Pacific Northwest National Laboratory. Goat anti-human IgG-peroxidase conjugate and non-relevant control human IgG were acquired from Sigma-Aldrich (St. Louis, MO). ImmunoPure immobilized Protein A plus resin, binding buffer, elution buffer and Supersignal® ELISA maximum sensitivity substrate were obtained from Pierce (Rockford, IL). Immunotoxin, goat-anti-human IgG-saporin conjugate, was purchased from Advanced Targeting System (San Diego, CA).

### **3.2.2 Isolation of Anti-HAAH Leads**

Six rounds of screening were performed to isolate  $\alpha$ -HAAH binders from  $3 \times 10^9$  human scFv-displaying yeasts. First two rounds of screening were carried out with magnetic colloids (Miltenyi) according to the manufacturing protocol. Briefly, cells were incubated with 300nM of biotinylated recombinant full-length HAAH protein at room temperature for 2hr, and then washed, chilled on ice and incubated with magnetic colloid at 4°C for 20min. After the incubation, cells were washed and binders (positive fraction) were isolated using Auto-MACS (Miltenyi). Collected yeast cells were then expanded in SD-CAA media and subsequently induced in SG-CAA media for another round of screening (Boder and Wittrup, 1997). After two rounds of magnetic screening, four rounds of fluorescence-activated cell sorting (FACS) were performed. Yeasts cells were co-incubated with 300nM of biotinylated HAAH and 1:100 of 9e10 antibody at 37°C in

PBS containing 1% bovine serum albumin (PBS/BSA). Cells were then washed with cold PBS/BSA, and co-labeled with 1:100 of streptavidin-phycoerythrin and 1:100 goat anti-mouse IgG-Alexa 488 in PBS/BSA at 4°C for 20min. Cells that have the highest 1% binding-to-display signal ratio were collected using FACS. These cells were then grown in SD-CAA and later induced for another round of screening. Three rounds of screening at 300nM of biotinylated HAAH and one final round of screening at 100nM of biotinylated HAAH were performed to isolate binders. In between rounds of screening against biotinylated HAAH antigen, cells were also labeled with just fluorophores streptavidin-phycoerythrin and goat anti-mouse IgG-Alexa 488 to eliminate fluorophores-binding clones using FACS. To confirm the binding against HAAH instead of biotinylation epitope, individual sorted clones was incubated with 300nM of unmodified full-length HAAH at 37°C, and then washed and labeled with either 200nM of FB-50 or 15c7 on ice for 20min. The binding was detected with goat anti-mouse IgG-phycoerythrin conjugate and then analyzed by flow cytometry.

### **3.2.3 Conversion of scFv to IgG**

The IgG1 plasmid contains the constant domains of the human heavy and light chains. The variable regions of the isolated  $\alpha$ -HAAH scFv were PCR out using primers targeting the light chain and heavy chain of the scFv. For example, for 6-22 IgG, heavy chain primers 5'-gatcgagcaacgcgtgtcttgtcccaggtacagctgcagcagtcagg-3' and 5'-gatcgagcagctagctgaggagacggtgaccagggtcc-3', and light chain primers 5'-tcacggtgcacgatgtgagcc tgtgtgactcagtcaccc-3' and 5'-tcacgcaccgtacgtaggacggtcagcttgggtcccag-3' were used. PCR reaction was carried out with *Vent* polymerase for 20 cycles according to the manufacturing protocol. The PCR products were then gel-purified. Heavy chain products

were restriction digested with *MluI* and *NheI*, and light chain products were digested with *BsiWI* and *DraIII*. The IgG backbone was also digested with the same four enzymes, and then the digested heavy and light chain PCR products were ligated sequentially into the digested backbone. The ligated plasmid was then transformed into *E.coli* for amplification.

Sixty microgram of plasmid per T-175 flask were used to transfect fully confluent COS-7L cells using lipofectamine 2000 (Invitrogen) according to the manufacturing protocol. Transiently transfected cells were cultured in Opti-MEM (Invitrogen) for up to 2 weeks and media containing the secreted IgG was replaced every two days. The media was then concentrated, buffer-exchanged with ImmunoPure IgG binding buffer and purified using the Protein A resin according to the manufacturing protocol. Purified IgG was then dialyzed in PBS and resolved in a denaturing, reduced 12% Tris-Glycine gel. The gel was stained with SilverXpress® silver staining kit (Invitrogen) according to the manufacturing protocol.

### **3.2.4 ELISA**

Either 0.3µg of recombinant full-length HAAH, 0.3µg of BSA or 0.4µg of catalytic domain of HAAH was coated on the well of a 96-well plate overnight at 4°C. The coated wells were then blocked with PBS/3% BSA/0.05% Tween20 for 2hr at 4°C, washed and incubated with various antibodies in PBS at room temperature for 2hr. The plates were washed with cold PBS/0.1% Tween20 and then incubated with 1:1000 of goat anti-human peroxidase conjugate in PBS at 4°C for 30min. The binding was detected with Supersignal® ELISA maximum sensitivity substrate and a luminescence plate reader.

### **3.2.5 Binding of the IgGs to Tumor Cells**

FOCUS cells were cultured as previously described (He, et al., 1984). H460 cells were cultured in RPMI with 10% fetal bovine serum (FBS), 2mM glutamine, 100U/ml of penicillin and 100µg/ml of streptomycin under 5% CO<sub>2</sub> at 37°C. Cells were dissociated from the culture plates using cell dissociation solution (Sigma). Cells were then washed with PBS/BSA supplemented with 2% FBS (PBS/BSA/FBS). 1x10<sup>5</sup> to 2x10<sup>5</sup> cells were incubated with various concentrations of antibodies in PBS/BSA/FBS at 4°C for 3 to 5hr. After the incubation, cells were washed, stained with 1:100 of goat anti-human IgG-phycoerythrin conjugate at 4°C for 30min, and finally resuspended in 1µg/ml of propidium iodide solution, used in this case as a marker of non-viable cells. Cell fluorescence was analyzed using a flow cytometer.

### **3.2.6 Immunohistochemistry**

Paraffin-embedded specimens of primary pancreatic ductal adenocarcinoma and adjacent chronic pancreatitis tissues were studied. The sections (5-µm thick) were deparaffinized in xylenes and rehydrated in alcohol solutions. Endogenous peroxidase activity of the tissues was quenched with 0.6% hydrogen peroxide in 60% methanol. Then the tissues were equilibrated in Tris-buffered saline (TBS, pH7.2), blocked with horse serum at room temperature, washed, and incubated overnight with 10nM of 6-22 IgG at 4°C in a humidified chamber. The sections were then immunostained with 1:1000 of goat anti-human IgG-peroxidase conjugate at room temperature for 30min and developed with peroxidase stain DAB from the Vector lab (Burlingame, CA).

### **3.2.7 Internalization Studies of 6-22 IgG**

6-22 IgG was labeled with Alexa-488 molecule using the Alexa Fluor® 488 protein labeling kit (Molecular Probe). FOCUS cells were grown on coverslips and 30nM of Alexa-488 labeled 6-22 IgG was incubated with the cells either at 4°C or 37°C for 4hr in media. Cells were also stained with 1:1000 of Hoechst dye (Molecular probe). Cells were then washed and imaged using a deconvolution microscope.

For the study of internalization kinetics, FOCUS cells were cultured in 96-well plates, and 60nM of Alexa-488 labeled 6-22 IgG or control Alexa-488 conjugated antibody was incubated with the cells for various times at 37°C in media. At each time point, cells from a single well were trypsinized at 37°C for 5min to dissociate the cells from the well and to remove any surface labeling. Separate experiment was performed to confirm that 37°C trypsinization was able to remove surface labeling of Alexa 488-6-22 IgG. Trypsinized cells were then washed, resuspended in 1µg/ml of propidium iodide solution, and fluorescence inside the cells was analyzed using a flow cytometer. For the recycling studies, FOCUS cells, cultured in 96-well plates, were pulsed with 60nM of Alexa-488 labeled 6-22 IgG for 3hr at 37°C. After the pulse, cells were washed, chilled, surface-quenched with 20µg/ml of rabbit anti-Alexa 488 IgG at 4°C for 30min, and then warmed back to 37°C under the continuous presence of quenching antibody for various times. At different times, cells were trypsinized, resuspended in 1µg/ml of propidium iodide solution, and then analyzed using a flow cytometer.

### **3.2.8 Cytotoxicity of 6-22 Immunotoxins**

The toxin used in this study was goat-anti-human IgG-saporin conjugates. FOCUS cells were cultured in 96-well plates. 10nM of 6-22 IgG or control antibody was

pre-incubated with 22nM of goat-anti-human IgG-saporin at room temperature. The complexes or 6-22 IgG alone was presented to the FOCUS cells. After 3 days of treatment, the viability of the cells was determined using alamarBlue® dye according to the manufacturing protocol (Biosource, Camarillo, CA).

### **3.2.9 Construction of Random Mutagenesis Library**

Mutagenic PCR of anti-HAAH scFv was performed using the nucleotide analogues 8-oxo-2'-deoxyguanosine-5'-triphosphate (8-oxodGTP) and 2-deoxy-P-nucleoside-5'-triphosphate (dPTP), which were both purchased from TriLink Biotechnologies (San Diego, CA) (Zaccolo and Gherardi, 1999; Zaccolo, et al., 1996). The forward primer (HA primer) was 5'-CGACGATTGAAGGTAGATACCCATACGACGTTCCAGACTACGCTCTGCAG-3' and reverse primer (c-myc primer) was 5'-CAGATCTCGAGCTATTACAAGTCTTCTTCAGAAATAAGCTTTTGTTC-3'. These primers have approximately 50 base pairs overlap with pCTCON that has been digested from *Nhe*1 to *Bam*H1. All mutagenic PCR reactions were carried out in a 100µL volume using 10-100ng of template, 1µM primers, 0.2mM of each dNTP, 6.25U *Taq* (Invitrogen, Carlsbad, CA), and 2mM MgCl<sub>2</sub>. To vary the mutation rate, both the concentration of the analogues and the number of PCR cycles was varied. Six separate PCRs were performed: 5 cycles with 200µM analogues, 10 cycles with 200µM analogues, 10 cycles with 20µM analogues, 10 cycles with 2µM analogues, 20 cycles with 20µM analogues, and 20 cycles with 2µM analogues. The cycling conditions used were 1 cycle of 94°C for 1 minute followed by either 5, 10 or 20 cycles of 94°C for 1 minute, 50°C for 1 minute, 72°C for 2 minutes, followed by 1 cycle of 72°C for 10 minutes. PCR products were gel purified using the Gel-Extraction kit from Qiagen (Valencia, CA). After purification, a

1:50 dilution of the 20 cycle purified PCR product and a 1:10 dilution of the 10 cycle PCR product were prepared and 5µl were used in a 100µl PCR reaction with the following cycling conditions: 1 cycle of 94°C for 1 minute followed by 30 cycles of 94°C for 1 minute, 50°C for 1 minute, 72°C for 2 minutes, followed by 1 cycle of 72°C for 10 minutes. For the 5-cycle PCR purified product, the PCR was performed in the same way except the purified template was not diluted. All amplifications were performed using the same concentrations of reagents as in the mutagenic PCR except the nucleotide analogies were omitted. The PCR amplified products were gel purified.

### **3.2.10 Construction of CDR Domain Shuffling Library of 6-22 scFv**

The CDR domain shuffling libraries were prepared utilizing the homologous recombination in yeast (Swers, et al., 2004b). First, fragments of non-immune human scFv library were amplified using the same set of HA and c-myc primers as the mutagenic PCR at 2.5µM. 25ng of human non-immune library DNA ( $7.2 \times 10^9$  copies) and 0.5µl of Tag polymerase (Invitrogen, CA) was used per PCR reaction. The reaction was annealed at 55°C for 1 min, extended at 72°C for 1min, and cycled for 35 times. The 900bp fragments from the PCR reaction containing the nonimmune human scFv flanked by HA and c-myc tags were then gel purified. Meanwhile, different fragments of anti-HAAH scFv 6-22 were prepared using primers targeting different heavy chain framework regions and sequence downstream of the c-myc tag. 6-22 fragment missing FW1 to CDR1 was generated using primer targeting heavy chain FW2 (5'-GGATCAGGCAGTCCCATCGAGAGGCCTTGAGTGGCTGGG-3') and primer targeting sequence downstream of c-myc (5'-ACAGTGGGAACAAAGTCGATTTTGTACATCTACAC-3'). Similarly, fragments missing FW1 to CDR2 and FW1 to CDR3 were generated by

replacing the previous FW2 primer with primers targeting FW3 (5'-CGAATAACCA TCAACCCAGACACATCCAAGAACCAGTTCTCCC-3') and FW4 (5'-GGGGCCAG GGAACCCTGGTCACCGTCTCCTCAGGGAGTGCATCC-3') respectively. 10ng of WT scFv and 2.5 $\mu$ M of primers were used in the reaction. The PCR reactions were performed using *Taq* polymerase at an annealing temperature of 54°C for 1min, and at an extension temperature of 72°C for 38sec to 65sec depending on the length of the desired fragments. The reaction was cycled for 35 times. The CDR domain shuffling libraries were then constructed by co-transforming the non-immune human scFv fragments, fragments missing the desired shuffled portion (either FW1 to CDR1, FW1 to CDR2 or FW1 to CDR3) and a *NheI*-to-*XhoI* cut pCTCON backbone into EBY100 yeast.

### **3.2.11 Construction of Heavy Chain Shuffling Library of 6-22 scFv**

Non-immune human heavy chain sequences were restriction digested out from the human scFv library plasmids using *NheI* and *BamHI*, and then gel purified. Similarly, the WT anti-HAAH scFv plasmid was digested with *NheI* and *BamHI* to remove the WT heavy chain, and after the digestion, the plasmid was gel purified. The non-immune heavy chain fragments were then ligated into the digested WT backbone at a mass ratio of 7.5 to 1. The ligated products were then electroporated into the Electro Ten-Blue® competent cells according to the manufacturer's protocol. The plasmids were then amplified and recovered using miniprep kit, and later electroporated into EBY100 cells.

### **3.2.12 Fluorescence Activated Cell Sorting of Mutant Library**

The library size of the 6-22 scFv random mutagenesis library was  $3 \times 10^6$  and this library was sorted six times. The 6-22 CDR domain shuffling libraries were of size  $1.1 \times 10^4$ ,  $1.2 \times 10^4$ , and  $1.1 \times 10^4$ , and were pooled together for screening. Six rounds of



screening were performed using FACS stepping down from 500nM to 160nM of HAAH antigen to screen for improved binders and without antigen to eliminate any binder against the detection antibodies. The 6-22 heavy chain shuffling library was of size  $1.2 \times 10^5$ . Six rounds of sorting, either stepping down from 800nM to 500nM of HAAH to screen for improved binders or without any HAAH to eliminate any binder against the detection antibodies, were performed using FACS. The library size of the C4 scFv random mutagenesis library was  $1 \times 10^7$  and this library was sorted five times. The first round of sorting was performed with the magnetic colloids (Miltenyi) at 50nM and then four more rounds of FACS screening were performed to isolate improved mutants.

### **3.3 Results**

#### **3.3.1 Isolation of Human Antibody Fragments against HAAH**

A non-immune human antibody library displayed on the surface of yeast was sorted to isolate novel binders against HAAH (Feldhaus, et al., 2003).  $1 \times 10^9$  yeast cells were screened against biotinylated HAAH ectodomain (bio-HAAH). Two rounds of MACS (magnetic activated cell sorting) at 300nM bio-HAAH, and then four rounds of FACS at 300nM bio-HAAH were performed to isolate binders. Individual isolated  $\alpha$ -bio-HAAH binder was then labeled with unmodified full length HAAH and detected with two previously isolated  $\alpha$ -HAAH mouse antibodies, FB-50 and 15c7, to confirm that the  $\alpha$ -bio-HAAH clones bind specifically to HAAH protein instead of biotinylation epitopes. Twelve clones were confirmed to bind specifically to recombinant HAAH protein, and their respective binding against 300nM of bio-HAAH on the surface of yeast is shown in Figure 3.1. Sequence analysis of these twelve clones (full sequences are shown in the

Appendix) showed that one of the binders, clone 4-6, contained only the variable region of heavy chain with no light chain (Appendix). Surprisingly, seven of the remaining 11 binders had very similar  $V_L$  sequences, but totally different  $V_H$ . These light chains were from the same family and the CDR3 of these light chains differed only at four residues, as shown in Table 3.1. In the human library used for binder isolation, the diversity of heavy chain is 80 fold higher than the diversity of light chain, so it is statistically rare for a binder to have one similar light chain to pair with seven different heavy chains (Feldhaus, et al., 2003). In addition, it was separately shown that antibody fragments containing only the light chain of clone 6-22 (one of the seven consensus clones) was able to bind HAAH on the surface of yeast (data not shown). Therefore, it is hypothesized that the light chain determines the binding of these clones against HAAH, and thus these seven clones were not functionally distinct from each other, and are likely to bind one common epitope. Of the seven similar clones, clone 6-22 was chosen for subsequent studies given its relatively higher affinity and expression (data not shown). The remaining four clones (6-23, 6-24, 6-27 and 6-28), which have distinct sequences, were also further characterized.

### **3.3.2 Conversion of scFv to IgG and ELISA**

The  $\alpha$ -HAAH scFv's were reformatted for expression as IgGs. The variable regions of the five  $\alpha$ -HAAH clones (6-22, 6-23, 6-24, 6-27 and 6-28) were subcloned into a human IgG1 vector containing the constant domains of the heavy and light chains. The ligated vectors were then transiently transfected into COS-7L cells. The  $\alpha$ -HAAH IgGs were secreted from the transfected COS-7L cells and purified using Protein A resin.

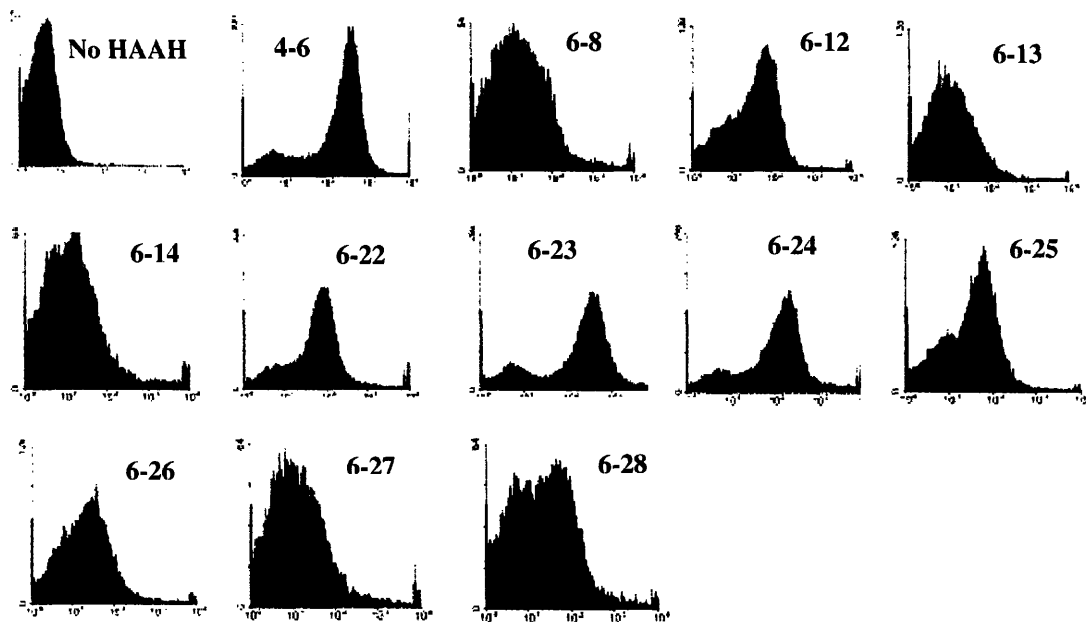


**Figure 3.1 Isolation of Human scFv against HAAH from Non-immune Human Library Displayed on Yeast.** Twelve clones were selected after six rounds of screening against recombinant HAAH protein. Individual clone displayed on yeast surface was allowed to bind 300nM of biotinylated HAAH and their binding level was detected with FACS. Without the HAAH antigen, a single negative peak is observed. When HAAH is present, all twelve clones have binding levels above the negative peak. These twelve clones conceivably have different binding affinities, as their binding levels to same concentration of HAAH are different.

**Table 3.1 Similar Light Chain Sequences for Seven out of the Twelve Isolated HAAH Binders.** The red, bold amino acid residues are the different residues among the consensus sequences.

Clone	CDR 1	CDR 2	CDR 3
6-8	SGSTSNIG <b>R</b> NYVYWY	KLLIYRNNQRPS	AAWDDSLSG-WV
6-12	SGSSSNIGNNYVYWY	KLLVYRNNQRPS	AAWDDSLSGRWV
6-13	SGSSSNIG <b>S</b> KYVYWY	KLLIYRNNQRPS	AAWDDSLSA-WV
6-14	SGSSSNIASNYVYWY	KLLIYTNNRRPS	AAWDDSLSG-WV
6-22	SGSSSNIGSNYVYWY	KLLIYKNNQRPS	AAWDDSLRG-YV
6-25	SGSSSNIGSNYVYWY	TLLIYRNNQRPS	AAWDDSLSGLYV
6-26	SGSRSNIGSNYVYWY	KLLIYRNHQRPS	AAWDDSLSG-YV

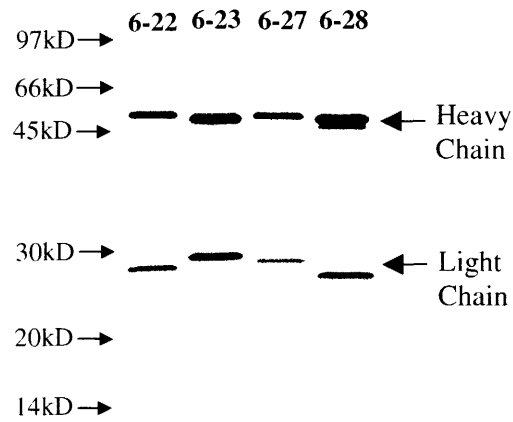
Figure 3.2A shows silver staining of four of the five purified antibodies. The binding of these five  $\alpha$ -HAAH IgG against full length HAAH was evaluated in ELISA. Either full-length recombinant HAAH or bovine serum albumin (BSA) was coated on the 96-wells plate overnight and various concentrations of IgG were then incubated in each well. The binding was detected with goat anti-human IgG-peroxidase conjugate and luminol /peroxide solution. Figure 3.2B shows that all five IgGs have higher binding signal to HAAH than to BSA. However, the binding of IgG 6-22 and 6-23 are significantly stronger than the other three IgGs, even though they are at lower concentration.

### **3.3.3 IgG Binding against Tumor Cell Lines**

HAAH expression has been observed on a variety of tumor cells. Binding of these human  $\alpha$ -HAAH IgGs against two HAAH-positive tumor cell lines were evaluated. Hepatocellular carcinoma cell line, FOCUS, and lung carcinoma cell line, H460, were used as the model cell lines. FOCUS cells and H460 cells were allowed to bind different concentrations of  $\alpha$ -HAAH IgGs at 4°C. Binding was detected with goat anti-human IgG-phycoerythrin conjugate and cell fluorescence was analyzed by flow cytometry. Figure 3.3A shows that compared to the non-relevant control human IgG, 6-22, 6-23, 6-24 and 6-28 IgGs all bind to both tumor cell lines. Meanwhile, no significant binding was observed when tumor cells were labeled with 100nM of 6-27 IgG. Consistent with the ELISA result, 6-22 and 6-23 IgGs give higher binding signals than the other IgGs, even though they are incubated at lower concentration. This indicates that 6-22 and 6-23 IgGs have higher binding affinity against HAAH than the other IgGs.

The apparent equilibrium binding constants (app.  $K_D$ ) of 6-22 and 6-23 IgGs against FOCUS cells at 4°C were determined by flow cytometry. Cells were labeled with

(A)



(B)

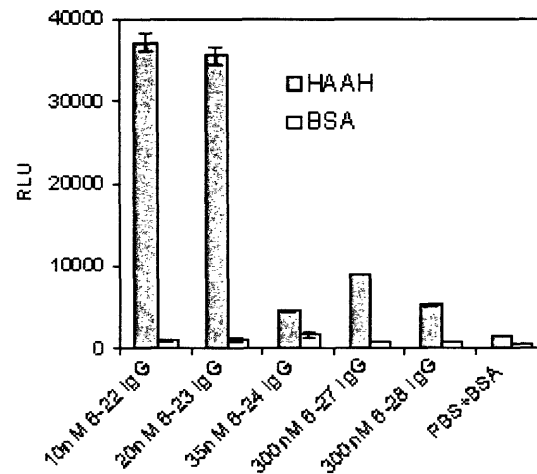
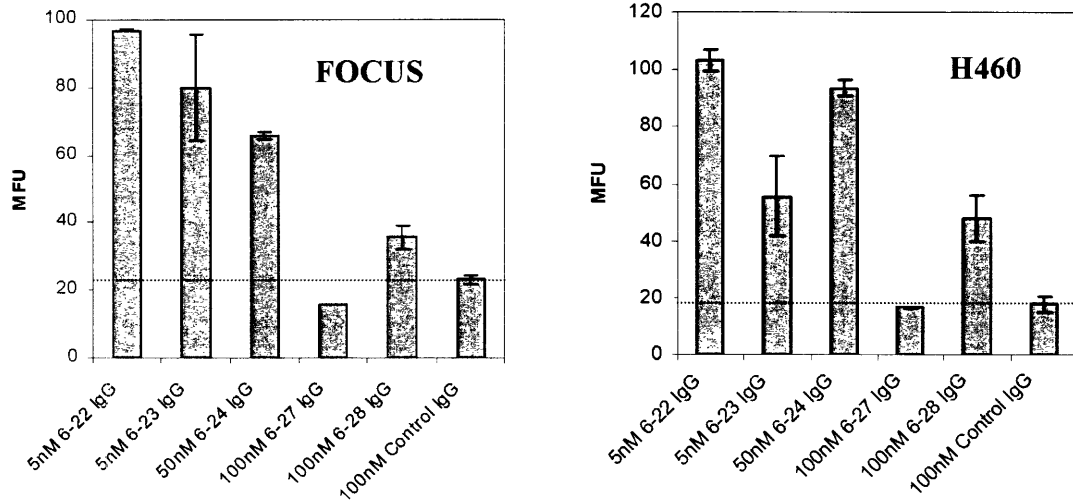


**Figure 3.2 Binding of Human anti-HAAH IgGs against Full-Length Recombinant HAAH Protein.** (A) Five human scFvs were reformatted into IgG. The IgGs were secreted from the COS-7L cells and purified using Protein A resin. Four of the five purified human IgGs were resolved in a denaturing SDS-PAGE gel, and silver staining of the gel is shown. (B) The binding of these five human IgGs against recombinant HAAH was evaluated in ELISA. Either full-length recombinant HAAH or bovine serum albumin (BSA) was coated in the ELISA wells, and different concentration of human IgG was allowed to bind in each well. IgG 6-22 and 6-23 show higher binding toward HAAH even though they are at lower concentrations than the other 3 human IgGs (6-24, 6-27 and 6-28). There is minimal binding of these human IgGs to BSA. Error bars in HAAH binding are result of triplicate trials.

(A)



(B)

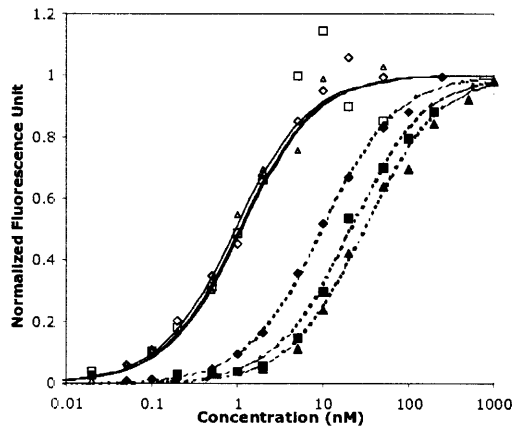


**Figure 3.3 Binding of Human anti-HAAH IgG Against Tumor Cell Lines.** (A) Different concentrations of human IgG were allowed to bind two tumor cell lines, FOCUS and H460. Their bindings were detected with FACS and their mean fluorescence units (MFU) are shown. At 5nM, both 6-22 and 6-23 IgGs gave significant binding to both tumor cell lines. IgG 6-24 and 6-28 bind the tumor cells only at high concentrations (50 to 100nM), while 6-27 IgG did not show any significant binding to the tumor cells. (B) The binding affinities of 6-22 and 6-23 IgG against FOCUS cells were then determined. Triplicate trials were performed. The apparent dissociation constants of 6-22 (open symbols) and 6-23 IgGs (dark, closed symbols) were determined to be  $1.0 \pm 0.2\text{nM}$  and  $20 \pm 10\text{nM}$  respectively.

different concentrations of IgGs, and then the binding was detected with goat anti-human IgG-phycoerythrin conjugate. Triplicate trials were performed for each IgG. Figure 3.3B shows that the app.  $K_D$  of 6-22 and 6-23 IgGs was determined to be  $1.0 \pm 0.2\text{nM}$  and  $20 \pm 10\text{nM}$  respectively.

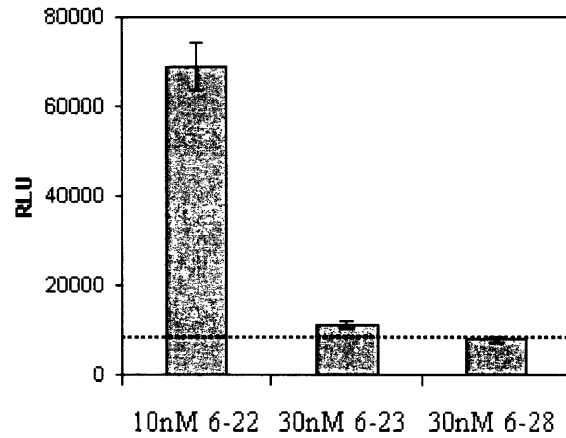
#### **3.3.4 Domain Mapping of Clone 6-22 and 6-23**

The respective binding domain of clone 6-22 and 6-23 were studied to determine whether they bind the catalytic domain of HAAH. Recombinant catalytic domain of HAAH was coated on the ELISA wells, then different IgGs were allowed to bind in each well. IgG 6-28, which did not display significant binding to full-length HAAH at 300nM (Figure 3.2B), was used as a human IgG1 isotype (negative) control. Figure 3.4A shows that 6-22 IgG gives significant binding to the catalytic domain of HAAH, while 6-23 IgG has minimal binding to the catalytic domain compared with 6-28 IgG. This indicates that 6-22 IgG binds the catalytic domain of HAAH, while 6-23 IgG binds the charged non-catalytic domain of HAAH, which along with the catalytic domain, was expressed on the surface of plasma membrane in tumor cells.

Although 6-22 IgG and 6-23 IgG bind different domains of HAAH, it is still conceivable that their binding epitopes are overlapping. To this end, we investigated whether the antibodies compete with each other on tumor cell binding. FOCUS cells were incubated simultaneously with Alexa-488-labeled 6-22 IgG (A488-6-22) and different concentrations of unlabeled 6-22, 6-23 and non-relevant control human antibody. Figure 3.4B shows that the binding of A488-6-22 is competed off with increasing concentration of unlabeled 6-22 IgG. However, the binding signal is not affected with the addition of



(A)



(B)

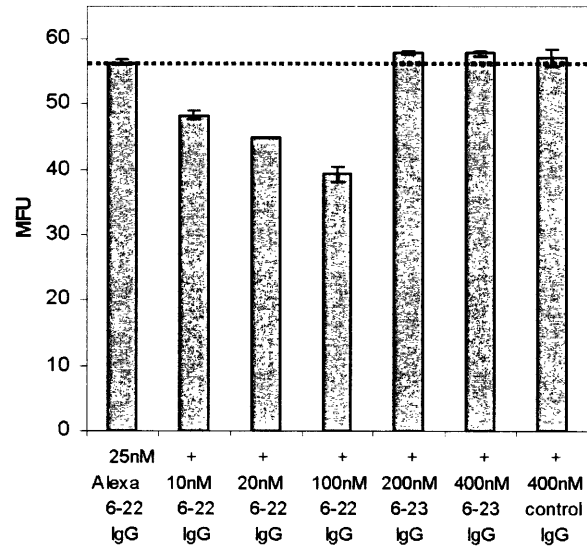


**Figure 3.4 Domain Mapping of 6-22 and 6-23 IgG.** (A) Binding of 6-22 and 6-23 IgGs to the catalytic domain of HAAH was evaluated in ELISA. Recombinant catalytic domain of HAAH was coated in ELISA cells, and IgG was allowed to bind in each well. 6-28 IgG, which show very weak binding to full-length HAAH in Figure 3.2B, was used as an isotype control. Results showed that 6-22 IgG showed strong binding to the catalytic domain of HAAH, while 6-23 IgG did not bind the catalytic domain. (B) Competition experiment was set up to determine if 6-22 and 6-23 bind overlapping epitopes. Alexa-488 labeled 6-22 IgG and different concentrations of unlabeled 6-22, 6-23 and non-relevant human control IgG were co-incubated with H460 cells. The binding level was detected with FACS. Results indicated that the fluorescence of Alexa-488 labeled 6-22 IgG was not competed off with increasing concentration of 6-23 IgG, demonstrating that 6-22 and 6-23 bind non-overlapping epitopes.

excess unlabeled 6-23 or control IgGs, indicating that neither IgG competes with 6-22 IgG on binding tumor cells. Unpublished work also illustrates that neither 6-22 nor 6-23 IgG competes with the mouse antibodies FB-50 and 15c7. Overall, 6-22 IgG and 6-23 IgG are two human antibodies targeting different epitopes of HAAH. Since 6-22 IgG has higher affinity and targets the catalytic domain of HAAH, it is further characterized.

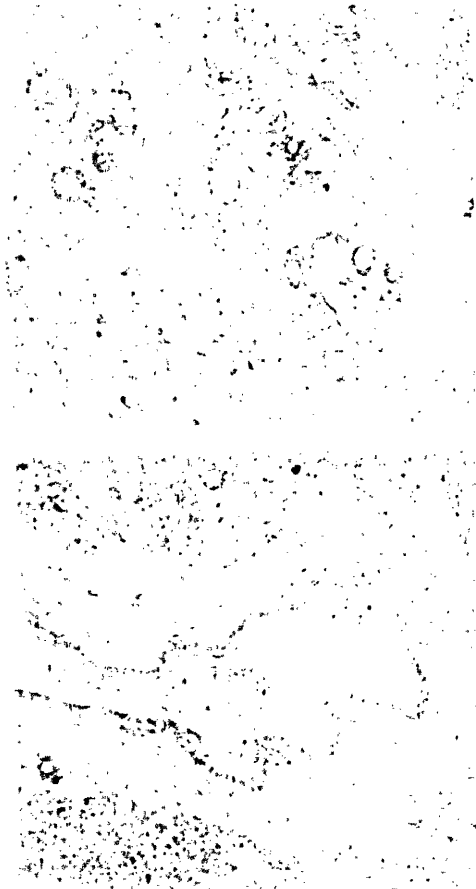
### **3.3.5 Immunohistochemistry using 6-22 IgG**

Paraffin-embedded tissue sections of pancreatic adenocarcinoma and adjacent chronic pancreatitis from the same patient were immunostained with 6-22 IgG. Immunoreactivity was revealed by the goat-anti human IgG-peroxide conjugate. HAAH expression in these pancreatic adenocarcinoma tissues was previously confirmed by a positive IHC stain using mouse antibody FB-50 (data not shown). Figure 3.5 shows the staining of both tumorous and adjacent non-tumorous tissues using 6-22 IgG. There is intense staining on the ductal areas of pancreatic adenocarcinoma using 6-22 IgG, while there is minimal staining on the ducts of adjacent pancreatitis tissues. Results here indicate that 6-22 IgG targets the HAAH-expressing tissues specifically, with minimal non-specificity against the non-tumorous tissues.

### **3.3.6 Internalization of 6-22 IgG into the Tumor Cells**

The internalization ability of the 6-22 IgG into tumor cells was studied. Alexa-488 labeled 6-22 IgG was incubated with the FOCUS cells at either 4°C or 37°C for 4 hr. The fluorescence of the cells was imaged by deconvolution microscopy. Figure 3.6A shows that incubating at 4°C, A488-6-22, which is denoted by the green fluorescence, primarily resides on the outer membrane of the cells. However, when incubated at 37°C, 6-22 IgG distributes throughout the inside of the cells, indicating extensive internalization

### Chronic Pancreatitis



### Adenocarcinoma of Pancreas, Ductal

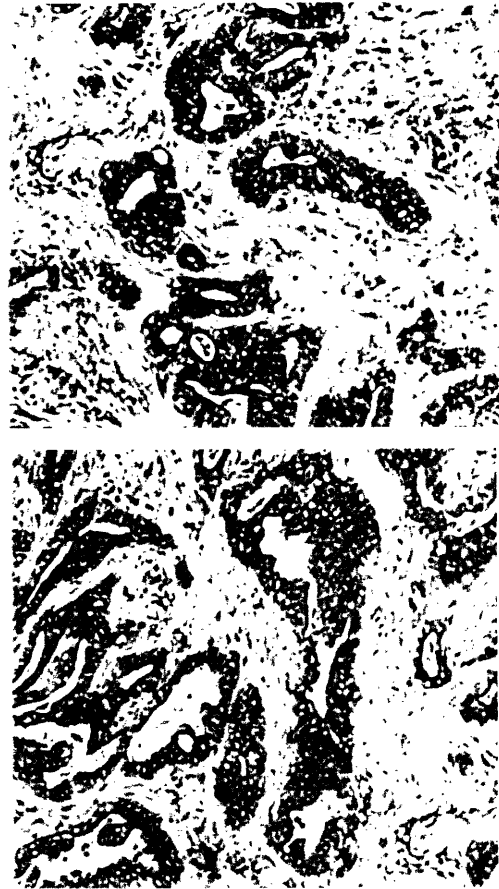


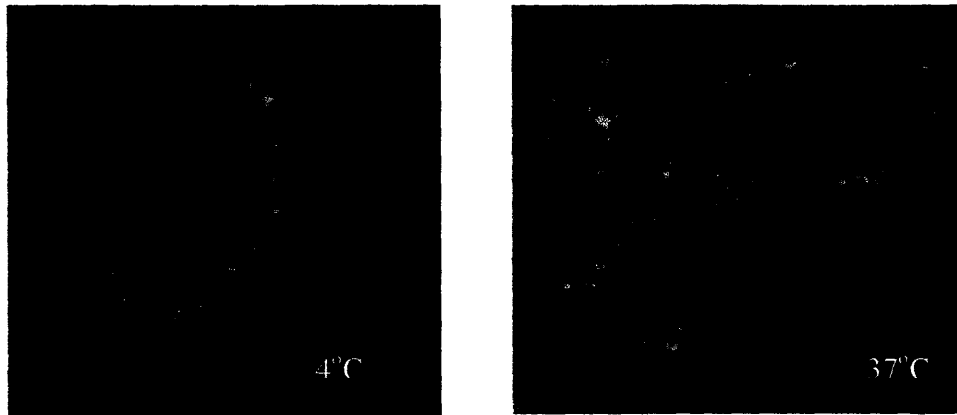
**Figure 3.5 Immunohistochemistry Staining of Human Tissue using 6-22 IgG.** Paraffin-embedded tissue sections of pancreatic adenocarcinoma and adjacent chronic pancreatitis were immunostained with 6-22 IgG. Immunoreactivity was revealed by the goat-anti human IgG-peroxide conjugate and DAB stain. There is intense staining of the ductal area of pancreatic adenocarcinoma using 6-22 IgG, while there is minimal staining on the duct of adjacent pancreatitis tissue.

of 6-22 IgG into the FOCUS cells. Similarly, internalization of 6-22 IgG was also observed on H460 cells, as shown in Figure 3.7.

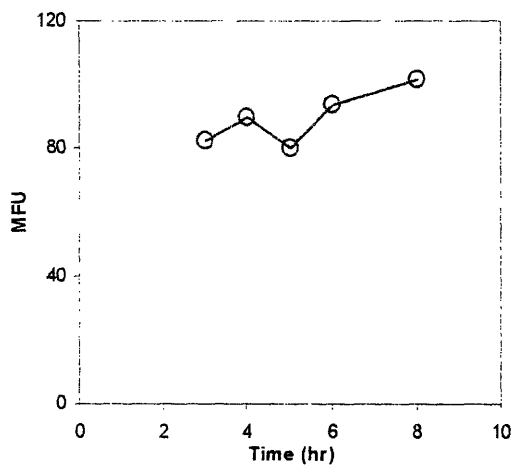
Internalization kinetics was investigated. First, a pulse-chase experiment was performed to probe the recycling of 6-22 IgG (Austin, et al., 2004). After a 3hr internalization pulse of A488-6-22, FOCUS cells were surface-quenched on ice with rabbit anti-Alexa 488 IgG, and then returned to 37°C incubation under the continuous presence of quenching antibody. At various times, cells were detached, surface-quenched on ice and then fluorescence inside the cells was analyzed by a flow cytometer. Figure 3.6B shows that cell fluorescence stays about the same within the 5hr chase period, indicating that fluorescence quenching was negligible. Thus, there was minimal amount of antibody recycling within the 5hr chase period.

Next, the internalization rate of 6-22 IgG was estimated. FOCUS cells were incubated at 37°C with either non-saturating concentrations of A488-6-22 or Alexa-488 control IgG; both IgGs have the same number of Alexa-488 molecules per IgG. At various times, cells were detached and fluorescence inside the cells was detected by flow cytometry. Figure 3.6C shows that A488-6-22 and Alexa-488 control IgG are taken up at a rate of 22.2 and 3.0MFU/hr respectively by the tumor cells. The uptake of the Alexa control IgG represents the solution phase (non-specific) uptake of fluorescent molecule in solution, which accounts for about 14% of A488-6-22 uptake rate in this case. When the cells were labeled with the incubating concentration of A488-6-22 on ice, the minus-background MFU was about 15 (data not shown). Accounting for solution phase uptake and minimal antibody recycling, an average internalization time of approximately 45min is calculated.

(A)



(B)



(C)

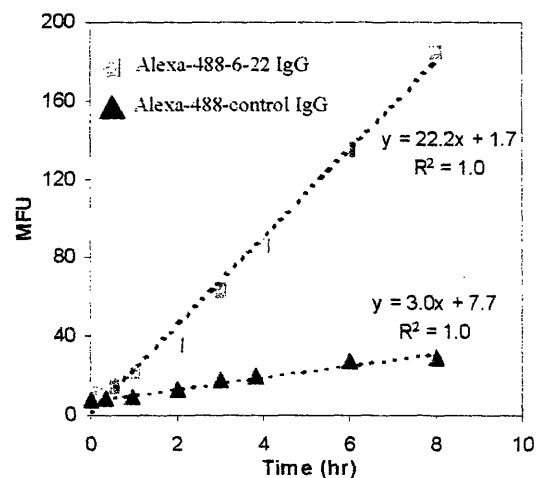


**Figure 3.6 Internalization of 6-22 IgG into FOCUS cells.** (A) Alexa-488 labeled 6-22 IgG was incubated with FOCUS cells at 4°C or 37°C for 4hr. Cells were then imaged using a deconvolution microscope. At 4°C, antibody mainly resided on the outside of the cells, while at 37°C antibody was internalized into the cells, illustrated by the green fluorescence inside the cell. The blue color indicated the Hoechst stain of the nuclei. (B) A pulse and chase experiment was set up to show that the fluorescence inside the cells stayed about constant within the 5hr of chase period (see *material and methods*). Therefore, there was minimal recycling of the antibody back to the surface. (C) The internalization rate of Alexa-488 labeled 6-22 IgG was investigated. A488-6-22 or control antibody was incubated with FOCUS cells at 37°C and at various times, fluorescence inside the cells was detected with FACS. Results indicated that the rise of fluorescence was 22.2MFU/hr and 3.0MFU/hr respectively for A488-6-22 and control antibody.

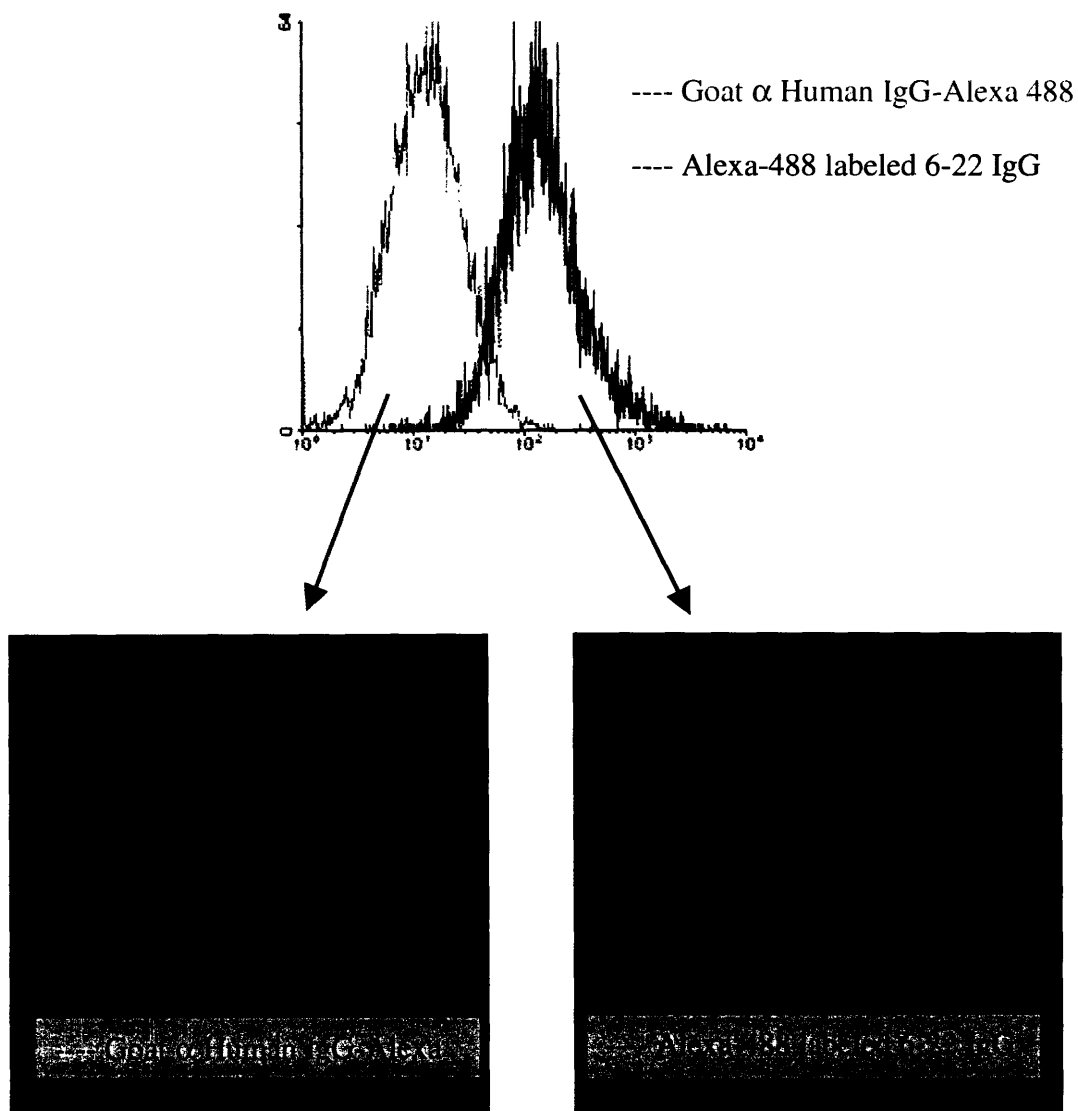


**Figure 3.7 Internalization of 6-22 IgG into H460 cells.** Alexa-488 labeled 6-22 IgG or control Alexa labeled IgG was incubated with H460 cells at 37°C for 24hr. Cells were trypsinized and fluorescence of the cells was analyzed using a flow cytometer. Trypsinized cells were also stained with Hoechst dye, allowed to settle on lysine-coated slides and then imaged using a deconvolution microscope. Cells that were incubated with Alexa-488 6-22 IgG have significant higher fluorescence than the cells incubated with control IgG. Microscopic study shows that the green fluorescence in the Alexa 488-6-22 IgG treated cells is from the inside of the cells. This indicates that 6-22 IgG is internalized into the H460 cells.

### 3.3.7 Cytotoxicity of 6-22 IgG Immunotoxin on Tumor Cell Lines

The capability of 6-22 IgG to serve as a targeting domain in immunotoxin therapy was tested. The toxin used in this study was saporin, a ribosome-inhibiting plant toxin. Commercially available secondary antibody-conjugate, goat-anti-human IgG-saporin conjugate (Hum-ZAP, H-Z), allows facile assessment of the potential immunoconjugate efficacy. H-Z binds primary human targeting antibody, and then through the internalization of primary antibody is delivered intracellularly to inhibit cellular proliferation. In our study, 6-22 IgG or non-relevant human control antibody was pre-incubated with H-Z and then the complex was presented to the FOCUS cells. *In-vitro* cell viability was determined after three days of incubation. Figure 3.8 shows that neither 10nM of 6-22 IgG nor 22nM of H-Z alone inhibits cell growth. In addition, there was no observable cytotoxicity when the complex of control human antibody and H-Z was presented to the cells. However, the viability of the 6-22/H-Z treated cells was lowered by about 30%, indicating that 6-22 IgG was able to specifically facilitate the internalization of the toxins. Similarly, increased cytotoxicity was also observed when 6-22/H-Z was used to treat H460 cells; however the extent of immunotoxin efficacy on H460 was not as high as on FOCUS, as H-Z alone had higher background toxicity to the H460 cells (Figure 3.8). Overall, results here suggest that 6-22 IgG can be employed as a targeting domain for conjugating immunotherapy for HAAH-expressing tumor cells.

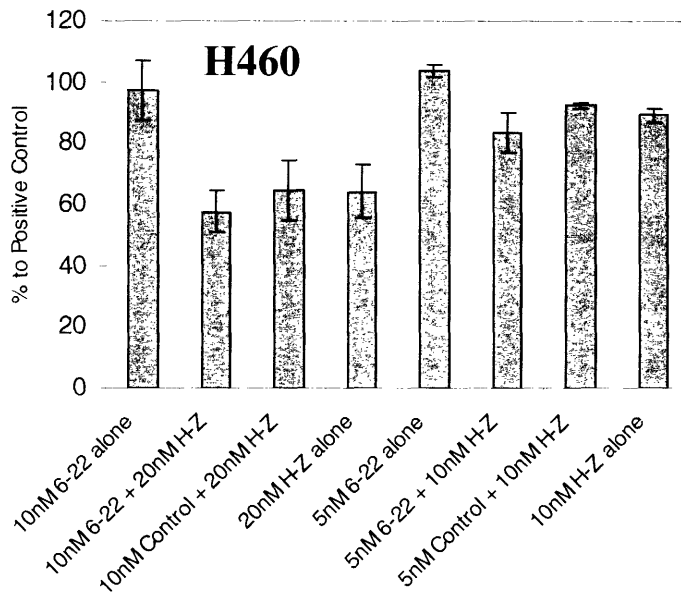
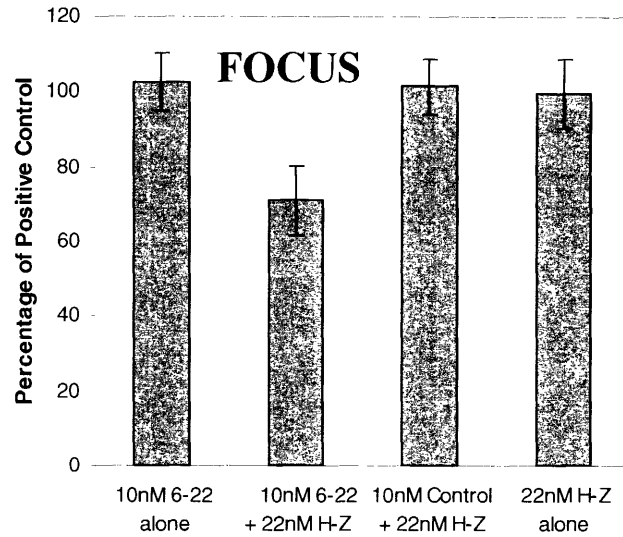


**Figure 3.8 Cytotoxicity of 6-22 Immunotoxins on FOCUS and H460 Cells.** Efficacy of using 6-22 IgG as the targeting module in immunotoxin was evaluated. 6-22 IgG or control human IgG was pre-incubated with H-Z (goat anti-human IgG-saporin conjugate). FOCUS or H460 cells were then exposed to the IgG alone, H-Z alone or the pre-incubated complexes. Viability of the cells was determined after 3 days of incubation. Results showed that 6-22 IgG alone did not have any cytotoxicity toward the tumor cells. For FOCUS cells, complex of 6-22 IgG/H-Z inhibits cell growth. However, the inhibition of H460 cell growth from 6-22IgG/H-Z complex is not as significant as for FOCUS cells.



### 3.3.8 Random Mutagenesis of 6-22 scFv

Three different mutagenesis strategies were directly compared for affinity maturation of 6-22 scFv: error-prone PCR (random mutagenesis), CDR shuffling (Figures 3.9A-C), and heavy chain shuffling (Figure 3.9D). Seven higher affinity clones isolated from the error-prone PCR mutagenized library were sequenced and found to possess a strikingly high average of  $25 \pm 16$  mutations, significantly higher than the number of mutations in the unscreened library ( $6.6 \pm 8.0$  for 17 unselected clones; difference statistically significant with  $p < 0.001$ ). The dissociation constant of the best-improved clone (11m1-2) was determined to be  $120 \pm 20$ nM, a two order of magnitude improvement (Figure 3.10). Upon closer examination of the amino acid sequences of these improved clones, cysteine deletion or insertion in the  $V_H$  domain was frequently observed. Five of the seven sequenced clones replaced the  $V_H22$  cysteine residue with either arginine or tyrosine, abolishing the  $V_H$  intra-domain disulfide bond. Of these five clones, three have mutations introducing a novel cysteine in either the heavy chain FW3 or light chain CDR3. For the two clones that did not alter  $V_H\text{Cys}22$ , one clone did not introduce a new cysteine, but had 19 amino acid changes. The other clone had 51 amino acid mutations, and also replaces a tyrosine with a cysteine in the heavy chain CDR3 loop, just four residues away from the consensus  $V_H22$  cysteine. The frequent cysteine mutations and extraordinarily high number of mutations in the selected clones suggest that fairly dramatic structural change in the heavy chain architecture is required to improve the affinity of this clone's starting binding motif. The starting scFv has respectively zero and four mutations from germline heavy and light chain framework sequences. The clones isolated from the random mutagenesis studies have germline

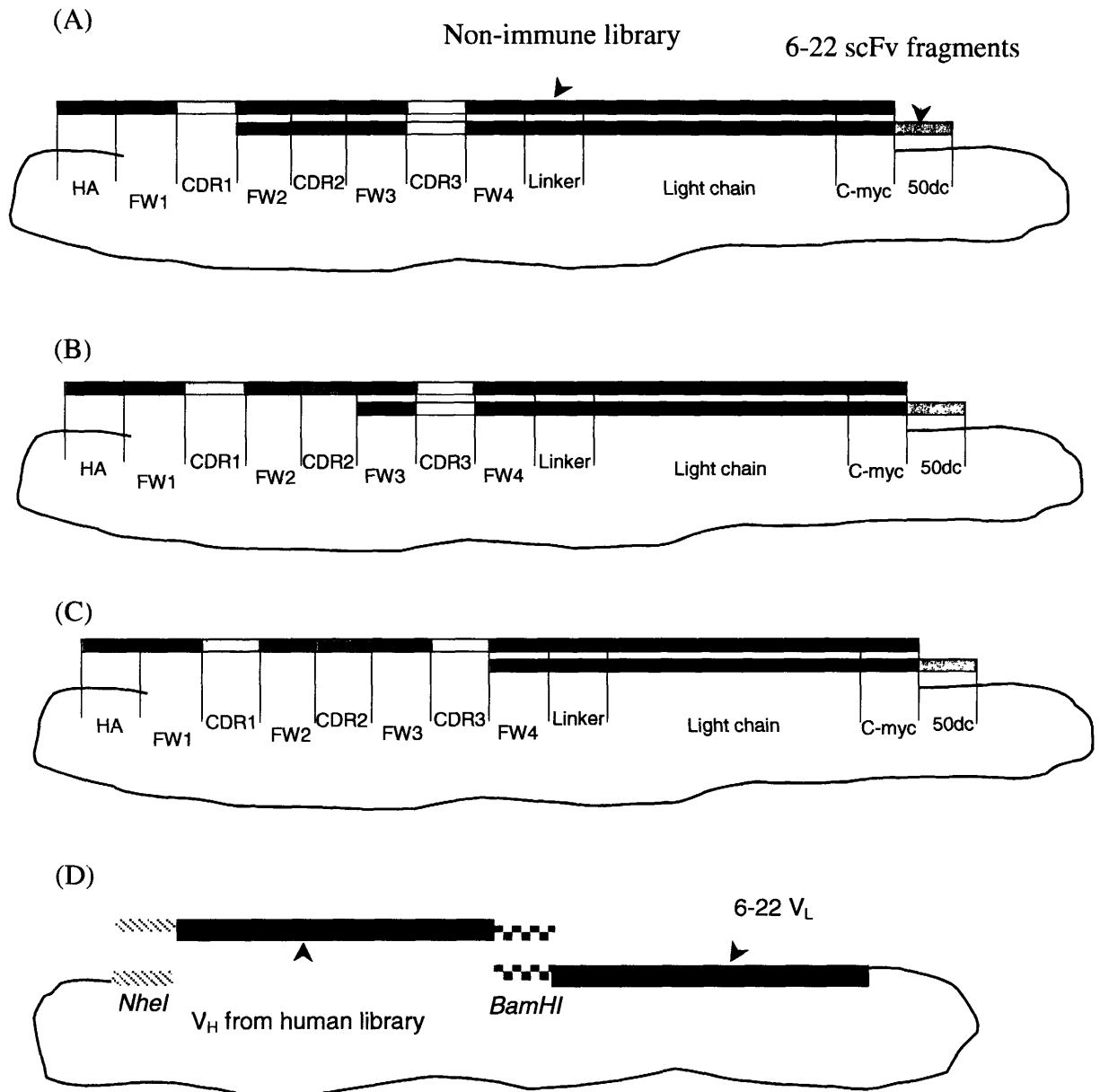


**Figure 3.9 Schematic of CDR Domain and Heavy Chain Shuffling Mutagenesis Methods.** CDR domain shuffling (A-C) employs *in vivo* homologous recombination in yeast, while heavy chain shuffling (D) employs ligation of heavy chain fragments into restriction digested 6-22 backbone. (A) 6-22  $V_H$ FW1 and  $V_H$ CDR1 are exchanged with the non-immune library fragments. (B) 6-22  $V_H$ FW1,  $V_H$ CDR1,  $V_H$ FW2, and  $V_H$ CDR2 are exchanged. (C) 6-22  $V_H$ FW1 to  $V_H$ CDR3 are exchanged. (D) Heavy chain fragments from non-immune human library are paired with the 6-22 light chain.

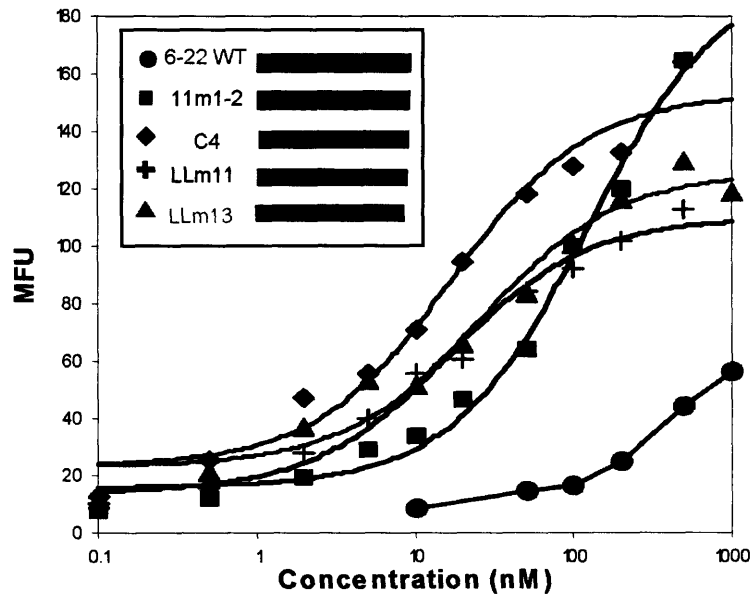
framework mutations ranging from 8 to 35, which would raise substantial concerns about immunogenicity in any potential therapeutic application of this antibody.

### **3.3.9 CDR Domain Shuffling of 6-22 scFv**

A CDR domain shuffling library was constructed by replacing either heavy chain FW1 to CDR1, FW1 to CDR2, or FW1 to CDR3 of the WT scFv with the non-immune heavy chain fragments (Figures 3.9A-C) respectively (Swers, et al., 2004), with all three pooled into a single library for screening. After sorting, four unique affinity-improved clones were isolated, of which three had replaced FW1 to CDR3 with a sequence from the nonimmune library, (effectively a full V<sub>H</sub> chain shuffling event), and the remaining clone replaced the FW1 to CDR2 sequence. Sequences of the clones are shown in the Appendix. As shown in Figure 3.10, the dissociation constant of this CDR (FW1 to CDR2) shuffled mutant (C4) was  $17 \pm 5$ nM, 3 order of magnitude improvement relative to the WT affinity, and one order of magnitude improvement over the random mutagenesis clone. This CDR shuffled mutant possesses only two mutations from the germline heavy chain framework sequence, significantly fewer than in the random mutagenesis clones.

### **3.3.10 Heavy Chain Shuffling of 6-22 scFv**

A heavy chain shuffling library was constructed by shuffling heavy chains from the nonimmune library against the WT light chain. (Figure 3.9D). Five clones from the unscreened library were sequenced and confirmed to have unique heavy chains (data not shown). Following six rounds of sorting, eleven clones were identified with unique heavy chains distinct from the initial scFv. Sequences of the clones are shown in the Appendix. The dissociation constants for two selected clones, LLm11 and LLm13, were determined



	Schematic	$K_D$
<b>WT</b>		
ScFv #6-22		> 10 $\mu$ M
<b>A. Random Mutagenesis</b>		
Clone 11m1-2 (with 9 mutations including CysH22Arg)		120 $\pm$ 20
<b>B. CDR Shuffling</b>		
Clone C4 (V <sub>H</sub> FR1, V <sub>H</sub> CDR1, V <sub>H</sub> FR2, V <sub>H</sub> CDR2 Preferentially Exchanged)		17 $\pm$ 5 nM
<b>C. Heavy Chain Shuffling</b>		
Clone LLm11		16 $\pm$ 4 nM
Clone LLm13		26 $\pm$ 8 nM

**Figure 3.10 Topology and Affinities of 6-22 WT scFv and Mutants Isolated from Different Mutagenesis Strategies.** The  $K_D$  was determined on the yeast surface using recombinant full-length HAAH protein. The  $K_D$  of the clone isolated from random mutagenesis was two orders of magnitude lower than the  $K_D$  of WT. Meanwhile, the clones isolated from CDR shuffling and heavy chain shuffling libraries have three orders of magnitude improvements in binding affinity over the WT scFv.

to be  $16 \pm 4\text{nM}$  and  $26 \pm 8\text{nM}$  respectively (Figure 3.10), a three order of magnitude improvement in affinity over the starting scFv. The extent of the affinity improvement in this heavy chain shuffling library was one order of magnitude higher than the extent of the affinity improvement in the random mutagenesis study, although the library sizes were 25 fold smaller than the random mutagenesis library. The affinities of these chain-shuffled mutants are comparable to the affinity of the CDR-shuffled mutant (C4). Similar to the CDR-shuffled mutants, these clones also have minimal deviation from the heavy chain germline framework sequence (on average  $4 \pm 2$  mutations).

### **3.3.11 Conversion of C4 scFv to C4 IgG**

CDR shuffled mutant C4 scFv, which has the same heavy chain CDR3 and light chain as 6-22 scFv, was reformatted as IgG. The binding affinities of C4 IgG on two FOCUS and H460 cells were determined and compared with the binding affinities of wild-type 6-22 IgG. Figure 3.11 shows that the binding affinities of C4 IgG are similar to those of 6-22 IgG on two different cell lines, indicating that the extent of affinity improvement on IgG level is not as significant as those of scFv format.

### **3.3.12 Random Mutagenesis of C4 scFv**

C4 scFv was further affinity matured using random mutagenesis. A library of  $1 \times 10^7$  mutants was constructed, and five rounds of screening were performed to isolate improved mutants. Two mutants (C4-8 and C4-18) that have higher ratio of binding-to-display signal than C4 scFv were isolated. The affinity of C4-8 was not determined, and its sequence is shown in the Appendix. The dissociation constant of C4-18 was determined to be  $0.6 \pm 0.1\text{nM}$  on yeast surface, which is two order of magnitude improvement over the C4 scFv (Figure 3.12). The nucleic acid and amino acid sequences

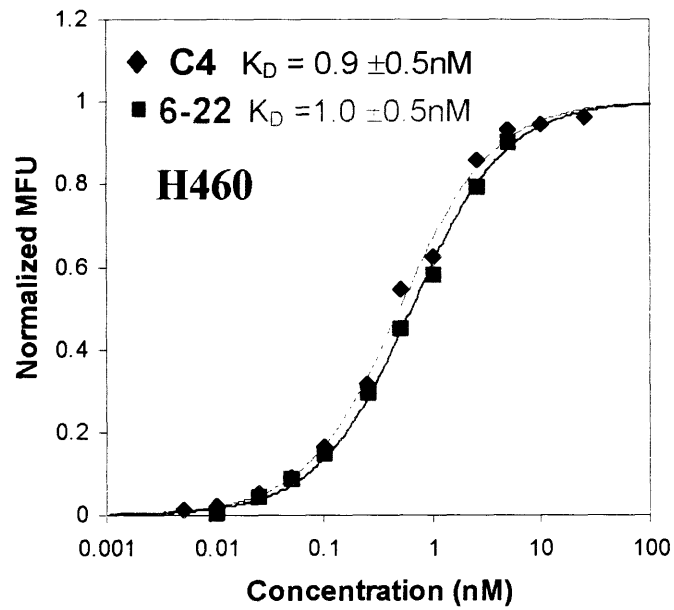
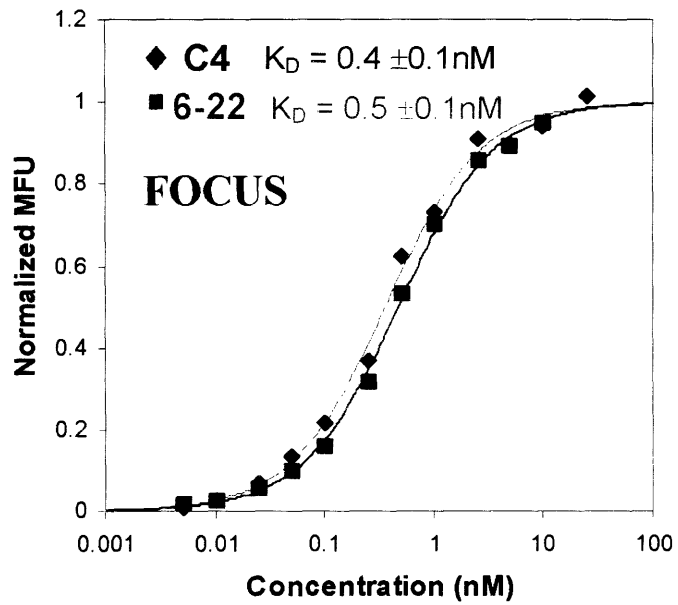
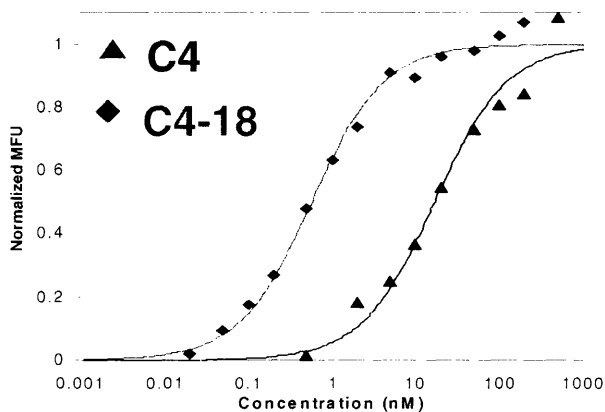


**Figure 3.11 Affinity Comparison of 6-22 and C4 IgGs against FOCUS and H460 Cells.** C4 scFv was reformatted as IgG. 6-22 and C4 IgGs were then titrated against tumor cell lines, FOCUS and H460. Results show that the affinities of 6-22 and C4 IgGs are similar on both tumor cell lines.

(A)



(B)

```
Q V Q L Q Q S G P G L V K P S P T L S L
1 caggtacagctgcagcagtcaggtccaggactgggtgaagccctcaccgaccctctcactc 60
  T C A I S G D S V S S N S A A W N W V R
61 acctgtgccatctccggggacagtgctctctagcaacagtgctgcttgggaactgggtcagg 120
  Q S S R G L E W L G R T Y Y R S K W Y
121 cagtcacctatcgagaggccttgagtggtgggaaggacatactacaggtccaagtggtat 180
  N G Y A V S V R I T T N D T S R N
181 aatggttatgcagtatctgtgaggggtcgaataaccaccaacgcggacacatccaggaac 240
  Q F S L Q L N S V T P E D T A V Y Y C A
241 cagttctccctgcagctgaactctgtgactcccaggacacggctgtgtattactgtgca 300
  R T G Y S S S W V V N S N Y W G Q G T L
301 aggaccgggtatagcagtagctgggtcgtaaattctaactactggggccagggaaacctg 360
  V T V S S G S A S A P T G I L G S G G G
361 gtcaccgtctcctcagggagtgcatccgcccccaaccggaattctagggtcgggtggcggt 420
  G S G G G G S G G G G S Q P A L T Q S P
421 ggcagcggcggtgggtgggtccggaggcggcggttctcagcctgcgctgactcagtcaccc 480
  S A S G T P G Q R V T I S C S G S S N
481 tcagcgtctgggacccccgggcagagggtcaccatctcttgttctggaagcagctccaac 540
  I G S N Y V Y W Y Q Q L P G T A P K L L
541 atcggaaagtaattatgtatactggtaaccagcagctcccaggaacggcccccaactctc 600
  I Y K N N Q R P S G V P G R F S G S K S
601 atctataagaataatcagcggccctcaggggtccctggccgattctctgggtccaagtct 660
  G T A A S L A I S G L R S K D E A D Y Y
661 ggcacgcagcctcctggccatcagtgggctccggcttaaggatgaggctgattattac 720
  C A A W D D S L R G Y V F G T G T K L T
721 tgtgcagcatgggatgacagcctgcgtgggttatgtcttcggaactgggaccaagctgacc 780
  V L
781 gtccta 786
```

**Figure 3.12 The Affinity and Sequences of C4-18 scFv.** (A) The affinity of C4-18 scFv was determined on the yeast surface. The  $K_D$  was determined to be 0.6nM, 2 order of magnitude improvement over C4 scFv (17nM). (B) The nucleic acid and amino acid sequences of C4-18 scFv. The CDRs are underlined. The difference between C4-18 and 6-22 sequences are highlighted in green (acquired from the CDR domain shuffling of 6-22) and yellow (acquired from the random mutagenesis of C4).

of C4-18 is also shown in Figure 3.12. Compared with the amino acid sequence of 6-22scFv, C4-18 has 15 mutations and five of the 15 mutations occur in the CDRs. Meanwhile, C4-18 has 11 mutations from C4, and three of the 11 mutations are located at the CDRs.

### 3.4 Discussion

In this study, novel human antibodies against human aspartyl (asparaginyl)  $\beta$ -hydroxylase were isolated from a non-immune human antibody library using yeast surface display. These antibodies have been shown to bind specifically to tumor cell lines and tumor tissues, while they have minimal activity against normal tissue. Two of the higher affinity IgGs, 6-22 and 6-23, were shown to bind different epitopes on HAAH. 6-22 IgG was also shown to internalize into the tumor cells, and able to deliver toxins into the tumor cells. Moreover, 6-22 scFv was affinity-matured using different mutagenesis methods, and the binding affinity of an isolated improved mutant (C4-18) had five order of magnitude improvements over the wild-type 6-22 scFv. Overall, these human  $\alpha$ -HAAH antibodies may be useful for targeting a variety of HAAH-expressing tumor cells, and they are also candidates for conjugating toxins, enzymes, radionuclides, liposomes or virus for targeted immunotherapy.

Human  $\alpha$ -HAAH antibodies with a range of affinities were isolated in our study. The apparent dissociation constants of the IgG-reformatted clones range from about micromolar for 6-28 IgG to about single digit nanomolar for 6-22 IgG. The scFv format of 6-22 has a binding affinity of about 80nM against both FOCUS and H460 cells (data not shown). Previously, antibodies against protein antigens were isolated from this non-



immune library and the binding affinities of the isolated protein binders ranged from single digit nanomolar to around micromolar (Feldhaus, et al., 2003). Other studies using phage non-immune human antibody libraries have also selected protein-binding leads ranging from 0.2nM to micromolar (de Haard, et al., 1999; Griffiths, et al., 1994; Hoet, et al., 2005; Knappik, et al., 2000; Marks, et al., 1991; Sheets, et al., 1998; Soderlind, et al., 2000; Vaughan, et al., 1996). Therefore, the affinities of the clones isolated against HAAH in this study are in accordance with those isolated from other non-immune human libraries. However, it is not certain beforehand that high affinity anti-HAAH clone can be directly isolated from a non-immune human library, as HAAH is a self-antigen. Such self-reactive clones may be deleted from the non-immune repertoire, which was used to construct our human antibody library. Usually, if such a weak lead is the only available clone, lengthy *in-vitro* affinity maturation probably is required to substantially improve the binding affinity of antibody (Pancook, et al., 2001). One advantage of isolating self-antigen binder from *in-vitro* human library is that *in-vitro* random pairing of V<sub>H</sub> and V<sub>L</sub> in the library construction generates greater antibody diversity. This may be in the case of clone 6-22; the light chain of 6-22 is very similar to the light chains of other clones and can bind the antigen weakly by itself. Pairing of different heavy chains with this similar light chain result in binders with different affinity, as shown in the differential binding signals in the selected clones (Figure 3.1 and Table 3.1). The pairing of 6-22 heavy chain with this consensus light chain appears to give the highest binding affinity. *In-vitro* affinity maturation involving shuffling heavy chain against this consensus light chain may further explore the possibility of different heavy chain pairing, hence improving the affinity of this particular clone (Marks, et al., 1992).

The affinities of FDA-approved antibodies range from 0.1nM to 10nM (Cardarelli, et al., 2002; Goldstein, et al., 1995; Spiridon, et al., 2002). The apparent  $K_D$  of 6-22 IgG is about 1nM, and within the affinity range for marketed antibodies. The reformatting of 6-22 scFv to IgG increases its affinity from 80nM to about 1nM. Therefore, it may be advantageous to reformat antibody fragment that directly isolated from the non-immune library to avoid lengthy affinity maturation. It was previously shown in the work of Nielsen and co-workers (Nielsen, et al., 2000) that reformatting the monovalent antibody fragments to bivalent formats when they were in lower affinity had greater benefit in apparent  $K_D$  improvement. They showed that reformatting three scFvs against ErbB2 with affinities of 360nM, 70nM and 3nM to diabodies resulted in affinity improvements of 65, 19 and 7.7 folds respectively. Similar apparent affinity improvement was also seen in reformatting a Fab against tumor-associated MUC1 into IgG (Henderikx, et al., 2002). However, if monovalent antibody fragment is desired for tumor penetration or targeting, *in-vitro* affinity maturation process can be carried out on the monovalent fragment of 6-22 to improve its affinity.

HAAH expression has been detected on the surfaces of numerous cancer cell types. In our study, the human  $\alpha$ -HAAH IgGs did not show any significant anti-proliferation effect *in-vitro* (Figure 3.8), however it does not preclude the therapeutic use of  $\alpha$ -HAAH antibodies *in vivo*. It was previously shown in some of the FDA-approved antibodies that the effector function of immune system triggered by the antibodies played an important, if not major, role in tumor reduction *in vivo*. Di Gaetano and co-worker's study on complement activation showed that tumor xenografts lacking the first component of the classical complement pathway were not protected from Rituxan (Di

Gaetano, et al., 2003). They concluded that complement activation was fundamental for the *in vivo* therapeutic effect of Rituxan. In addition, two separate studies both showed that polymorphism in Fc gamma receptor IIIa (FCGR3A) was associated with the therapeutic effect of Rituxan in patients (Cartron, et al., 2002; Dall'Ozzo, et al., 2004). A significant difference in objective response rate was observed for the FCGR3A-158V homozygous patients and FCGR3A-158F carriers patients (response rate of 90% vs. 51% after 1 year) (Cartron, et al., 2002). The observed difference was due to more efficient antibody-dependent cell-mediated cytotoxicity (ADCC) against the CD20+ cells (Dall'Ozzo, et al., 2004). Other studies also showed that the Fc receptor on human antibody and its interactions with effector cells were important for the therapeutic effect of both Rituxan and Herceptin *in vivo* (Clynes, et al., 2000). In addition, Spiridon and co-worker compared the *in vitro* and *in vivo* activities of anti-HER-2 IgG and F(ab')<sub>2</sub> (Spiridon, et al., 2004). They found out that even though the *in vitro* anti-proliferation and proapoptotic effects of the IgG and F(ab')<sub>2</sub> were similar, their therapeutic effects *in vivo* were dramatically different. *In vivo* studies showed that IgG, which can mediate ADCC and complement dependent cytotoxicity, exhibited significant antitumor activity, while their F(ab')<sub>2</sub> fragments were only marginally effective. These studies in general show that *in vivo* activities of Herceptin and Rituxan are largely Fc dependent, although both antibodies have *in vitro* anti-proliferation effects. Additional studies indicated that even targeting a biologically inactive tumor antigen like Ep-CAM with human antibodies was also able to trigger ADCC both *in vitro* and *in vivo* (Naundorf, et al., 2002; Prang, et al., 2005). Therefore, perhaps simply targeting tumor cell surface antigens with human

antibodies *in vivo* can elicit therapeutic effect by activating the effector function of the immune system.

Different options of tumor therapy targeting the HAAH have been explored in previous studies. Antisense oligodeoxynucleotides (ODN) targeting HAAH mRNA was used to inhibit HAAH expression in tumor cells (Ho, et al., 2002; Maeda, et al., 2003). Maeda et al. showed that transfecting the cholangiocarcinoma cells with antisense ODN was able to substantially reduce the motility of the tumor cells *in vitro* (Maeda, et al., 2003). Ho and co-workers also developed a set of antisense oligonucleotides to regulate the expression of HAAH and humbug. They used an antisense oligonucleotide that inhibited the expression of both HAAH and humbug *in vitro* to target lung tumor cells in nude mice. Their results showed that the antisense oligo had poor penetration into the tumor cells. Even though there was modest effect on tumor growth *in vivo*, the expression of HAAH transcript in antisense-treated group was unaltered comparing with the control group. In general, antisense therapy was developed to inhibit HAAH expression *in vitro*, however their usages *in vivo* is still being hampered by issues such as stability and binding specificity. On the other hand, antibody therapy has the advantage of targeting tumor cells specifically. In our study, in addition to targeting the tumor cells, 6-22 IgG was shown to internalize into the tumor cells. The internalization time is about 45min, which is similar to the time of constitutive membrane turnover (Thilo, 1985). Thus, there may not be any active mechanism involved in the internalization of the HAAH/6-22 IgG bound complex. Moreover, our recycling experiment, modified from the work of Austin and co-workers (Austin, et al., 2004), shows that once internalized 6-22 IgG is not recycled back to the surface within the incubation time. This is different from both

Herceptin and transferrin, which were shown to rapidly recycle (Austin, et al., 2004). In general, utilizing the internalization ability of the antibody, toxins, liposome and viruses can be conjugated to 6-22 IgG for targeted therapy. Different protein toxins including *Pseudomonas* exotoxin, *Diphtheria* toxin, gelonin, ricin A chain, as well as small molecule toxins such as maytansinoids and calicheamycins have been either chemically conjugated or genetically fused to different antibodies to construct immunotoxins and immunochemotherapeutics (Bera, et al., 1999; Hexham, et al., 2001; Ma, et al., 2001; Rosenblum, et al., 2003; Safavy, et al., 2003; Thompson, et al., 2001). In our work, a commercially available secondary antibody-saporin conjugates (H-Z) was used. Our study shows that 6-22 IgG can facilitate the internalization of saporin, hence eliciting cytotoxicity to the tumor cells *in vitro*. The work here is a proof of concept that 6-22 IgG can be used as a targeting module for delivering toxins and other moieties into the cells. For future clinical or animal study, the choice of toxins and the conjugating methods will need further consideration and optimization.

For the engineering of 6-22 scFv, affinity improvement by error prone PCR mutagenesis required extremely high substitution rates, and the structurally important cysteine (H22) in the heavy chain was frequently mutated, implying that small changes in structure or CDR were insufficient to improve the complementary of interaction with the antigen. This high level of deviation from germline framework sequence in the isolated mutants could very well create immunogenic epitopes, and consequently in the absence of an alternative mutagenesis strategy this antibody lineage would be unlikely to be developed further. In contrast, recombinational mutagenesis (CDR shuffling and heavy chain shuffling mutagenesis) generated mutants with substantial changes from the WT

sequence while conserving the germline framework sequence in the mutants. Recombinational mutagenesis is much more preferable in this case as the isolated mutants have the higher affinity improvement (3 order of magnitude) but far fewer framework mutations. In cases such as this, it is favorable to use recombinational mutagenesis over somatic hypermutation to generate improved mutants with substantial changes from the first generation antibody, while keeping the sequence similar to the germline framework sequence.

In summary, novel human antibodies targeting HAAH have been isolated. These antibodies have been shown to bind specifically to the HAAH-expressing tumor cells. One of the antibodies, 6-22 IgG, was also shown to internalize into the tumor cells and facilitate the internalization of toxins. The scFv format of 6-22 was also engineered to 0.6nM in two rounds of mutagenesis (CDR domain shuffling and random mutagenesis). These  $\alpha$ -HAAH IgG and scFv can potentially be used in the diagnosis and therapeutic treatments of HAAH-expressing tumor cells.

# Chapter 4: Quantitative Screening of Yeast Surface-Displayed Polypeptide Libraries by Magnetic Bead Capture

## 4.1 Introduction

Directed evolution is the most effective method currently available for exploration and engineering of new protein functions and properties. Directed evolution involves displaying a diverse array of protein mutants on a scaffold (Shusta, et al., 1999), and favorable mutants are selected or screened from the pool. Such scaffolds include bacteriophage (Griffiths and Duncan, 1998; McCafferty, et al., 1990; Smith, 1985; Wilson and Finlay, 1998), *Escherichia coli* (Georgiou, et al., 1997; Griffiths and Duncan, 1998) and *Saccharomyces cerevisiae* (Boder and Wittrup, 1997).

Appropriate quantitative selection or screening methodologies for polypeptide libraries are critical for successful recovery of favorable mutants. Different methodologies exist for different display systems. For example, phage libraries are typically screened by immobilized ligand, such as panning and affinity columns (Marks, et al., 1991). To avoid avidity artifacts in panning, phage library screening is also performed with biotinylated ligand and streptavidin-coated paramagnetic beads (Griffiths, et al., 1994; Hawkins, et al., 1993; Hawkins, et al., 1992). Meanwhile, flow cytometric analysis with fluorescent probe labeling has been used to screen for improved mutants from cell surface-displayed combinatorial libraries (Boder, et al., 2000; Christmann, et al., 1999; Daugherty, et al., 1998; Daugherty, et al., 2000b; Francisco, et al., 1993; Kieke, et al., 1999; Wentzel, et al., 1999). Flow cytometric analysis has the advantages of being a reliable, and quantitative high-throughput screening method for

libraries of  $10^8$  cells. However, many laboratories do not have ready access to flow cytometers, somewhat restricting the use of cell-based libraries for protein engineering.

In addition to the availability issue, sorting a library greater than  $10^{10}$  clones by cytometer would be time-consuming. Commercially available flow cytometers are capable of sorting cells at a rate  $10^7$  to  $10^8$  cells/hr, with state-of-the-art machines sorting at about  $4 \times 10^8$  cells/hr (Ashcroft and Lopez, 2000). To sort a library of  $10^{10}$  clones, flow cytometric analysis would require about one day of sorting time. Example of such a large library is naive human antibody library. An initial library of  $1 \times 10^{10}$  clones may be required to obtain antibodies with affinities in the nanomolar range (Griffiths and Duncan, 1998). To reduce both initial library size and sorting time, magnetic cell sorting has been employed to pre-enrich target cells from a library greater than  $10^8$  cells prior to flow cytometric screening (Christmann, et al., 1999; Wentzel, et al., 1999). Magnetic separation is convenient, simple, fast and has been utilized in many applications for cell isolation (Chalmers, et al., 1998; Safarik and Safarikova, 1999). However, the quantitative enrichment capabilities of magnetic bead capture have not been demonstrated previously. Therefore, we have used model antibody systems to test the feasibility of magnetic bead separation as an alternative, quantitative screening tool for cell-based polypeptide library screening.

The model antibodies used for most of the studies were anti-fluorescein antibodies (an antibody/hapten system). 4-4-20 is an anti-fluorescein antibody with  $K_D$  of  $0.7 \pm 0.3$  nM (in PBS). The single chain Fv (scFv) fragment of 4-4-20 was expressed on the yeast surface as described previously (Boder, et al., 2000). Higher affinity scFv mutants, namely 4M2.5, 4M3.6 and 4M3.7, which were previously isolated by screening



randomly mutagenized libraries of yeast surface-displayed anti-fluorescein scFv (Boder, et al., 2000), were also displayed on yeast and employed in this study, along with the 4-4-20 scFv. Different ratios of 4-4-20-displaying cells to cells displaying no scFv were mixed, incubated with biotinylated antigen and then captured by streptavidin-coated magnetic beads. This method was used to capture 4-4-20 displaying cells (binders) from an excess of non-displaying cells (nonbinders). The ability to isolate binders from nonbinders by magnetic bead capture was further explored in an antibody/protein system, D1.3 scFv / hen egg lysozyme. Furthermore, a kinetic screen for slower dissociation was performed to enrich 4M3.6-displaying cells from an excess of 4M2.5-displaying cells (7.7-fold lower in dissociation rate than 4M3.6). The effects of shear on the enrichments of favorable mutant by magnetic bead capture in binder identification and kinetic screening cases were also determined. The abilities of magnetic beads to both quantitatively isolate binders in an excess of non-binders, and isolate improved mutants in a kinetic screen for slower dissociation were assessed.

## **4.2 Materials and Methods**

### **4.2.1 Yeast Strains and Plasmids**

The yeast strain used in this study was EBY100 (Boder and Wittrup, 1997). Four display plasmids containing different anti-fluorescein single chain Fv (scFv) fragments genes: pCT302 (4-4-20, wild-type), pCT4M2.5, pCT4M3.6 and pCT4M3.7 were previously prepared (Boder, et al., 2000). The pCT201-D1.3, an anti-hen egg lysozyme D1.3 scFv displaying plasmid, was also previously prepared (VanAntwerp and Wittrup, 2000). Each of the plasmids previously described contained a Trp marker and was

transcribed for a single copy of scFv per display unit (a disulfide-bonded Aga1 and Aga2 yeast cell wall proteins) (Boder and Wittrup, 1997). A standard pRS315 CEN shuttle vector providing the LEU2 marker was used for the differentiation of different scFv displaying cells on selective media (Sikorski and Hieter, 1989). Plasmids were transformed into yeast (EBY100) using Frozen EZ Yeast Transformation II™ (ZYMO Research, Orange, CA).

#### **4.2.2 Materials and Media**

2.8µm-diameter streptavidin-labeled paramagnetic beads (Dynabead® M-280 streptavidin, magnetic mass susceptibility of  $100 \pm 25 \times 10^{-6} \text{ m}^3/\text{kg}$ ) were obtained from DYNAL (Lake Success, NY). Antigens including fluorescein-biotin, and hen egg lysozyme (HEL) were purchased from Sigma (St. Louis, MO). HEL was biotinylated using the FluoReporter Protein Labeling Kits (Molecular Probes, Eugene, OR). Streptavidin-phycoerythrin (PharMingen, San Diego, CA) was used as labeling reagents. The buffer used was phosphate-buffered saline (PBS) with 0.1% bovine serum albumin (BSA) (0.14M NaCl, 2.7mM KCl, 10mM Na<sub>2</sub>HPO<sub>4</sub> and 1.8mM KH<sub>2</sub>PO<sub>4</sub>, 1g/L BSA, pH adjusted to 7.4). All experiments were performed in PBS/BSA.

Both rich medium and synthetic mediums were used for yeast cultures. Rich medium YPD was prepared with 10g/L yeast extract, 20g/L peptone and 20g/L dextrose. Synthetic medium SD-CAA contained 20g/L glucose, 7g/L yeast nitrogen base, 5.4g/L Na<sub>2</sub>HPO<sub>4</sub>, 7.4g/L NaH<sub>2</sub>PO<sub>4</sub> and 5g/L casamino acid (-ura, -trp, DIFCO, Franklin Lakes, NJ). SG-CAA was prepared in the same way as SD-CAA, except glucose was replaced with 20g/L of galactose. SD-SCAA and SG-SCAA (-ura, -trp, -leu) were also prepared similarly, except 2x SCAA synthetic amino acid instead of casamino acid was used

(Shusta, et al., 1998). SD-SCAA agar plates with different amino acid supplements were prepared similarly as the media listed above, except with additional 17g/L of agar (DIFCO) and 182g/L of sorbitol.

#### **4.2.3 Growth and Induction**

Yeasts containing single display plasmid (pCT302, pCT4M2.5, pCT4M3.6, pCT4M3.7 or pCT201-D1.3) were grown in SD-CAA at 30°C (in a 250rpm shaker) for 24 hr. To induce the display of scFv, cells from the SD-CAA cultures were collected to inoculate 5 ml of SG-CAA to a starting OD<sub>600</sub> of about 1. These cultures were grown at 20°C for 20 to 22hr. Yeasts containing one display plasmid and an extra LEU2 plasmid (pRS315) were grown and induced identically, except the media used for growth and induction were SD-SCAA and SG-SCAA (-ura, -trp, -leu) respectively. Non-displaying cells (nonbinders) were prepared by growing yeasts containing only LEU2 plasmid (pRS315) in SD-SCAA (-ura, -leu) media at 30°C for 24 hr.

#### **4.2.4 Fluorescence Labeling and Measurements**

About  $2 \times 10^6$  yeast cells display anti-fluorescein scFv were incubated with 80nM fluorescein-biotin (FL-B) at 25°C for 30min (time for equilibrium binding). There was about 50-fold molar excess of FL-B over antibody, assuming  $10^5$  scFv per cell. After the primary label, cells were washed in cold PBS/BSA (4°C) and then incubated on ice with streptavidin-phycoerythrin (1:100 dilution) for 30min. Shorter secondary labeling time (about 7 min) was used for labeling wild-type 4-4-20 displaying cells to prevent extensive dissociation of primary label. Cells, with secondary label, were washed and then suspended in cold PBS/BSA. The mean fluorescence of the cells was measured by Coulter® Epic® XL™ flow cytometer.

#### 4.2.5 Binder Identification from Magnetic Bead Capture

Experiments with different initial ratios of 4-4-20 displaying cells (binder) to nonbinders were performed. At least 1000 4-4-20 cells were used to avoid stochastic effects of small numbers (small number of binders recovered from the magnetic beads) on experimental results. The initial concentrations of nonbinders were either  $1 \times 10^7$  cells/ml or  $1 \times 10^8$  cells/ml, depending on the binder to nonbinder ratio required. In each experiment, 4-4-20-displaying cells and excess of nonbinders were mixed in 1ml PBS/BSA, and incubated with 80nM of FL-B (about 50-fold molar excess) at 21°C for 1 hr on a rotator (20rpm). Excess ligand was washed away in cold PBS/BSA (4°C), and then cells with FL-B bound were mixed with streptavidin-labeled magnetic bead at a ratio of 10 beads to 1 cell displaying scFv (bead to binder ratio was optimal at a ratio about 10:1 and at least  $10^8$  beads/ml was required to prevent bead loss during procedural handling, data not shown). Microcentrifuge tube containing magnetic beads and cells was simply end-over-end turned at 4°C for 2min. Capture was performed at 4°C to prevent the dissociation of bound ligand. A magnet was then applied to select out the beads, and the supernatants were removed. The magnetic beads with attached cells were cultured in 2ml YPD media at 30°C (in a 250rpm shaker) for about 3 hours (more than one doubling time) to separate the captured cells from the beads. Dilutions of starting culture, supernatant collected and culture grown from the beads were plated on SD-SCAA (-ura, -leu, 4-4-20 + NB) and SD-SCAA (-trp, -ura, -leu, 4-4-20) agar plates to determine the enrichment ratio and supernatant loss percentage.

Selection with applied shear force was performed to isolate binders from excess of nonbinders. About 960 4-4-20-displaying cells and  $1.07 \times 10^8$  non-binders were

mixed, incubated with 80nM FL-B at 21°C for 1hr on a rotator (20rpm), washed and then captured by magnetic beads at 4°C, as previously described. After the first capture, magnetic beads with attached cells were washed, vortexed for about 15sec and resuspended in room temperature PBS/BSA. The magnet was applied and the supernatant was removed. The supernatant collected from the wash was incubated with 80nM FL-B at 21°C for 1hr on a rotator again and then captured by magnetic beads at 4°C without additional vortexing (simple end-over-end turning). The magnetic beads from the first and second captures were pooled together and grown in 2ml YPD media at 30°C for about 3 hours to isolate cells from the cell/bead complexes. Dilutions of starting culture, supernatant collected and culture grown from the beads were then plated on SD-SCAA(-ura, -leu, 4-4-20 + NB) and SD-SCAA(-trp, -ura, -leu, 4-4-20) agar plates. The same procedure (selection with shear) was performed to enrich 1600 D1.3 displaying cells from  $1.68 \times 10^8$  nonbinders, except cells were labeled with 80nM of biotinylated HEL, instead of FL-B, at 21°C.

#### **4.2.6 Dissociation Kinetics by Fluorescent Measurement and Magnetic Bead**

$2 \times 10^6$  anti-fluorescein displaying cells were incubated with 80nM FL-B at 21°C for 1 hr, washed with cold PBS/BSA, and then incubated with 560nM of 5-aminofluorescein, a competitor (about 350-fold molar excess) at 21°C for different length of time. At different points in the competition phase, cells were washed with cold PBS/BSA and labeled with streptavidin-phycoerythrin at 4°C for 30min. After secondary labels, the cells were washed and their mean fluorescence was detected by a flow cytometer. The decrease of mean fluorescence (F) as a function of time was fitted with an exponential decay function ( $F = F_0 e^{-kt} + F_\infty$ , where  $F_0$  is the initial mean fluorescence of

labeled cells and  $F_{\infty}$  is the background fluorescence of unlabeled cells) to determine the dissociation rate constant ( $k$ ) of polypeptide/ligand complex. Meanwhile, magnetic bead capture was also used to determine the dissociation kinetics. The procedures were similar to those by mean fluorescence measurement. Instead,  $3 \times 10^6$  anti-fluorescein displaying cells were used, and instead of labeling with streptavidin-phycoerythrin, cells at different points of competition phase were captured by  $10^8$  magnetic beads at  $4^{\circ}\text{C}$ . A magnet was applied to isolate the magnetic beads and the supernatant was removed. The optical density ( $\text{OD}_{600}$ ) of the supernatant was then measured to determine the amount of cells captured by magnetic beads. The decrease in binder amount ( $B$ ) as a function of time was fitted with an exponential decay function ( $B=B_0e^{-Kt}+B_{\infty}$ , where  $B_0$  is the initial amount of binder and  $B_{\infty}$  is the amount captured due to non-specific binding) to determine the dissociation rate constant ( $K$ ) of bead/cell complex.

#### **4.2.7 Kinetic Screening by Magnetic Bead Capture**

4M3.6-displaying cells were transformed with a standard pRS315 CEN shuttle vector providing the Leu marker. This additional plasmid did not affect cell growth or surface expression but allowed for the differentiation of cells on selective media plate. About  $5.4 \times 10^3$  of 4M3.6 cells and  $8.7 \times 10^6$  of 4M2.5 cells were mixed, saturated with 80nM FL-B at  $21^{\circ}\text{C}$  for 1 hr on a rotator (20rpm), washed and incubated with 5-aminofluorescein at  $21^{\circ}\text{C}$  on a rotator (20rpm) for different lengths of competition times. Then, at different points of competition phase, cells were washed with minimal shear force and then captured by the magnetic beads at  $4^{\circ}\text{C}$ . The magnetic beads with attached cells were cultured in 2ml YPD media at  $30^{\circ}\text{C}$  (in a 250rpm shaker) for about 3 hr. Dilutions of the starting culture, supernatant collected and cultures grown from magnetic

beads, were plated on SD-SCAA (-ura, -trp, -leu, 4M3.6) and SD-SCAA (-ura,-trp, 4M2.5 + 4M3.6) media.

Selection with applied shear force was carried out to kinetically screen for improved mutants. About 600 4M3.6 cells and  $5.7 \times 10^7$  4M2.5 cells were mixed and screened kinetically as described above with 90min of competition time. However, after the first capture, isolated magnetic beads with cells bound were vortexed in PBS/BSA solution for about 10sec. Then, supernatant was removed and those vortexed magnetic beads were cultured in YPD media at 30°C for about 3 hr. Dilutions of cultures were plated as described above.

### **4.3 Results**

#### **4.3.1 Model System Validation**

The model antibody used for most of these studies is the anti-fluorescein antibody 4-4-20 and higher affinity mutants, which were described earlier (Boder, et al., 2000). Four different anti-fluorescein scFv fragments with varying dissociation rate constants, namely 4-4-20 (wild type), 4M2.5, 4M3.6, and 4M3.7, were displayed as a monolayer on the surface of *Saccharomyces cerevisiae* cells.

Flow cytometry quantitatively discriminates cell surface ligand density variations via fluorescence intensity differences. The capability of magnetic bead capture to discriminate cell surface ligand density differences was tested. Yeast cells displaying anti-fluorescein scFvs were labeled with different surface densities of fluorescein biotin (as described in *Materials and Methods*), and then captured with streptavidin-coated magnetic beads. Figure 4.1 shows that the cell capture probability (capture fraction) by

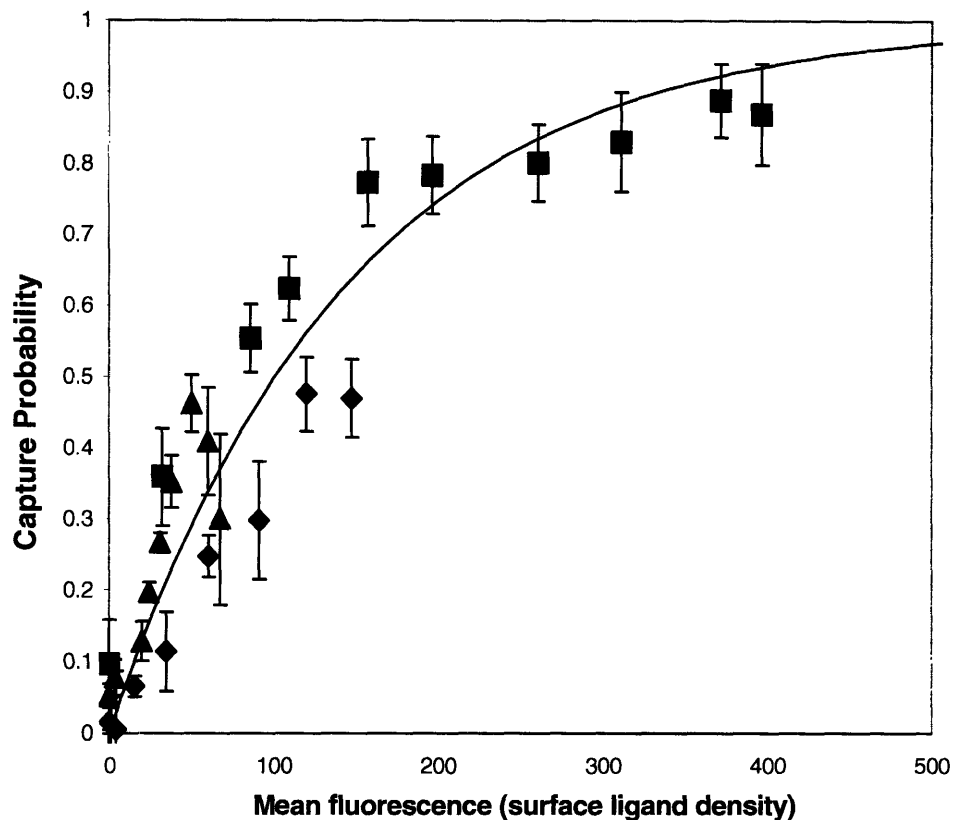


**Figure 4.1 Capture Probability of anti-Fluorescein scFv Displaying Cells by Magnetic Beads Increases with Increasing Surface Ligand Density.** Cells labeled with varying levels of fluorescein-biotin ligand were captured by streptavidin-labeled magnetic beads. Cells were also labeled with streptavidin-phycoerythrin and their mean fluorescence is determined by flow cytometer. Capture probabilities of cells displaying three different scFv mutants are plotted as a function of mean fluorescence of the mutants. The line represents an exponential least-square fit of all three data sets, simply as an empirical correlation without a theoretical basis. ◆ = cells displaying scFv 4M2.5 ( $k_{\text{off}} = 6.9 \times 10^{-2} \text{min}^{-1}$  at  $21^{\circ}\text{C}$ ), ■ = cells displaying scFv 4M3.6 ( $k_{\text{off}} = 8.9 \times 10^{-3} \text{min}^{-1}$  at  $21^{\circ}\text{C}$ ), and ▲ = cells displaying scFv 4M3.7 ( $k_{\text{off}} = 4.0 \times 10^{-3} \text{min}^{-1}$  at  $21^{\circ}\text{C}$ ). Error bars represent mean standard deviations of three replicates.



magnetic beads increases with increasing surface ligand density and levels off at high surface ligand density. Cells with higher surface ligand density have a monotonically higher probability of being captured by the magnetic beads. Furthermore, the correlation between ligand density and bead capture is surprisingly quantitative given the potential variability in multivalency, shear, and mixing conditions. This result indicates that magnetic beads are able to preferentially capture cells with higher ligand density in a fashion analogous to flow cytometric sorting, and provides the fundamental basis for using magnetic beads to perform quantitative screening.

Two important indicators were considered to gauge the success of a screening experiment: the single-pass enrichment ratio (defined as the ratio of the fraction consisting of the desired subpopulation before and after screening) and the percentage loss of cells displaying the binding protein of interest (“binders”). Ideally, the single-pass enrichment ratio should be as close to the theoretical maximum enrichment ratio as possible (high purity), whereas the percentage loss should be as low as possible (high yield). However, a tradeoff between yield and purity is generally to be expected, as for all separations processes.

Direct plating of the cells on selective media was validated as a measure of screen success by comparison with mean fluorescence measurements by flow cytometry. Approximately equal numbers of 4-4-20-displaying cells (yeast strain EBY100 transformed with pCT302) and non-displaying cells (yeast strain EBY100 transformed with pRS315) were mixed, incubated with FL-B, washed and then captured with magnetic beads. Separately, those cultures were also labeled with streptavidin-phycoerythrin, and immunofluorescent labeling was measured in a flow cytometer. The

percentage loss of binders and the enrichment ratio were then determined by each method. Table 4.1 shows the initial proportion of binders to non-binders, the supernatant loss percentage and the enrichment ratio from direct plating and flow cytometric analysis. Note that the initial proportion of binder to non-binder calculated from the direct plating is somewhat different from flow cytometric analysis. A certain measurable proportion (about 20-50%) of cells carrying plasmid pCT302 (4-4-20) do not display scFv on the surface (likely due to retention in the secretory pathway) (Robinson and Wittrup, 1995), and are characterized by a negative peak in the histogram. However, these cells are still capable of synthesizing tryptophan due to the presence of the TRP1 gene on the pCT302 plasmid, and survive in SD-SCAA (-trp,-ura) media. This accounts for the higher initial binder proportion measured by the plating method. After correcting the display fraction in 4-4-20-displaying cells, Table 4.1 shows that the supernatant loss percentage and enrichment ratio determined from the direct plating agree well with those from the flow cytometric analysis. Therefore, direct plating was used to determine the supernatant loss percentages and enrichment ratios in subsequent experiments where the percentage of binders is too small to reliably measure by flow cytometry.

#### **4.3.2 Isolation of binders from nonbinders**

Identification of lead molecules from large diverse repertoires requires selection of rare binding events from a large excess of nonfunctional clones. The proficiency of magnetic bead separation to isolate binders from excess nonbinders was examined. Experiments with different ratios of nonbinders to binders were performed to determine their respective enrichment ratio and supernatant loss percentage. Minimal shear force was applied in the washing step to avoid separating captured cells from the magnetic

**Table 4.1 Agreement of Direct Plating and Fow Cytometer Results for Displayed Fraction.** Supernatant loss percentage and single-pass enrichment ratio of 4-4-20-displaying cells from excess of non-displaying cells (EBY100::pRS315) are determined from direct plating and flow cytometry.

(Method)	-Trp plates (4-4-20)	+Trp plates (4-4-20 + NB <sup>a</sup> )	Proportion
Initial Population			
(Plating)	$4.36 \pm 0.07 \times 10^6$	$1.13 \pm 0.08 \times 10^7$	$39 \pm 4 \% ^b$
(Cytometer)			$18.9 \pm 0.9\%$
Corrected for the display population of 4-4-20			
Methods	Supernatant loss %	Enrichment ratio	Maximum theoretical enrichment ratio
Plating	$4.4 \pm 0.4\%$	$5.0 \pm 0.7$	5.3
OD + Cytometry	$7.49 \pm 0.16\%$	$4.02 \pm 0.11$	

<sup>a</sup> NB- Non-Binder, EBY100::pRS315

<sup>b</sup> Average and standard deviation of three replicates

beads (i.e. manual end-over-end turning of a microcentrifuge tube for 2 minutes). As shown in Table 4.1, under a starting proportion of about 5 nonbinders to 1 binder, the enrichment ratio is about 4 to 5-fold and the supernatant loss percentage is about 4 to 7%. Figure 4.2 shows the single-pass enrichment ratio and supernatant loss percentage of binders at binders to non-binder ratios of 1:14 to 1:60000. The initial total cell concentration (binders + nonbinders) was about  $10^7$  cells/ml for all but one ratios, at 1:60000, the initial total concentration was about  $10^8$  cells/ml. This tenfold higher concentration of initial non-binder at 1:60000 leads to a somewhat higher extent of steric effect and non-specific binding to the magnetic beads, resulting in a lower single-pass enrichment ratio.

To enhance the single-pass enrichment ratio, shear force was applied in the washing step to lower non-specific binding of cells to the magnetic beads (refer to *Materials and Methods* section for detailed procedure.) Table 4.2 shows that with a starting ratio of about 1 binder in  $1 \times 10^5$  nonbinders, the single-pass enrichment ratio is 9400 fold and the supernatant loss percentage is 85%. The results indicate that shear force increases the single-pass enrichment ratio, at the cost of an increase in the supernatant loss percentage, as shear force strips specific binders from beads. As expected, higher enrichment ratio is attained at the cost of a decreased yield of binders. Having demonstrated that the magnetic bead capture protocol is capable of isolating binders in an antibody/hapten (4-4-20/fluorescein) recognition system, an antibody /protein antigen recognition system was tested to generalize this protocol. The antibody/protein system used was D1.3, an anti-hen egg lysozyme (HEL) antibody, and HEL. The scFv fragment of D1.3 was displayed on the surface of yeast cells. The D1.3

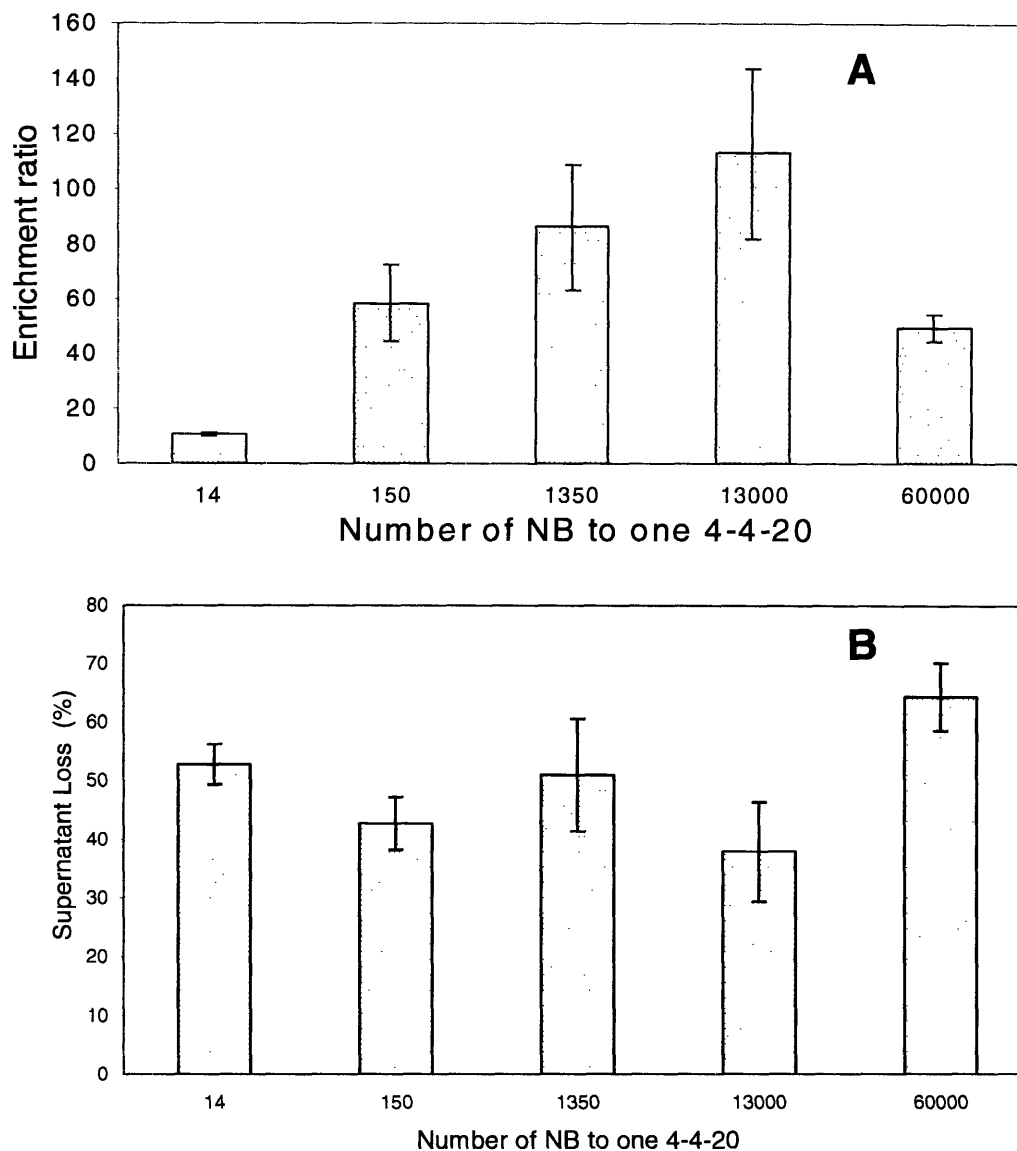


**Figure 4.2 Single-Pass Enrichment Ratio (A) and Supernatant Loss Percentage (B) of Binders (4-4-20-Displaying Cells) from Non-Binders (NB, Non-Displaying Cells) at Different Initial Ratios.** The single-pass enrichment ratio and supernatant loss percentage are calculated from the direct plating of the starting culture, supernatant and the culture captured on bead. Minimal shear force is applied to remove captured cells on the magnetic beads (i.e. end-over-end mixing). Individual data set (each ratio of binder to non-binder) is performed on separate days and with freshly prepared cells. The initial total cell concentration is  $10^7$  cells/ml for all experiments except at 1:60000, where total cell concentration is  $10^8$  cells/ml. Error bars represent mean standard deviation of three replicates.

**Table 4.2 Vigorous Shear Force Increases the Single-Pass Enrichment Ratio of Binder from Non-Binder.** Supernatant loss percentage and single-pass enrichment ratio of 4-4-20-displaying cells from excess of non-displaying cells (EBY100::pRS315) with shear force applied in the washing step.

(Method)	-Trp plates (4-4-20)	+Trp plates (4-4-20 + NB <sup>a</sup> )	Proportion	Enrichment Loss (max. theoretical)
Start	960 ± 140	1.07 ± 0.02 x 10 <sup>8</sup>	9.0 ± 1.4x10 <sup>-4</sup> % <sup>b</sup>	
Supernatant	810 ± 60	1.05 ± 0.09 x 10 <sup>8</sup>	7.7 ± 0.8x10 <sup>-4</sup> %	85 ± 6%
Recovered from bead	120 ± 40	1500 ± 700	8.4 ± 1.5%	<b>9400 ± 1800 fold</b> (110000-fold)

<sup>a</sup> NB- Non-Binder, EBY100::pRS315

<sup>b</sup> Average and standard deviation of three replicates

procedure was similar to the procedure of isolating 4-4-20-displaying cells under shear condition, except biotinylated HEL was used as linker. Table 4.3 shows that the single-pass enrichment ratio of D1.3-displaying cells is about 1200 fold, and the supernatant loss percentage is about 80%. Variability was somewhat higher for this antibody/antigen system in three independent replicate experiments, for unknown reasons. These data show that magnetic bead isolation is generalizable to antibody/protein antigen systems.

### **4.3.3 Affinity Maturation**

In addition to isolating new binding molecules, a common application of library screening is affinity maturation of a lead-binding molecule. The ability of magnetic beads to isolate improved library mutants from an excess of lower-affinity mutants was examined. Improved binding mutants within a library may be isolated by selectively labeling in an equilibrium binding screen or by a kinetic screen for slowed dissociation (Boder and Wittrup, 1998). Magnetic bead screening utilizes analogous equilibrium and kinetic screens as in flow cytometric screening. In an equilibrium screen, cells displaying polypeptides are incubated at a concentration of labeled ligand below the equilibrium dissociation constant of the wild-type polypeptide/ligand complex. Cells displaying high-affinity polypeptides will be preferentially labeled compared to those cells displaying low-affinity polypeptides. As shown in Figure 4.1, cells labeled with higher surface ligand density will be preferentially captured on the magnetic bead. Concentration of the labeled ligand will likely determine the range of enrichment achieved in an equilibrium screen. In a kinetic screen, an excess of unlabeled ligand is added to cells displaying polypeptides that are first labeled to saturation with labeled ligand. The decrease in cell-

**Table 4.3 Enrichment of Binder from Non-Binders using Protein Antigen (Lysozyme).** Supernatant loss percentage and single-pass enrichment ratio of D1.3-displaying cells from non-displaying cells (EBY100::pRS315) with shear forces applied in the washing step.

(Method)	-Trp plates (D1.3)	+Trp plates (D1.3 + NB <sup>a</sup> )	Proportion	Loss	<b>Enrichment</b> (max. theoretical)
Start	1600 ± 400	1.68 ± 0.11 x 10 <sup>8</sup>	9.5 ± 1.7x 10 <sup>-4</sup> % <sup>b</sup>		
Supernatant	1260 ± 130	1.6 ± 0.2 x 10 <sup>8</sup>	7.9 ± 1.1x 10 <sup>-4</sup> %	80 ± 20%	
Recovered from bead	310 ± 160	1.4 ± 2.1 x 10 <sup>5</sup>	1.2 ± 1.6%		<b>1200 ± 1400-fold</b> (110000-fold)

<sup>a</sup> NB- Non-Binder, EBY100::pRS315

<sup>b</sup> Average and standard deviation of three replicates



bound labeled ligand is followed with time. Mutants with slower polypeptide/ligand dissociation constant will preferentially have higher labeled ligand density on their surfaces, resulting in a higher probability of capture by magnetic beads. In a kinetic screen, the duration of competition time will determine the range of affinity improvement likely to be selected from the library.

Dissociation kinetics of 4M2.5, 4M3.6 and 4M3.7 displaying cells were tracked by mean fluorescence measurement and magnetic bead capture. The dissociation of bound ligands from cell surfaces directly resulted in a decrease of mean fluorescence of the cells. The monovalent polypeptide/ligand dissociation rate constants could be determined by fitting the decrease in mean fluorescence to an exponential decay. Meanwhile, cells with decreasing surface-bound ligands also resulted in a decrease of the amount of binders captured by magnetic beads. The multivalent cell/bead dissociation rate constants could be determined by monitoring the decreasing capture probability. Figure 4.3 shows the dissociation kinetics of three different scFv displaying cells: 4M2.5, 4M3.6 and 4M3.7 determined both by mean fluorescence measurement and magnetic bead capture at 21°C. (The data presented in Figure 4.3 were those used to construct the relationship shown in Figure 4.1.) The dissociation rate constants determined by mean fluorescence measurement at 21°C were  $6.9 \times 10^{-2} \text{min}^{-1}$ ,  $8.9 \times 10^{-3} \text{min}^{-1}$ , and  $4.0 \times 10^{-3} \text{min}^{-1}$  for 4M2.5, 4M3.6 and 4M3.7 respectively. Meanwhile, the dissociation rate constants determined by magnetic bead capture at 21°C were  $4.9 \times 10^{-2} \text{min}^{-1}$ ,  $2.9 \times 10^{-3} \text{min}^{-1}$ , and  $2.1 \times 10^{-3} \text{min}^{-1}$  for 4M2.5, 4M3.6 and 4M3.7 respectively. The dissociation kinetics of antibody/hapten and cell/bead complexes tracked by respective methods were surprisingly similar. The characteristic dissociation rate constants determined by bead

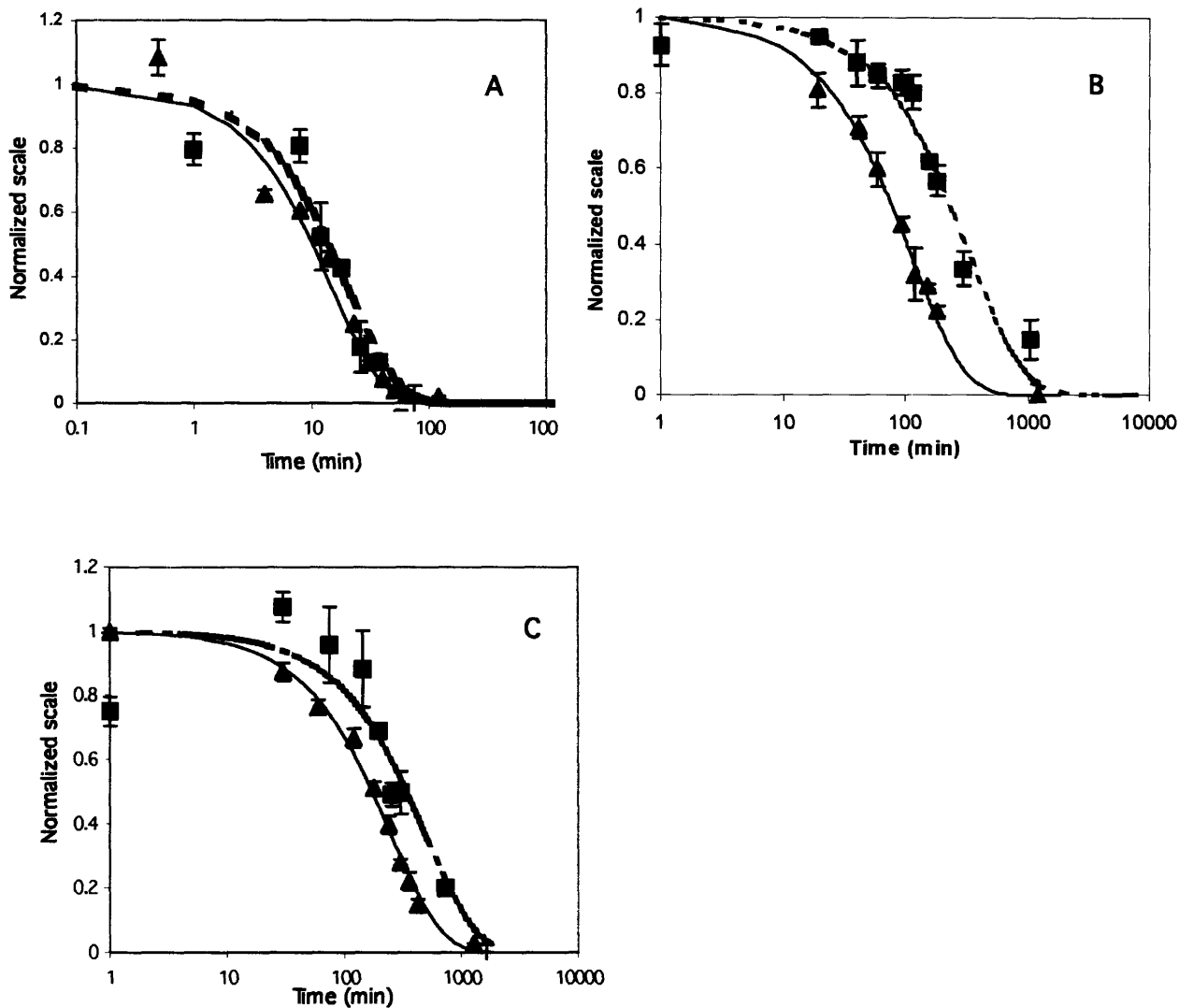


**Figure 4.3 Quantitative Dissociation Rates Tracked by Magnetic Bead Capture.** Dissociation rates of ligand from cell surfaces are determined for three anti-fluorescein scFv displaying cells: (A) 4M2.5, (B) 4M3.6 and (C) 4M3.7 by magnetic bead capture and mean fluorescence measurement. ■ = dissociation rate by magnetic bead capture. ▲ = dissociation rate by mean fluorescence measurement. Data are fit to an exponential decay with nonlinear least-square regression (solid line for mean fluorescence measurement, dashed line for magnetic bead capture). Mean fluorescence is normalized by initial fluorescence, and amount of cell capture is normalized by the initial amount of binder. Error bars represent mean standard deviations of three replicates.

capture were lower than the dissociation rate constants from the fluorescence measurement. Bead/cell complex formation involves multivalent interactions of antibody and hapten on the beads and cell surfaces, and this avidity effect would be expected to contribute to the observed slower dissociation rate. These results indicate that magnetic bead capture is capable of tracking dissociation rates in nearly as quantitative a fashion as mean fluorescence measurement.

A validation experiment for a magnetic bead kinetic screening protocol was performed to enrich 4M3.6-displaying cell (high affinity mutant) from an excess of 4M2.5-displaying cells (7.7-fold slower in polypeptide/ligand dissociation rate). The initial ratio of improved mutant (4M3.6) to “wild-type” (4M2.5) was 1:1600 (refer to Materials and Methods for procedure). During the experiment, cells were washed with minimal shear force. Figure 4.4 shows the enrichment ratio and supernatant loss percentage of 4M3.6 as a function of competition time. As in kinetic screening by flow cytometry, the enrichment ratio increases initially with competition time, peaks at an optimal competition time, and eventually decays back to about 1 (no enrichment) as labeling reaches background (Figure 4.4A). Meanwhile, the loss of 4M3.6 increases with increasing times (Figure 4.4B), as the labeled ligand on 4M3.6 displaying cells continue to dissociate. Thus, magnetic bead separation can kinetically screen for slower dissociation mutants, as with flow cytometry.

The effect of applied shear force on the enrichment ratio and supernatant loss percentage of a kinetic screen was determined. The initial ratio of improved mutants to wild type was 1:10<sup>6</sup>. After the first capture, the magnetic beads with cells attached were vortexed in PBS/BSA (refer to *Materials and Methods* for detail procedure). Table 4.4

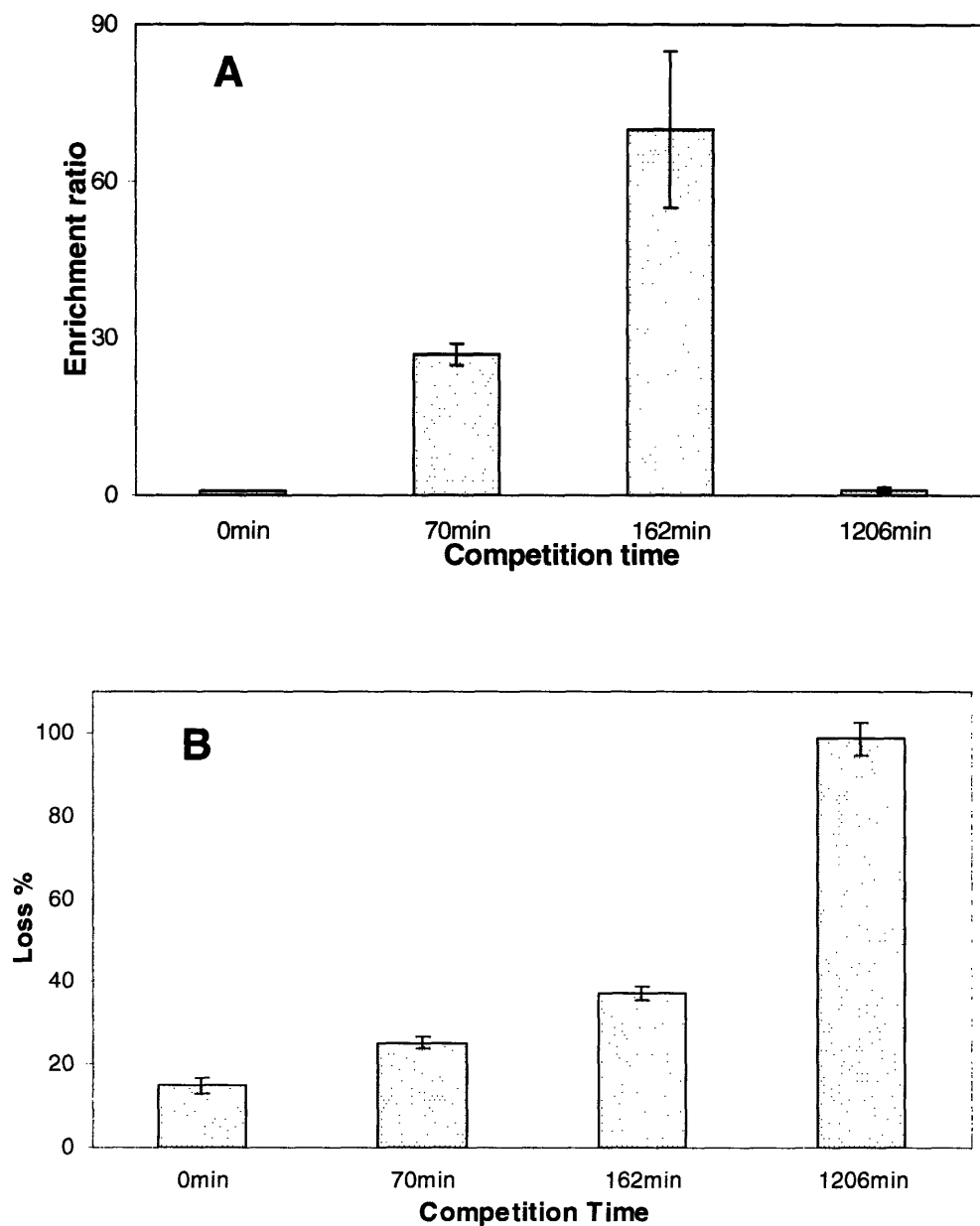


**Figure 4.4 Kinetic Screen for Slower Dissociation Rate Mutants.** Single-pass enrichment ratio (A) and supernatant loss percentage (B) of 4M3.6-displaying cells from excess of 4M2.5 displaying cells as a function of the competition time. Using magnetic bead, kinetic screen is performed to enrich 4M3.6-displaying cells ( $k_{\text{off}}=8.9 \times 10^{-3} \text{min}^{-1}$  at  $21^{\circ}\text{C}$ ) from excess of 4M2.5-displaying cells ( $k_{\text{off}}=6.9 \times 10^{-2} \text{min}^{-1}$  at  $21^{\circ}\text{C}$ ). Initially, the ratio of 4M3.6-displaying cells to 4M2.5-displaying cells is 1:1600. 5-aminofluorescein is used as a competitor and the competition is performed at room temperature ( $21^{\circ}\text{C}$ ). Minimal shear force is applied during the bead washing step. Error bars represent mean standard deviation of three replicates.

**Table 4.4 Shear Enhancement of Enrichment Ratio in the Kinetic Screen.** Supernatant loss percentage and single-pass enrichment ratio of 4M3.6-displaying cells from excess of 4M2.5-displaying cells under kinetic screen without and with additional shear force applied in washing step.

(Method)	-Leu plates (4M3.6)	+Leu plates (4M3.6 + 4M2.5)	Proportion	Loss	Enrichment <sup>a</sup> (max. theoretical)
Start	600 ± 170	5.7 ± 0.7 × 10 <sup>7</sup>	1.04 ± 0.12 × 10 <sup>-3</sup> % <sup>b</sup>		
<b>Without Shear</b>					
Supernatant	180 ± 30	5.1 ± 0.3 × 10 <sup>7</sup>		26 ± 10%	
Recovered from bead	590 ± 70	7.5 ± 0.3 × 10 <sup>5</sup>	8.0 ± 1.0 × 10 <sup>-2</sup> %		<b>70 ± 20-fold</b> (96000-fold)
<b>With Shear</b>					
Supernatant	410 ± 40	5.11 ± 0.11 × 10 <sup>7</sup>		75 ± 24%	
Recovered from bead	157 ± 15	2.81 ± 0.19 × 10 <sup>4</sup>	0.56 ± 0.07%		<b>600 ± 200-fold</b> (96000-fold)

<sup>a</sup> 90min of competition time

<sup>b</sup> Average and standard deviation of three replicates

shows the enrichment ratio and supernatant loss percentages for the kinetic screen with and without additional shear applied. With additional shear, there is about a 10-fold increase in single-pass enrichment ratio and about 3-fold increase in supernatant loss percentage. Table 4.4 shows that shear reduces the amount of cells captured by beads, with more significant effect on low-affinity binders. Low-affinity binders have relative lower surface ligand density than high-affinity binders after the competition, rendering the low-affinity binders more easily removed by shear. Thus, shear can increase single-pass enrichment ratio in a kinetic screen by magnetic beads, at the expense of higher percentage loss of improved mutants. Therefore magnetic beads are capable of quantitatively screening for both novel binders and improved mutants.

#### **4.4 Discussion**

Magnetic bead capture has been shown to quantitatively discriminate varying surface ligand density as in flow cytometry, with magnetic bead cell capture probability correlated strongly with cell surface ligand density. Magnetic bead capture is able to isolate binders from an excess of nonbinders in both antibody/hapten and antibody/protein systems. Particularly, with an initial ratio of a one antibody-displaying cell (binder) in  $1.1 \times 10^5$  non-displaying cells (a frequency of binders typical for a small library), a single-pass enrichment ratio of  $9400 \pm 1800$  fold with a  $85 \pm 6\%$  binders loss are achieved from screening an antibody/hapten library. In addition, magnetic bead capture is capable of tracking dissociation kinetics of ligand/cell complexes and performing a quantitative kinetic screen for improved mutants with slower dissociation rate. With the presence of 7.7-fold higher affinity clones at 1: 95,000 in the initial library,

the magnetic bead method is able to enrich the improved mutant  $600 \pm 200$ -fold, at the expense of  $75 \pm 24\%$  probability of loss.

The sticking probability of cells mediated by specific cell surface interactions such as antibody/antigen under uniform shear force has been examined previously both theoretically and experimentally (Bell, 1978; Bell, 1981; Capo, et al., 1982; Long, et al., 1999). The models developed are generally based on two-body collision (formation of doublets), whereas in the experiments reported here, a cluster of (more than two) beads and cells in complex is formed by multiple collisions. These models, however, can still give some insight into the dependence of surface ligand density, intrinsic dissociation rate and shear effect on the formation and breakage of bead/cell complexes. Bell employed the frequency and duration of cell-cell collision and the number of bonds needed and required to hold the cells together to determine the sticking probability (Bell, 1981). Long et al. extended Bell's model to formulate the sticking probability from a set of binding kinetics equations of receptors and ligands (Long, et al., 1999). Both models and experimental results (Capo, et al., 1982) demonstrate that the two-body collision capture frequency (doublet formation rate) is linearly proportional to the cell surface ligand density at low surface ligand density. This dependence provides the fundamental basis for using magnetic beads to perform quantitative screening and agrees with our experimental results that higher surface ligand density leads to higher capture probability. In addition, once the bead/cell complexes are formed, external force (shear) on the bonds tends to accelerate their dissociation. Bell formulated the shear effect as an exponential dependence on the apparent reverse rate constant ( $k^n$ ) as follows (Bell, 1978)

$$k^n = k^0 \exp\left(\frac{\gamma F}{kTN}\right) \quad (1)$$

where  $k^0$  is the zero-force (intrinsic) reverse rate constant,  $\gamma$  is the bond interaction parameter,  $F$  is the force,  $N$  is the number of bonds,  $k$  is the Boltzmann constant and  $T$  is the absolute temperature. Equation 1 shows that increasing the shear force or having fewer bonds will increase the apparent reverse rate constant. During kinetic screening, the dissociation of ligands from cells displaying lower affinity receptors will be faster. Cell with lower surface density will be under high force per bond rendering them easier to separate from the bead/cell complex. This is shown by the shear enhancement of enrichment ratio in both binder identification and kinetic screening cases, as the shear force preferentially removes the lower affinity binder (binder with lower surface density).

The enrichment ratios obtained from magnetic bead screening indicate that magnetic bead capture is able to quantitatively screen for improved mutants, as with flow cytometric analysis. It is very difficult to exactly compare the enrichment ratios obtained here with those from flow cytometric analysis, because of the different experimental conditions, but a comparison should provide some insight into the potential for the magnetic screening method. Francisco et al. were able to achieve an enrichment ratio of about 300 fold each round in purifying the binders from  $10^5$ -fold excess background bacteria to almost homogeneous in two rounds (Francisco, et al., 1993). Enrichment factors of 2,000-10,000 fold per round may be achieved under optimal conditions (Georgiou, et al., 1997). These enrichment factors are comparable to those reported here. Using kinetic screening by flow cytometry, VanAntwerp and Wittrup were able to enrich a two-fold higher affinity mutant  $125 \pm 65$  fold with the presence of high-affinity mutant at a starting ratio 1:1000 (VanAntwerp and Wittrup, 2000). The magnetic bead method is able to achieve 70 to 600-fold enrichment factors in kinetic screening. Overall, based on



the single-pass enrichment ratios obtained, magnetic bead screening of cell-based polypeptide libraries appears to be approximately equivalent to flow cytometry.

Compared to flow cytometric analysis, magnetic bead screening method has both advantages and disadvantages. Magnetic bead screening is cheap, simple, fast, and convenient. It also has higher throughput than flow cytometric analysis, facilitating easy scale-up of library size to increase the number of clones of interest if needed. Therefore, larger libraries ( $> 10^8$  clones) can be sorted as readily and quickly as smaller library ( $10^6 - 10^7$  clones). However, a potentially significant disadvantage of magnetic bead screening is that it cannot discriminate an expression mutant (higher expression level) from true functional mutant (higher binding affinity). Due to the avidity effect from magnetic bead capture, a highly expressed low-affinity mutant may be captured at the same probability as a poorly expressed high-affinity mutant. By contrast, flow cytometric analysis can explicitly account for variation in the expression level with epitope normalization (two-color FACS). The fluorescence intensity of a second probe, which is used to specifically label a constant part of the displayed protein and quantify the expression level, is used to normalize the binding signal, facilitating the selection of functional traits independent of expression level (Boder and Wittrup, 1997). In addition, magnetic bead screening is not able to provide real-time quantitative multi-parameter statistical analysis of every library member as in flow cytometry. Although varying amounts of magnetic beads can potentially alter the amount of cells captured, the number of cells to be collected cannot be easily set as for flow cytometry. The gate setting of flow cytometric analysis can be readily modified to collect any desired fraction of the library. With a more sophisticated approach, such fine discrimination and fractionation of immunomagnetically labeled cells

may be achievable with colloidal or molecular magnetic labels in the near future (Chalmers, et al., 1998).

Magnetic beads have been utilized extensively in screening phage display libraries. For affinity maturation of D1.3 using phage display, 5 rounds of magnetic bead screening were used to enrich a mutant  $10^6$  fold by kinetic screening (Hawkins, et al., 1993). From our kinetic screening results, initial single-pass enrichment ratio of  $600 \pm 200$  fold is achieved. Therefore, we would predict that three to four rounds of magnetic bead screening should be sufficient to purify an improved mutant from a yeast-surface displayed library. As an approximate comparison, magnetic bead screening of yeast-surfaced displayed library compares well with phage display. In addition, adsorptive losses of rare clones are less significant in a yeast library, because phage particles, being much smaller than yeast cells, have higher tendencies to stick to glassware or beads. Also, only three to five copies of polypeptides are displayed on phage, so molecular randomness or stochastic effects inherent in the small number of binding reactions can lead to loss of rare clones. High copies of polypeptides ( $10^4$ - $10^5$  (Boder and Wittrup, 1997)), however, are displayed on the yeast surface, essentially eliminating random fluctuations by extensive averaging.

Earlier efforts at directed evolution with multivalently displayed phage were found to lead to extensive avidity effects that obscured the desired monovalent binding properties being engineered (e.g., only 2/11 selected antibodies exhibit higher affinity against pHOx antigen (Griffiths, et al., 1994)). Such artifacts are not a substantial issue for the approach described here, because the intrinsic competition occurs relative to a monovalent interaction with soluble biotinylated antigen, followed by a rapid capture step

that depends only on surface ligand density. The likely multivalent interactions between cells and beads serve only to define the bead capture probability relationship represented in Figure 4.1, whereas the surface ligand density is related directly to the monovalent binding equilibria and kinetics at the cell surface. Therefore, the capture probability is governed by well-defined monovalent binding interactions rather than the ill-defined (but empirically reproducible) cell-bead complex formation kinetics.

Magnetic bead capture has been shown to be a high-through quantitative screening tool for cell-based libraries. Magnetic bead screening can potentially be employed to screen cell-based naive antibody libraries of  $>10^9$  clones to identify antibodies against antigens of interest. As described here, magnetic bead screening currently utilizes soluble biotinylated antigen. One obstacle to use of a cell-based polypeptide library is the incapability of screening or selecting mutant cells against a membrane-bound antigen. Magnetic separation holds a conceivable solution to this problem. The understanding of the formation and breakage of bead/cell complexes should provide further insight into the cell/cell interactions, such as avidity effect, external shear effect, steric effect, non-specific binding and so on, and eventually could lead to development of screening protocols for cell-based polypeptide library against a membrane-bound antigen.

#### **4.5 Conclusion**

Currently, flow cytometric analysis has been employed extensively to quantitatively screen cell-based library for novel binders and improved mutants. Due to the limited availability of flow cytometers in many laboratories, magnetic bead screening

has been developed as an alternative quantitative screening tool for cell-based libraries. Specifically, the library is first equilibrated with biotinylated ligand, and then binders are isolated with streptavidin-coated magnetic beads. Results indicate that close to 10000-fold single-pass enrichment ratio are possible in screening for novel binder, and 600-fold single-pass enrichment ratio is achievable in a kinetic screening for a 7.7-fold higher affinity mutants. Magnetic bead separation is fast, simple, and convenient. The described methods are similar to procedures in common use for phage display, and should lower the barriers to entry for use of cell surface display libraries.

## Appendix

**Amino acid sequences of anti-HAAH scFv directly isolated from the non-immune library.** CDRs of the antibody are highlighted in yellow.

Clone 4-6

QVQLVQSEGGVVQPGRSLRLSCAASGFTFSSYAMHWVRQAPGKGLEWVAVISY  
DGSNKYYADSVKGRFTISRDN SKNTLYLQMNSLRAEDTAVYYCARDYYDFWSG  
SSPSYYYYGMDVWGQGT TTVVSSGSASAPTRNSRIRWRWQRRWWFRRRRAAGI  
L

Clone 6-8

QVQLQQSGPGLVKPSQTL SLTCAISGDSVSSNSAAWNWIRQSPSRGLEWLGRTY  
YRTK WYNEYAASVKGRATINPDT SKNQFSLQLNSVTPEDTAVYYCATDPKGVTT  
QYWGQGT LTVVSSGSASASTGILGSGGGGSGGGGSGGGGSGQPVL TQSPSASGTP  
GQRVTISCSGSTS NIGNRNYVYWYQRLPGTAPKLLIYRNNQRPSGAPARFSGSKSG  
TSTSLAISGLRSEDEAEYFCAAWDDSLSGWVFGGGTQLTVL

Clone 6-12

QVQLQQSGPGLVKPSQTL SLTCGISGDSVSSNSAAWNWIRQSPSRGLEWLGRTY  
YRSR WYNDYAASVKS RITVNADTSKNQFSLQLNSVTPEDTAVYYCARSVRYSSG  
WGF DYWGQGT LTVVSSGILGSGGGGSGGGGSGGGGSGQPVL TQSPSASGTPGQRI  
TISCSGSSSNIGNNYVYWYQQFPGTAPKLLVYRNNQRPSGVPDRFSGSKSGTSAS  
LAISGLRSEDEADYYCAAWDDSLSGRWVFGGGTKLTVL

Clone 6-13

QVQLQQSGPGLVKPSQTL SLTCAISGDSVSRNSAAWNLIRQSPSRGLEWLGRTYY  
RSK WYTDYAVSVKS RITINPDT SKNQFSLRLNSVTPEDTAVYYCARSGGGHAAAG  
KFDS WGRGTLTVVSSGILGSGGGGSGGGGSGGGGSGQPVL TQSPSASGTPGQRVTI  
PCSGSSSNIGSKYVYWYQHLPGTAPKLLIYRNNQRPSGVPDRFSGSKSGTSASLAI  
SGLRSEDEADYYCAAWDDSLSAWVFGGGTKLTVL

Clone 6-14

QVQLQQSGPGLVKPSQTL SLTCAISGDSVSSNSATWNWIRQSPSRGLEWLGRTY  
YRSK WYNDYAVSVKS RMTINPDT SKNQFSLQLNSVTPDDRAVYYCARGGRLGG  
GMDV WGQGT TTVVSSGILGSGGGGSGGGGSGGGGSGQPVL TQSPSASGTPGQRV  
TISCSGSSSNIASNYVYWYQHLPGTAPKLLIYTNRRRPSGVPDRFSGSKSGTSASL  
AISGLRSEDEADYFCAAWDDSLSGWVFGGGTKVTVL

Clone 6-22

QVQLQQSGPGLVKPSQTL SLTCAISGDSVSSNSAAWNWIRQSPSRGLEWLGRTY  
YRSK WYNDYAVSVKS RITINPDT SKNQFSLQLNSVTPEDTAVYYCARTGYSSSW  
VVNF DYWGQGT LTVVSSGSASAPTGILGSGGGGSGGGGSGGGGSGQPVL TQSPSA  
SGTPGQRVTISCSGSSSNIGSNYVYWYQQLPGTAPKLLIYKNNQRPSGVPDRFSGS  
KSGTAASLAI SGLQSEDEADYYCAAWDDSLRGYVFGTGKLTVLS

Clone 6-23

QVQLVQSEGGVVQPGRSLRLSCGVSGFTFSSYAMHWVRQAPGKGLEWVAVISY  
DGSKKYYADSVKGRFTISRDN SKNTLYLQMNSLRAEDTAVYYCARRVTTGITRY  
FDLWGRGTLVTVSSGILGSGGGGSGGGGSGGGGSQSVLTQPASVSGSPGQSITIS  
CTGTNSDIGGYNYSWYQQHPGKAPKLMIFEVTNRPSGVPDRFSASKSGNTASL  
TISGLQADDEADYYCSSYAGSNTPSVFGTGTKLTVL

Clone 6-24

QVQLVESEGGVVQPGRSLRLSCAASGFTFSSYAMHWVRQAPGKGLEWVAVVSY  
DGSQDYADSVKGRFTISRDN SKNTLYLQMNSLRPEDTGVYYCAKVRSSNWF  
SRYYYYGMDVWGQGTTVTVSSGILGSGGGGSGGGGSGGGGSEIVLTQSPATLSL  
SPGERATLSCRASQSVSHYLA WYQQKPGQAPRVLIYDVANRAAGTPARFSGSGS  
GTDFTLTISSEPEDFAVYYCQQRSNWPQTFGPGTKVDIK

Clone 6-25

QVQLQQSGPGLVKPSQTL SLTCAISGDSVSSDAAWNWIRQSPSRGLEWLGRTY  
YRSKWyNDYAVSVKSRISINPDTSKNQFSLQLNSVTPEDTAVYYCARAQNNAV  
AGFDYWGLGTLVTVSSGILGSGGGGSGGGGSGGGGSQPVL TQSPSASGTPGQRV  
TISCSGSSNIGSNYVYWYQQLPGTAPLLIYRNNQRPSGVPDRFSGSKSGTSASL  
AISGLRSEDEAEYYCAA WDDSLSGLYVFGTGTKVTVLS

Clone 6-26

QVQLQQSGPGLVKPSQTL SLTCAISGDSVSSNSAAWNWIRQSPSRGLEWLGRTY  
YRSKWyNDYAVSVKGRITINPDTSKNQFSLQLNSVTPEDTAMYVCVRSGGGRV  
DPWGQGT LTVTVSSGILGSGGGGSGGGGSGGGGSQPVL TQSPSASGTPGQRTISC  
SGSRNIGSNYVYWYQQLPGTAPKLLIYRNHQ RPSGVPDRFSASKSGTSASLAISG  
LRSEDEADYYCAA WDDSLSGYVFGTGTKLTVL

Clone 6-27

QVQLVESEGGVVQPGRSLRLSCAASGFTFGTYAMHWVRQAPGKGLEWVAVISN  
DGGHKYYADSVKGRFTISRDN SKDSMYLQMNSLRAEDTAVYHCAKGRPWYDP  
GAEYFQHWGQGT LTVTVSSGILGSGGGGSGGGGSGGGGSQSALIQPASVSGSPGQ  
WITISCTGTSSDVG GYNYSWYQQHPGKAPKLLIYDVSDRPSGVS NRFSGSKSGN  
TASLTISGLQAEDEADYYCSSYTSSNTVLFGGGTKLTVLS

Clone 6-28

QVQLVQSEGGVVQPGRSLRLSCAASGFTFNDYAMHWVRQAPGKGLEWVAVIS  
YDGSNKYYTDSVKGRFTISRDN SKNTLYLQMDSL RPEDTALYYCAREASSGWYI  
DSWGQGT LTVTVSSASTKGPSGILGSGGGGSGGGGSGGGGSEIVLTQSPGTLSP  
GERATLSCRASQSVSSSYLA WYQQKPGQAPRLLIYGASSRATGIPDRFSGSGSGT  
DFTLTISRLEPEDFAVYYCQQYGSSQVTFGQGT RLEVKS

**Amino acid sequences of anti-HAAH scFv isolated from CDR domain shuffling mutagenesis. CDRs of the antibody are highlighted in yellow.**

Clone C1

PVQLQQSGPGLVKPSQTL<sup>SL</sup>PC<sup>AI</sup>SGDSVSSNSAAWNWIRQSLSRGLEWLGRTYY  
RSK<sup>WY</sup>NDYAVSVKSRITINPDT<sup>SK</sup>NQFSLQLNSVTPDDTAIYYCARASDYGDYF  
YYFDYWGQGT<sup>LV</sup>VSSGSASAPT<sup>GIL</sup>GSGGGGGSGGGGGSGGGGSQPVL<sup>TQ</sup>SPSAS  
GTPGQRVTISCSGSSSNIGSNYVYWYQQLPGTAPKLLIYKNNQRPSGVPDRFSGS  
KSGTAASLAISGLQSEDEADYYCAAWDDSLRGYVFGTGTKLTVLSGIL

Clone C2

QVQLQQSGPGLVKPSQTL<sup>SL</sup>TCAISGDSVSSNSAAWNWIRQSPSRGLEWLGRIYY  
RSK<sup>WY</sup>YDYAVSVKSRIA<sup>IK</sup>PD<sup>TS</sup>KNQFSLQLNSVTPEDTAVYYCARGAGRSFDL  
WGRGTL<sup>LV</sup>VSSGSASAPT<sup>GIL</sup>GSGGGGGSGGGGGSGGGGSQPVL<sup>TQ</sup>SPSASGTPGQ  
RVTISCSGSSSNIGSNYVYWYQQLPGTAPKLLIYKNNQRPSGVPDRFSGSKSGTA  
ASLAISGLQSEDEADYYCAAWDDSLRGYVFGTGTKLTVLSGIL

Clone C3

QVQLQQSSPGLVKPSQTL<sup>SL</sup>TCAVSGDSVSGNSGVWNWIRQSPSRGLEWLGRTY  
YYTYK<sup>WY</sup>IDYAVSVKSRITVNPDT<sup>SR</sup>NQFSLQLNSVTPEDTAVYYCARVDYTG  
PVWGQGT<sup>LV</sup>VSSGSASAPT<sup>GIL</sup>GSGGGGGSGGGGGSGGGGSQPVL<sup>TQ</sup>SPSASGTP  
GQRVTISCSGSSSNIGSNYVYWYQQLPGTAPKLLIYKNNQRPSGVPDRFSGSKSG  
TAASLAISGLQSEDEADYYCAAWDDSLRGYVFGTGTKLTVLSGIL

Clone C4

QVQLQQSGPGLVKPSQTL<sup>SL</sup>TCAISGDSVSSNSAAWNWIRQSLSRGLEWLGRTY  
YRSK<sup>WY</sup>NDYAVSVRGRITINAD<sup>TS</sup>KNQFSLQLNSVTPEDTAVYYCARTGYSSSW  
VNF<sup>FD</sup>YWGQGT<sup>LV</sup>VSSGSASAPT<sup>GIL</sup>GSGGGGGSGGGGGSGGGGSQPVL<sup>TQ</sup>SPSA  
SGTPGQRVTISCSGSSSNIGSNYVYWYQQLPGTAPKLLIYKNNQRPSGVPDRFSGS  
KSGTAASLAISGLQSEDEADYYCAAWDDSLRGYVFGTGTKLTVLSGIL

**Sequences of anti-HAAH scFv isolated from heavy chain shuffling mutagenesis.**  
CDRs of the antibody are highlighted in yellow.

Clone LLm1

QVQLQQSGPGLVKPSQTLTCAISGDSVSSITAAWNWLQRQSPSRGLEWLGRTY  
HRSKWYYDYAVSVKSRIIVNPDTSKNQFSLHLNSVTPEDTAVYYCARGLAARG  
GGPSAHAFEIWGQGTMTVSSASTKGPSGILGSGGGGSGGGGSGGGGSGQPVLVLTQ  
SPSASGTPGQRTVISCSSGSSNIGSNYVYWYQQLPGTAPKLLIYKNNQRPSGVPDR  
FSGSKSGTAASLAISGLQSEDEADYYCAAWDDSLRGYVFGTGTKLTVLSGIL

Clone LLm3

QVQLQQSGPGLVKPSQTLTLCVISGDSVSNNSAVWNWIRQSLSRGLEWLGRTY  
YRSKWYNDYAVSVKSRIIINPDTSKNQFSLQLNSVTPEDTAVYYCARRTGAGVD  
YWGQGTLVTVSSGILGSGGGGSGGGGSGGGGSGQPVLVLTQSPSASGTPGQRTVISC  
GSSSNIGSNYVYWYQQLPGTAPKLLIYKNNQRPSGVPDRFSGSKSGTAASLAISG  
LQSEDEADYYCAAWDDSLRGYVFGTGTKLTVLSGIL

Clone LLm5

QVQLQQSGPGLVKPSQTLTCAISGDGVSNNVIWNWIRQSPSRGLEWLGRTY  
YRSKWYYDLLPSVKSRIAINPDTSKSQFSLQLSSVTPEDTAVYYCARTRAVAGNQ  
YFDLWGRGTLTVVSSGILGSGGGGSGGGGSGGGGSGQPVLVLTQSPSASGTPGQRTV  
SCSSGSSNIGSNYVYWYQQLPGTAPKLLIYKNNQRPSGVPDRFSGSKSGTAASLA  
ISGLQSEDEADYYCAAWDDSLRGYVFGTGTKLTVLSGIL

Clone LLm6

QVQLQQSGPGLVKPSQTLTCAISGDSVSSYSAAWNWIRQSLSRGLEWLGRTY  
YRSKWYNDYAVSVKSRIINPDTSKNQFSLQLNSVTPEDTAVYYCASLAAAAGT  
VDYWGQGTLVTVSSGSASAPTGILGSGGGGSGGGGSGGGGSGQPVLVLTQSPSASG  
TPGQRTVISCSSGSSNIGSNYVYWYQQLPGTAPKLLIYKNNQRPSGVPDRFSGSKS  
GTAASLAISGLQSEDEADYYCAAWDDSLRGYVFGTGTKLTVLSGIL

Clone LLm8

QVQLQQSGPGLVKPSQTLTCAISGDSVSSNSAAWNWIRQSLSRGLEWLGRTY  
YRSKWYNDYALS VKSRININADTSKSKQFSLQLDSVTPEDTAVYFCAKDRLLYNY  
GSNAMDVWGQGTTVTVSSGILGSGGGGSGGGGSGGGGSGQPVLVLTQSPSASGTPG  
QRTVISCSSGSSNIGSNYVYWYQQLPGTAPKLLIYKNNQRPSGVPDRFSGSKSGT  
AASLAISGLQSEDEADYYCAAWDDSLRGYVFGTGTKLTVLSGIL

Clone LLm9

QVQLQQSGPGLVKPSETLSLTCAISGDSVSSNSAAWNWIRQSLSRGLEWLGRTY  
YRSKWYNDYAVSVKSRIINPDTSKNQFSLQLNSVTPEDTAVYYCARDTPRYCS  
GGSCYKYFDYWGQGTLVTVSSASTKSPSGILGSGGGGSGGGGSGGGGSGQPVLVLTQ  
SPSASGTPGQRTVISCSSGSSNIGSNYVYWYQQLPGTAPKLLIYKNNQRPSGVPDR  
FSGSKSGTAASLAISGLQSEDEADYYCAAWDDSLRGYVFGTGTKLTVLSGIL



Clone LLm11

QVQLQQSGPGLVKSSQTLSLTCAISGDSVSSKGAAWNWIRQSPSRGLEWLGRAY  
YWSKWYYDYAVSVKSRITINPDTSKNQFSLQLNSLTPEDTAVFYCARGATSTYY  
LPGGLDVWGQGTTVTVSSGILGSGGGGSGGGGSGGGGSGQPVLTSQSPSASGTPGQ  
RVTISCSGSSSNIGSNYVYWYQQLPGTAPKLLIYKNNQRPSGVPDRFSGSKSGTA  
ASLAISGLQSEDEADYYCAAWDDSLRGYVFGTGTKLTVLSGIL

Clone LLm13

QVQLQQSGAGLVKPSQTLSLTCTISGDSVSADRVAVWNWIRQSPLRGLEWLGRIF  
YRSKWMVDYAVSVKSRISINPDTSKNQFSLQLNSVTPEDTAMYYCARATTRGYF  
DLWGRGTLTVSSGILGSGGGGSGGGGSGGGGSGQPVLTSQSPSASGTPGQRVTISC  
SGSSSNIGSNYVYWYQQLPGTAPKLLIYKNNQRPSGVPDRFSGSKSGTAASLAIS  
GLQSEDEADYYCAAWDDSLRGYVFGTGTKLTVLSGIL

Clone LLm14

QVQLQQSGPGLVKPSQTLSLTCVVSVDGVSSNSAAAWNWIRQSLSRGLEWLGRIT  
YYRSKWYNDYAVSMKGRITINPDTSKNQFSLQLDSVTPEDTAVYYCARRSGRTG  
GYFDLWGRGTLVAVSSGILGSGGGGSGGGGSGGGGSGQPVLTSQSPSASGTPGQRV  
TISCSGSSSNIGSNYVYWYQQLPGTAPKLLIYKNNQRPSGVPDRFSGSKSGTAASL  
AISGLQSEDEADYYCAAWDDSLRGYVFGTGTKLTVLSGIL

Clone LLm15

QVQLQQSGPGLVKPSQTLSLTCAIPGHSVGSSNAAWNWIRQSPSRGLEWLGRIFY  
GSKWYNDYAVSLKSRLTINPDTSKNQFSLQLNSVTPEDTAVYYCARRTGTGIDY  
WGQGTTLTVTVSSGILGSGGGGSGGGGSGGGGSGQPVLTSQSPSASGTPGQRVTISCSG  
SSSNIGSNYVYWYQQLPGTAPKLLIYKNNQRPSGVPDRFSGSKSGTAASLAISGL  
QSEDEADYYCAAWDDSLRGYVFGTGTKLTVLSGIL

Clone LLm20

QVQLQQSGPGLVKPSQTLSLTCAISGHSVGSSNAAWNWIRQSPSRGLEWLGRIFY  
RSKWYNDYAVSVKTRISINPDTAKNQFSLHLNSVTAEDTGYYCARGQQKRLDS  
WGQGTTLTVTVSSGILGSGGGGSGGGGSGGGGSGQPVLTSQSPSASGTPGQRVTISCSG  
SSSNIGSNYVYWYQQLPGTAPKLLIYKNNQRPSGVPDRFSGSKSGTAASLAISGL  
QSEDEADYYCAAWDDSLRGYVFGTGTKLTVLSGIL

**Amino acid sequences of anti-HAAH scFv isolated from random mutagenesis of C4 scFv. CDRs of the antibody are highlighted in yellow.**

Clone C4-8

RVQLQQLGPGLVKPSQTLTCAIFGDSVSSNGAAWSWIRQSLSRGLEWLGRAY  
YRSKWYNDYAVSVRGRITINADTSKNQFSLQLNSVTPEDTAVYYCARTGYSSSR  
VVSSGYWGQGTLLVAVSSGSASAPIGILGSGGGGSGGGGSGGGGSSQPVLTSPPSAS  
GTPGQRVTISCSGSSSNIGSNYVYWYQQLPGTAPKLLIYKSNRRPSGVPGRFSGSK  
SGTAASLAISGLQSEDEADYYCAAWDDSLRGYVFGTGTCLTVL

Clone C4-18

QVQLQQSGPGLVKPSPTLSLTCAISGDSVSSNSAAWNWVRQSLSRGLEWLGRTY  
YRSKWYNGYAVSVRGRITTNADTSRNQFSLQLNSVTPEDTAVYYCARTGYSSS  
WVNSNYWGQGTLLVTVSSGSASAPTGILGSGGGGSGGGGSGGGGSSQPALTSPPS  
ASGTPGQRVTISCSGSSSNIGSNYVYWYQQLPGTAPKLLIYKNNQRPSGVPGRFS  
GSKSGTAASLAISGLRSKDEADYYCAAWDDSLRGYVFGTGTCLTVL

## References

- Adams, G. P., McCartney, J. E., Tai, M. S., Oppermann, H., Huston, J. S., Stafford, W. F., 3rd, Bookman, M. A., Fand, I., Houston, L. L. and Weiner, L. M. (1993). Highly specific in vivo tumor targeting by monovalent and divalent forms of 741F8 anti-c-erbB-2 single-chain Fv. *Cancer Res* **53**, 4026-34.
- Adams, G. P. and Schier, R. (1999). Generating improved single-chain Fv molecules for tumor targeting. *J Immunol Methods* **231**, 249-60.
- Adams, G. P., Schier, R., McCall, A. M., Crawford, R. S., Wolf, E. J., Weiner, L. M. and Marks, J. D. (1998). Prolonged in vivo tumour retention of a human diabody targeting the extracellular domain of human HER2/neu. *Br J Cancer* **77**, 1405-12.
- Akinc, A. and Langer, R. (2002). Measuring the pH environment of DNA delivered using nonviral vectors: implications for lysosomal trafficking. *Biotechnol Bioeng* **78**, 503-8.
- Ashcroft, R. G. and Lopez, P. A. (2000). Commercial high speed machines open new opportunities in high throughput flow cytometry (HTFC). *J Immunol Methods* **243**, 13-24.
- Austin, C. D., De Maziere, A. M., Pisacane, P. I., van Dijk, S. M., Eigenbrot, C., Sliwkowski, M. X., Klumperman, J. and Scheller, R. H. (2004). Endocytosis and sorting of ErbB2 and the site of action of cancer therapeutics trastuzumab and geldanamycin. *Mol Biol Cell* **15**, 5268-82.
- Bell, G. I. (1978). Models for the specific adhesion of cells to cells. *Science* **200**, 618-27.
- Bell, G. I. (1981). Estimate of the sticking probability for cells in uniform shear flow with adhesion caused by specific bonds. *Cell Biophys* **3**, 289-304.
- Bera, T. K., Onda, M., Brinkmann, U. and Pastan, I. (1998). A bivalent disulfide-stabilized Fv with improved antigen binding to erbB2. *J Mol Biol* **281**, 475-83.
- Bera, T. K., Viner, J., Brinkmann, E. and Pastan, I. (1999). Pharmacokinetics and antitumor activity of a bivalent disulfide-stabilized Fv immunotoxin with improved antigen binding to erbB2. *Cancer Res* **59**, 4018-22.
- Boder, E. T., Midelfort, K. S. and Wittrup, K. D. (2000). Directed evolution of antibody fragments with monovalent femtomolar antigen-binding affinity. *Proc Natl Acad Sci U S A* **97**, 10701-5.
- Boder, E. T. and Wittrup, K. D. (1997). Yeast surface display for screening combinatorial polypeptide libraries. *Nat Biotechnol* **15**, 553-7.
- Boder, E. T. and Wittrup, K. D. (1998). Optimal screening of surface-displayed polypeptide libraries. *Biotechnol Prog* **14**, 55-62.
- Boder, E. T. and Wittrup, K. D. (2000). Yeast surface display for directed evolution of protein expression, affinity, and stability. *Methods Enzymol* **328**, 430-44.
- Bretthauer, R. K. and Castellino, F. J. (1999). Glycosylation of Pichia pastoris-derived proteins. *Biotechnol Appl Biochem* **30** ( Pt 3), 193-200.
- Cadwell, R. C. and Joyce, G. F. (1992). Randomization of genes by PCR mutagenesis. *PCR Methods Appl* **2**, 28-33.
- Capo, C., Garrouste, F., Benoliel, A. M., Bongrand, P., Ryter, A. and Bell, G. I. (1982). Concanavalin-A-mediated thymocyte agglutination: a model for a quantitative study of cell adhesion. *J Cell Sci* **56**, 21-48.

- Cardarelli, P. M., Quinn, M., Buckman, D., Fang, Y., Colcher, D., King, D. J., Bebbington, C. and Yarranton, G. (2002). Binding to CD20 by anti-B1 antibody or F(ab')(2) is sufficient for induction of apoptosis in B-cell lines. *Cancer Immunol Immunother* **51**, 15-24.
- Carter, P. (2001). Improving the efficacy of antibody-based cancer therapies. *Nat Rev Cancer* **1**, 118-29.
- Cartron, G., Dacheux, L., Salles, G., Solal-Celigny, P., Bardos, P., Colombat, P. and Watier, H. (2002). Therapeutic activity of humanized anti-CD20 monoclonal antibody and polymorphism in IgG Fc receptor FcgammaRIIIa gene. *Blood* **99**, 754-8.
- Chalmers, J. J., Zborowski, M., Moore, L., Mandal, S., Fang, B. B. and Sun, L. (1998). Theoretical analysis of cell separation based on cell surface marker density. *Biotechnol Bioeng* **59**, 10-20.
- Chowdhury, P. S. and Pastan, I. (1999). Improving antibody affinity by mimicking somatic hypermutation in vitro. *Nat Biotechnol* **17**, 568-72.
- Christmann, A., Walter, K., Wentzel, A., Kratzner, R. and Kolmar, H. (1999). The cystine knot of a squash-type protease inhibitor as a structural scaffold for Escherichia coli cell surface display of conformationally constrained peptides. *Protein Eng* **12**, 797-806.
- Clynes, R. A., Towers, T. L., Presta, L. G. and Ravetch, J. V. (2000). Inhibitory Fc receptors modulate in vivo cytotoxicity against tumor targets. *Nat Med* **6**, 443-6.
- Cramer, A., Cwirla, S. and Stemmer, W. P. (1996). Construction and evolution of antibody-phage libraries by DNA shuffling. *Nat Med* **2**, 100-2.
- Dall'Ozzo, S., Tartas, S., Paintaud, G., Cartron, G., Colombat, P., Bardos, P., Watier, H. and Thibault, G. (2004). Rituximab-dependent cytotoxicity by natural killer cells: influence of FCGR3A polymorphism on the concentration-effect relationship. *Cancer Res* **64**, 4664-9.
- Daugherty, P. S., Chen, G., Iverson, B. L. and Georgiou, G. (2000a). Quantitative analysis of the effect of the mutation frequency on the affinity maturation of single chain Fv antibodies. *Proc Natl Acad Sci U S A* **97**, 2029-34.
- Daugherty, P. S., Chen, G., Olsen, M. J., Iverson, B. L. and Georgiou, G. (1998). Antibody affinity maturation using bacterial surface display. *Protein Eng* **11**, 825-32.
- Daugherty, P. S., Iverson, B. L. and Georgiou, G. (2000b). Flow cytometric screening of cell-based libraries. *J Immunol Methods* **243**, 211-27.
- de Haard, H. J., van Neer, N., Reurs, A., Hufton, S. E., Roovers, R. C., Henderikx, P., de Bruine, A. P., Arends, J. W. and Hoogenboom, H. R. (1999). A large non-immunized human Fab fragment phage library that permits rapid isolation and kinetic analysis of high affinity antibodies. *J Biol Chem* **274**, 18218-30.
- Di Gaetano, N., Cittera, E., Nota, R., Vecchi, A., Grieco, V., Scanziani, E., Botto, M., Inrona, M. and Golay, J. (2003). Complement activation determines the therapeutic activity of rituximab in vivo. *J Immunol* **171**, 1581-7.
- Dinchuk, J. E., Focht, R. J., Kelley, J. A., Henderson, N. L., Zolotarjova, N. I., Wynn, R., Neff, N. T., Link, J., Huber, R. M., Burn, T. C., Rupar, M. J., Cunningham, M. R., Selling, B. H., Ma, J., Stern, A. A., Hollis, G. F., Stein, R. B. and Friedman, P. A. (2002). Absence of post-translational aspartyl beta-hydroxylation of epidermal

- growth factor domains in mice leads to developmental defects and an increased incidence of intestinal neoplasia. *J Biol Chem* **277**, 12970-7.
- Downing, A. K., Knott, V., Werner, J. M., Cardy, C. M., Campbell, I. D. and Handford, P. A. (1996). Solution structure of a pair of calcium-binding epidermal growth factor-like domains: implications for the Marfan syndrome and other genetic disorders. *Cell* **85**, 597-605.
- Ellmark, P., Esteban, O., Furebring, C., Malmborg Hager, A. C. and Ohlin, M. (2002). In vitro molecular evolution of antibody genes mimicking receptor revision. *Mol Immunol* **39**, 349-56.
- El-Serag, H. B., Davila, J. A., Petersen, N. J. and McGlynn, K. A. (2003). The continuing increase in the incidence of hepatocellular carcinoma in the United States: an update. *Ann Intern Med* **139**, 817-23.
- El-Serag, H. B. and Mason, A. C. (1999). Rising incidence of hepatocellular carcinoma in the United States. *N Engl J Med* **340**, 745-50.
- Falasca, A., Gasperi-Campani, A., Abbondanza, A., Barbieri, L. and Stirpe, F. (1982). Properties of the ribosome-inactivating proteins gelonin, Momordica charantia inhibitor, and dianthins. *Biochem J* **207**, 505-9.
- Feldhaus, M. J., Siegel, R. W., Opresko, L. K., Coleman, J. R., Feldhaus, J. M., Yeung, Y. A., Cochran, J. R., Heinzelman, P., Colby, D., Swers, J., Graff, C., Wiley, H. S. and Wittrup, K. D. (2003). Flow-cytometric isolation of human antibodies from a nonimmune *Saccharomyces cerevisiae* surface display library. *Nat Biotechnol* **21**, 163-70.
- Francisco, J. A., Campbell, R., Iverson, B. L. and Georgiou, G. (1993). Production and fluorescence-activated cell sorting of *Escherichia coli* expressing a functional antibody fragment on the external surface. *Proc Natl Acad Sci U S A* **90**, 10444-8.
- Francisco, J. A., Earhart, C. F. and Georgiou, G. (1992). Transport and anchoring of beta-lactamase to the external surface of *Escherichia coli*. *Proc Natl Acad Sci U S A* **89**, 2713-7.
- Georgiou, G., Stathopoulos, C., Daugherty, P. S., Nayak, A. R., Iverson, B. L. and Curtiss, R., 3rd (1997). Display of heterologous proteins on the surface of microorganisms: from the screening of combinatorial libraries to live recombinant vaccines. *Nat Biotechnol* **15**, 29-34.
- Gietz, R. D. and Schiestl, R. H. (1991). Applications of high efficiency lithium acetate transformation of intact yeast cells using single-stranded nucleic acids as carrier. *Yeast* **7**, 253-63.
- Goldstein, N. I., Prewett, M., Zuklys, K., Rockwell, P. and Mendelsohn, J. (1995). Biological efficacy of a chimeric antibody to the epidermal growth factor receptor in a human tumor xenograft model. *Clin Cancer Res* **1**, 1311-8.
- Goyenechea, B. and Milstein, C. (1996). Modifying the sequence of an immunoglobulin V-gene alters the resulting pattern of hypermutation. *Proc Natl Acad Sci U S A* **93**, 13979-84.
- Graff, C. P., Chester, K., Begent, R. and Wittrup, K. D. (2004). Directed Evolution of an Anti-Carcinoembryonic Antigen scFv with a Four-Day Monovalent Dissociation Half-time at 37{degrees}C. *Protein Eng Des Sel*.
- Griffiths, A. D. and Duncan, A. R. (1998). Strategies for selection of antibodies by phage display. *Curr Opin Biotechnol* **9**, 102-8.

- Griffiths, A. D., Williams, S. C., Hartley, O., Tomlinson, I. M., Waterhouse, P., Crosby, W. L., Kontermann, R. E., Jones, P. T., Low, N. M., Allison, T. J. and et al. (1994). Isolation of high affinity human antibodies directly from large synthetic repertoires. *Embo J* **13**, 3245-60.
- Groner, B., Hartmann, C. and Wels, W. (2004). Therapeutic antibodies. *Curr Mol Med* **4**, 539-47.
- Gronke, R. S., VanDusen, W. J., Garsky, V. M., Jacobs, J. W., Sardana, M. K., Stern, A. M. and Friedman, P. A. (1989). Aspartyl beta-hydroxylase: in vitro hydroxylation of a synthetic peptide based on the structure of the first growth factor-like domain of human factor IX. *Proc Natl Acad Sci U S A* **86**, 3609-13.
- Gunyuzlu, P. L., Hollis, G. F. and Toyn, J. H. (2001). Plasmid construction by linker-assisted homologous recombination in yeast. *Biotechniques* **31**, 1246, 1248, 1250.
- Gura, T. (2002). Therapeutic antibodies: magic bullets hit the target. *Nature* **417**, 584-6.
- Haisma, H. J., Grill, J., Curiel, D. T., Hoogeland, S., van Beusechem, V. W., Pinedo, H. M. and Gerritsen, W. R. (2000). Targeting of adenoviral vectors through a bispecific single-chain antibody. *Cancer Gene Ther* **7**, 901-4.
- Hammarstrom, S. (1999). The carcinoembryonic antigen (CEA) family: structures, suggested functions and expression in normal and malignant tissues. *Semin Cancer Biol* **9**, 67-81.
- Hammond, C. and Helenius, A. (1995). Quality control in the secretory pathway. *Curr Opin Cell Biol* **7**, 523-9.
- Hanuske-Abel, H. M. and Popowicz, A. M. (2003). The HAG mechanism: a molecular rationale for the therapeutic application of iron chelators in human diseases involving the 2-oxoacid utilizing dioxygenases. *Curr Med Chem* **10**, 1005-19.
- Hanes, J., Jermutus, L., Weber-Bornhauser, S., Bosshard, H. R. and Pluckthun, A. (1998). Ribosome display efficiently selects and evolves high-affinity antibodies in vitro from immune libraries. *Proc Natl Acad Sci U S A* **95**, 14130-5.
- Hawkins, R. E., Russell, S. J., Baier, M. and Winter, G. (1993). The contribution of contact and non-contact residues of antibody in the affinity of binding to antigen. The interaction of mutant D1.3 antibodies with lysozyme. *J Mol Biol* **234**, 958-64.
- Hawkins, R. E., Russell, S. J. and Winter, G. (1992). Selection of phage antibodies by binding affinity. Mimicking affinity maturation. *J Mol Biol* **226**, 889-96.
- He, L., Isselbacher, K. J., Wands, J. R., Goodman, H. M., Shih, C. and Quaroni, A. (1984). Establishment and characterization of a new human hepatocellular carcinoma cell line. *In Vitro* **20**, 493-504.
- He, M. and Taussig, M. J. (1997). Antibody-ribosome-mRNA (ARM) complexes as efficient selection particles for in vitro display and evolution of antibody combining sites. *Nucleic Acids Res* **25**, 5132-4.
- Henderikx, P., Coolen-van Neer, N., Jacobs, A., van der Linden, E., Arends, J. W., Mullberg, J. and Hoogenboom, H. R. (2002). A human immunoglobulin G1 antibody originating from an in vitro-selected Fab phage antibody binds avidly to tumor-associated MUC1 and is efficiently internalized. *Am J Pathol* **160**, 1597-608.
- Hexham, J. M., Dudas, D., Hugo, R., Thompson, J., King, V., Dowling, C., Neville, D. M., Jr., Digan, M. E. and Lake, P. (2001). Influence of relative binding affinity on efficacy in a panel of anti-CD3 scFv immunotoxins. *Mol Immunol* **38**, 397-408.

- Ho, S. P., Scully, M. S., Krauthauser, C. M., Wexler, E. J., Stow, M. D., Dinchuk, J. E., Kerr, J. S. and Friedman, P. A. (2002). Antisense oligonucleotides selectively regulate aspartyl beta-hydroxylase and its truncated protein isoform in vitro but distribute poorly into A549 tumors in vivo. *J Pharmacol Exp Ther* **302**, 795-803.
- Hoet, R. M., Cohen, E. H., Kent, R. B., Rookey, K., Schoonbroodt, S., Hogan, S., Rem, L., Frans, N., Daukandt, M., Pieters, H., van Hegelsom, R., Neer, N. C., Nastri, H. G., Rondon, I. J., Leeds, J. A., Hufton, S. E., Huang, L., Kashin, I., Devlin, M., Kuang, G., Steukers, M., Viswanathan, M., Nixon, A. E., Sexton, D. J., Hoogenboom, H. R. and Ladner, R. C. (2005). Generation of high-affinity human antibodies by combining donor-derived and synthetic complementarity-determining-region diversity. *Nat Biotechnol*.
- Horton, R. M., Hunt, H. D., Ho, S. N., Pullen, J. K. and Pease, L. R. (1989). Engineering hybrid genes without the use of restriction enzymes: gene splicing by overlap extension. *Gene* **77**, 61-8.
- Houghton, A. N. and Scheinberg, D. A. (2000). Monoclonal antibody therapies—a 'constant' threat to cancer. *Nat Med* **6**, 373-4.
- Hu, S., Shively, L., Raubitschek, A., Sherman, M., Williams, L. E., Wong, J. Y., Shively, J. E. and Wu, A. M. (1996). Minibody: A novel engineered anti-carcinoembryonic antigen antibody fragment (single-chain Fv-CH3) which exhibits rapid, high-level targeting of xenografts. *Cancer Res* **56**, 3055-61.
- Hudson, P. J. and Souriau, C. (2001). Recombinant antibodies for cancer diagnosis and therapy. *Expert Opin Biol Ther* **1**, 845-55.
- Ince, N., de la Monte, S. M. and Wands, J. R. (2000). Overexpression of human aspartyl (asparaginyl) beta-hydroxylase is associated with malignant transformation. *Cancer Res* **60**, 1261-6.
- Jain, R. K. and Baxter, L. T. (1988). Mechanisms of heterogeneous distribution of monoclonal antibodies and other macromolecules in tumors: significance of elevated interstitial pressure. *Cancer Res* **48**, 7022-32.
- Jia, S., McGinnis, K., VanDusen, W. J., Burke, C. J., Kuo, A., Griffin, P. R., Sardana, M. K., Elliston, K. O., Stern, A. M. and Friedman, P. A. (1994). A fully active catalytic domain of bovine aspartyl (asparaginyl) beta-hydroxylase expressed in *Escherichia coli*: characterization and evidence for the identification of an active-site region in vertebrate alpha-ketoglutarate-dependent dioxygenases. *Proc Natl Acad Sci U S A* **91**, 7227-31.
- Jirholt, P., Ohlin, M., Borrebaeck, C. A. and Soderlind, E. (1998). Exploiting sequence space: shuffling in vivo formed complementarity determining regions into a master framework. *Gene* **215**, 471-6.
- Kashentseva, E. A., Seki, T., Curiel, D. T. and Dmitriev, I. P. (2002). Adenovirus targeting to c-erbB-2 oncoprotein by single-chain antibody fused to trimeric form of adenovirus receptor ectodomain. *Cancer Res* **62**, 609-16.
- Kettleborough, C. A., Saldanha, J., Heath, V. J., Morrison, C. J. and Bendig, M. M. (1991). Humanization of a mouse monoclonal antibody by CDR-grafting: the importance of framework residues on loop conformation. *Protein Eng* **4**, 773-83.
- Kieke, M. C., Shusta, E. V., Boder, E. T., Teyton, L., Wittrup, K. D. and Kranz, D. M. (1999). Selection of functional T cell receptor mutants from a yeast surface-display library. *Proc Natl Acad Sci U S A* **96**, 5651-6.

- Kikuchi, Y., Uno, S., Yoshimura, Y., Otabe, K., Iida, S., Oheda, M., Fukushima, N. and Tsuchiya, M. (2004). A bivalent single-chain Fv fragment against CD47 induces apoptosis for leukemic cells. *Biochem Biophys Res Commun* **315**, 912-8.
- Knappik, A., Ge, L., Honegger, A., Pack, P., Fischer, M., Wellnhofer, G., Hoess, A., Wolle, J., Pluckthun, A. and Virnekas, B. (2000). Fully synthetic human combinatorial antibody libraries (HuCAL) based on modular consensus frameworks and CDRs randomized with trinucleotides. *J Mol Biol* **296**, 57-86.
- Krebber, A., Bornhauser, S., Burmester, J., Honegger, A., Willuda, J., Bosshard, H. R. and Pluckthun, A. (1997). Reliable cloning of functional antibody variable domains from hybridomas and spleen cell repertoires employing a reengineered phage display system. *J Immunol Methods* **201**, 35-55.
- Kuan, C. T., Reist, C. J., Foulon, C. F., Lorimer, I. A., Archer, G., Pegram, C. N., Pastan, I., Zalutsky, M. R. and Bigner, D. D. (1999). 125I-labeled anti-epidermal growth factor receptor-vIII single-chain Fv exhibits specific and high-level targeting of glioma xenografts. *Clin Cancer Res* **5**, 1539-49.
- Lavaissiere, L., Jia, S., Nishiyama, M., de la Monte, S., Stern, A. M., Wands, J. R. and Friedman, P. A. (1996). Overexpression of human aspartyl(asparaginyl)beta-hydroxylase in hepatocellular carcinoma and cholangiocarcinoma. *J Clin Invest* **98**, 1313-23.
- Leung, D. W., Chen, E., Goeddel, D.V. (1989). A methods for random mutagenesis of a defined DNA segment using a modified polymerase chain reaction. *Technique* **1**, 11-15.
- Long, M., Goldsmith, H. L., Tees, D. F. and Zhu, C. (1999). Probabilistic modeling of shear-induced formation and breakage of doublets cross-linked by receptor-ligand bonds. *Biophys J* **76**, 1112-28.
- Ma, J., Chen, D. and Tian, Y. (2001). A modified method for preparation of adriamycin carried by magnetic albumin microspheres. *J Tongji Med Univ* **21**, 233-5.
- Maeda, T., Sepe, P., Lahousse, S., Tamaki, S., Enjoji, M., Wands, J. R. and de la Monte, S. M. (2003). Antisense oligodeoxynucleotides directed against aspartyl (asparaginyl) beta-hydroxylase suppress migration of cholangiocarcinoma cells. *J Hepatol* **38**, 615-22.
- Maeda, T., Taguchi, K., Aishima, S., Shimada, M., Hintz, D., Larusso, N., Gores, G., Tsuneyoshi, M., Sugimachi, K., Wands, J. R. and de la Monte, S. M. (2004). Clinicopathological correlates of aspartyl (asparaginyl) beta-hydroxylase overexpression in cholangiocarcinoma. *Cancer Detect Prev* **28**, 313-8.
- Marks, J. D., Griffiths, A. D., Malmqvist, M., Clackson, T. P., Bye, J. M. and Winter, G. (1992). By-passing immunization: building high affinity human antibodies by chain shuffling. *Biotechnology (N Y)* **10**, 779-83.
- Marks, J. D., Hoogenboom, H. R., Bonnert, T. P., McCafferty, J., Griffiths, A. D. and Winter, G. (1991). By-passing immunization. Human antibodies from V-gene libraries displayed on phage. *J Mol Biol* **222**, 581-97.
- Mattheakis, L. C., Bhatt, R. R. and Dower, W. J. (1994). An in vitro polysome display system for identifying ligands from very large peptide libraries. *Proc Natl Acad Sci U S A* **91**, 9022-6.
- May, R. D., Wheeler, H. T., Finkelman, F. D., Uhr, J. W. and Vitetta, E. S. (1991). Intracellular routing rather than cross-linking or rate of internalization determines



- the potency of immunotoxins directed against different epitopes of sIgD on murine B cells. *Cell Immunol* **135**, 490-500.
- McCafferty, J., Griffiths, A. D., Winter, G. and Chiswell, D. J. (1990). Phage antibodies: filamentous phage displaying antibody variable domains. *Nature* **348**, 552-4.
- McGinnis, K., Ku, G. M., VanDusen, W. J., Fu, J., Garsky, V., Stern, A. M. and Friedman, P. A. (1996). Site-directed mutagenesis of residues in a conserved region of bovine aspartyl (asparaginyl) beta-hydroxylase: evidence that histidine 675 has a role in binding Fe<sup>2+</sup>. *Biochemistry* **35**, 3957-62.
- McGrath, M. S., Rosenblum, M. G., Philips, M. R. and Scheinberg, D. A. (2003). Immunotoxin resistance in multidrug resistant cells. *Cancer Res* **63**, 72-9.
- Mohr, L., Schauer, J. I., Boutin, R. H., Moradpour, D. and Wands, J. R. (1999). Targeted gene transfer to hepatocellular carcinoma cells in vitro using a novel monoclonal antibody-based gene delivery system. *Hepatology* **29**, 82-9.
- Mohr, L., Shankara, S., Yoon, S. K., Krohne, T. U., Geissler, M., Roberts, B., Blum, H. E. and Wands, J. R. (2000). Gene therapy of hepatocellular carcinoma in vitro and in vivo in nude mice by adenoviral transfer of the Escherichia coli purine nucleoside phosphorylase gene. *Hepatology* **31**, 606-14.
- Moradpour, D., Compagnon, B., Wilson, B. E., Nicolau, C. and Wands, J. R. (1995). Specific targeting of human hepatocellular carcinoma cells by immunoliposomes in vitro. *Hepatology* **22**, 1527-37.
- Naundorf, S., Preithner, S., Mayer, P., Lippold, S., Wolf, A., Hanakam, F., Fichtner, I., Kufer, P., Raum, T., Riethmuller, G., Baeuerle, P. A. and Dreier, T. (2002). In vitro and in vivo activity of MT201, a fully human monoclonal antibody for pancarcinoma treatment. *Int J Cancer* **100**, 101-10.
- Nettelbeck, D. M., Rivera, A. A., Kupsch, J., Dieckmann, D., Douglas, J. T., Kontermann, R. E., Alemany, R. and Curiel, D. T. (2004). Retargeting of adenoviral infection to melanoma: combining genetic ablation of native tropism with a recombinant bispecific single-chain diabody (scDb) adapter that binds to fiber knob and HMWMAA. *Int J Cancer* **108**, 136-45.
- Nielsen, U. B., Adams, G. P., Weiner, L. M. and Marks, J. D. (2000). Targeting of bivalent anti-ErbB2 diabody antibody fragments to tumor cells is independent of the intrinsic antibody affinity. *Cancer Res* **60**, 6434-40.
- Nishikawa, K., Rosenblum, M. G., Newman, R. A., Pandita, T. K., Hittelman, W. N. and Donato, N. J. (1992). Resistance of human cervical carcinoma cells to tumor necrosis factor correlates with their increased sensitivity to cisplatin: evidence of a role for DNA repair and epidermal growth factor receptor. *Cancer Res* **52**, 4758-65.
- Palumbo, K. S., Wands, J. R., Safran, H., King, T., Carlson, R. I. and de la Monte, S. M. (2002). Human aspartyl (asparaginyl) beta-hydroxylase monoclonal antibodies: potential biomarkers for pancreatic carcinoma. *Pancreas* **25**, 39-44.
- Pancook, J. D., Beuerlein, G., Pecht, G., Tang, Y., Nie, Y., Wu, H., Huse, W. D. and Watkins, J. D. (2001). In vitro affinity maturation of human IgM antibodies reactive with tumor-associated antigens. *Hybrid Hybridomics* **20**, 383-96.
- Panyam, J., Zhou, W. Z., Prabha, S., Sahoo, S. K. and Labhasetwar, V. (2002). Rapid endo-lysosomal escape of poly(DL-lactide-co-glycolide) nanoparticles: implications for drug and gene delivery. *Faseb J* **16**, 1217-26.

- Parekh, R., Forrester, K. and Wittrup, D. (1995). Multicopy overexpression of bovine pancreatic trypsin inhibitor saturates the protein folding and secretory capacity of *Saccharomyces cerevisiae*. *Protein Expr Purif* **6**, 537-45.
- Prang, N., Preithner, S., Brischwein, K., Goster, P., Woppel, A., Muller, J., Steiger, C., Peters, M., Baeuerle, P. A. and da Silva, A. J. (2005). Cellular and complement-dependent cytotoxicity of Ep-CAM-specific monoclonal antibody MT201 against breast cancer cell lines. *Br J Cancer* **92**, 342-9.
- Przysiecki, C. T., Staggers, J. E., Ramjit, H. G., Musson, D. G., Stern, A. M., Bennett, C. D. and Friedman, P. A. (1987). Occurrence of beta-hydroxylated asparagine residues in non-vitamin K-dependent proteins containing epidermal growth factor-like domains. *Proc Natl Acad Sci U S A* **84**, 7856-60.
- Rebay, I., Fleming, R. J., Fehon, R. G., Cherbas, L., Cherbas, P. and Artavanis-Tsakonas, S. (1991). Specific EGF repeats of Notch mediate interactions with Delta and Serrate: implications for Notch as a multifunctional receptor. *Cell* **67**, 687-99.
- Robinson, A. S., Hines, V. and Wittrup, K. D. (1994). Protein disulfide isomerase overexpression increases secretion of foreign proteins in *Saccharomyces cerevisiae*. *Biotechnology (NY)* **12**, 381-4.
- Robinson, A. S. and Wittrup, K. D. (1995). Constitutive overexpression of secreted heterologous proteins decreases extractable BiP and protein disulfide isomerase levels in *Saccharomyces cerevisiae*. *Biotechnol Prog* **11**, 171-7.
- Roguska, M. A., Pedersen, J. T., Keddy, C. A., Henry, A. H., Searle, S. J., Lambert, J. M., Goldmacher, V. S., Blattler, W. A., Rees, A. R. and Guild, B. C. (1994). Humanization of murine monoclonal antibodies through variable domain resurfacing. *Proc Natl Acad Sci U S A* **91**, 969-73.
- Rosenblum, M. G., Cheung, L., Kim, S. K., Mujoo, K., Donato, N. J. and Murray, J. L. (1996). Cellular resistance to the antimelanoma immunotoxin ZME-gelolin and strategies to target resistant cells. *Cancer Immunol Immunother* **42**, 115-21.
- Rosenblum, M. G., Cheung, L. H., Liu, Y. and Marks, J. W., 3rd (2003). Design, expression, purification, and characterization, in vitro and in vivo, of an antimelanoma single-chain Fv antibody fused to the toxin gelolin. *Cancer Res* **63**, 3995-4002.
- Safarik, I. and Safarikova, M. (1999). Use of magnetic techniques for the isolation of cells. *J Chromatogr B Biomed Sci Appl* **722**, 33-53.
- Safavy, A., Bonner, J. A., Waksal, H. W., Buchsbaum, D. J., Gillespie, G. Y., Khzaeli, M. B., Arani, R., Chen, D. T., Carpenter, M. and Raisch, K. P. (2003). Synthesis and biological evaluation of paclitaxel-C225 conjugate as a model for targeted drug delivery. *Bioconjug Chem* **14**, 302-10.
- Sapra, P. and Allen, T. M. (2002). Internalizing antibodies are necessary for improved therapeutic efficacy of antibody-targeted liposomal drugs. *Cancer Res* **62**, 7190-4.
- Schier, R., Bye, J., Apell, G., McCall, A., Adams, G. P., Malmqvist, M., Weiner, L. M. and Marks, J. D. (1996a). Isolation of high-affinity monomeric human anti-c-erbB-2 single chain Fv using affinity-driven selection. *J Mol Biol* **255**, 28-43.
- Schier, R., McCall, A., Adams, G. P., Marshall, K. W., Merritt, H., Yim, M., Crawford, R. S., Weiner, L. M., Marks, C. and Marks, J. D. (1996b). Isolation of picomolar affinity anti-c-erbB-2 single-chain Fv by molecular evolution of the

- complementarity determining regions in the center of the antibody binding site. *J Mol Biol* **263**, 551-67.
- Sepe, P. S., Lahousse, S. A., Gemelli, B., Chang, H., Maeda, T., Wands, J. R. and de la Monte, S. M. (2002). Role of the aspartyl-asparaginyl-beta-hydroxylase gene in neuroblastoma cell motility. *Lab Invest* **82**, 881-91.
- Sheets, M. D., Amersdorfer, P., Finnern, R., Sargent, P., Lindquist, E., Schier, R., Hemingsen, G., Wong, C., Gerhart, J. C. and Marks, J. D. (1998). Efficient construction of a large nonimmune phage antibody library: the production of high-affinity human single-chain antibodies to protein antigens. *Proc Natl Acad Sci U S A* **95**, 6157-62.
- Shusta, E. V., Raines, R. T., Pluckthun, A. and Wittrup, K. D. (1998). Increasing the secretory capacity of *Saccharomyces cerevisiae* for production of single-chain antibody fragments. *Nat Biotechnol* **16**, 773-7.
- Shusta, E. V., VanAntwerp, J. and Wittrup, K. D. (1999). Biosynthetic polypeptide libraries. *Curr Opin Biotechnol* **10**, 117-22.
- Siegel, R. W., Coleman, J. R., Miller, K. D. and Feldhaus, M. J. (2004). High efficiency recovery and epitope-specific sorting of an scFv yeast display library. *J Immunol Methods* **286**, 141-53.
- Sikorski, R. S. and Hieter, P. (1989). A system of shuttle vectors and yeast host strains designed for efficient manipulation of DNA in *Saccharomyces cerevisiae*. *Genetics* **122**, 19-27.
- Smith, G. P. (1985). Filamentous fusion phage: novel expression vectors that display cloned antigens on the virion surface. *Science* **228**, 1315-7.
- Soderlind, E., Strandberg, L., Jirholt, P., Kobayashi, N., Alexeiva, V., Aberg, A. M., Nilsson, A., Jansson, B., Ohlin, M., Wingren, C., Danielsson, L., Carlsson, R. and Borrebaeck, C. A. (2000). Recombining germline-derived CDR sequences for creating diverse single-framework antibody libraries. *Nat Biotechnol* **18**, 852-6.
- Spiridon, C. I., Ghetie, M. A., Uhr, J., Marches, R., Li, J. L., Shen, G. L. and Vitetta, E. S. (2002). Targeting multiple Her-2 epitopes with monoclonal antibodies results in improved antigrowth activity of a human breast cancer cell line in vitro and in vivo. *Clin Cancer Res* **8**, 1720-30.
- Spiridon, C. I., Guinn, S. and Vitetta, E. S. (2004). A comparison of the in vitro and in vivo activities of IgG and F(ab')<sub>2</sub> fragments of a mixture of three monoclonal anti-Her-2 antibodies. *Clin Cancer Res* **10**, 3542-51.
- Srinivas, U., Tagliabue, E., Campiglio, M., Menard, S. and Colnaghi, M. I. (1993). Antibody-induced activation of p185HER2 in the human lung adenocarcinoma cell line Calu-3 requires bivalency. *Cancer Immunol Immunother* **36**, 397-402.
- Swers, J. S., Kellogg, B. A. and Wittrup, K. D. (2004a). Shuffled antibody libraries created by in vivo homologous recombination and yeast surface display, *Nucleic Acids Res*, pp. e36.
- Swers, J. S., Kellogg, B. A. and Wittrup, K. D. (2004b). Shuffled antibody libraries created by in vivo homologous recombination and yeast surface display. *Nucleic Acids Res* **32**, e36.
- Takahashi, H., Ozturk, M., Wilson, B., Maki, A., Ozawa, K., Koizumi, M., Endo, K., Strauss, W., Shouval, D. and Wands, J. (1989). In vivo expression of two novel

- tumor-associated antigens and their use in immunolocalization of human hepatocellular carcinoma. *Hepatology* **9**, 625-34.
- Thilo, L. (1985). Quantification of endocytosis-derived membrane traffic. *Biochim Biophys Acta* **822**, 243-66.
- Thompson, J., Stavrou, S., Weetall, M., Hexham, J. M., Digan, M. E., Wang, Z., Woo, J. H., Yu, Y., Mathias, A., Liu, Y. Y., Ma, S., Gordienko, I., Lake, P. and Neville, D. M., Jr. (2001). Improved binding of a bivalent single-chain immunotoxin results in increased efficacy for in vivo T-cell depletion. *Protein Eng* **14**, 1035-41.
- Trail, P. A. and Bianchi, A. B. (1999). Monoclonal antibody drug conjugates in the treatment of cancer. *Curr Opin Immunol* **11**, 584-8.
- Trail, P. A., Willner, D., Lasch, S. J., Henderson, A. J., Hofstead, S., Casazza, A. M., Firestone, R. A., Hellstrom, I. and Hellstrom, K. E. (1993). Cure of xenografted human carcinomas by BR96-doxorubicin immunoconjugates. *Science* **261**, 212-5.
- Treves, S., Feriotto, G., Moccagatta, L., Gambari, R. and Zorzato, F. (2000). Molecular cloning, expression, functional characterization, chromosomal localization, and gene structure of junctate, a novel integral calcium binding protein of sarco(endo)plasmic reticulum membrane. *J Biol Chem* **275**, 39555-68.
- Urban, J. L. and Schreiber, H. (1992). Tumor antigens. *Annu Rev Immunol* **10**, 617-44.
- van den Beucken, T., van Neer, N., Sablon, E., Desmet, J., Celis, L., Hoogenboom, H. R. and Hufton, S. E. (2001). Building novel binding ligands to B7.1 and B7.2 based on human antibody single variable light chain domains. *J Mol Biol* **310**, 591-601.
- Van Rossenberg, S. M., Sliedregt-Bol, K. M., Meeuwenoord, N. J., Van Berkel, T. J., Van Boom, J. H., Van Der Marel, G. A. and Biessen, E. A. (2002). Targeted lysosome disruptive elements for improvement of parenchymal liver cell-specific gene delivery. *J Biol Chem* **277**, 45803-10.
- VanAntwerp, J. J. and Wittrup, K. D. (2000). Fine affinity discrimination by yeast surface display and flow cytometry. *Biotechnol Prog* **16**, 31-7.
- Vaughan, T. J., Williams, A. J., Pritchard, K., Osbourn, J. K., Pope, A. R., Earnshaw, J. C., McCafferty, J., Hodits, R. A., Wilton, J. and Johnson, K. S. (1996). Human antibodies with sub-nanomolar affinities isolated from a large non-immunized phage display library. *Nat Biotechnol* **14**, 309-14.
- Viti, F., Tarli, L., Giovannoni, L., Zardi, L. and Neri, D. (1999). Increased binding affinity and valence of recombinant antibody fragments lead to improved targeting of tumoral angiogenesis. *Cancer Res* **59**, 347-52.
- Wadia, J. S., Stan, R. V. and Dowdy, S. F. (2004). Transducible TAT-HA fusogenic peptide enhances escape of TAT-fusion proteins after lipid raft macropinocytosis. *Nat Med* **10**, 310-5.
- Wands, J. R., Lavaissiere, L., Moradpour, D., de la Monte, S., Mohr, L., Nicolau, C. and Tanaka, S. (1997). Immunological approach to hepatocellular carcinoma. *J Viral Hepat* **4 Suppl 2**, 60-74.
- Wentzel, A., Christmann, A., Kratzner, R. and Kolmar, H. (1999). Sequence requirements of the GPNG beta-turn of the Ecballium elaterium trypsin inhibitor II explored by combinatorial library screening. *J Biol Chem* **274**, 21037-43.
- Wilson, B., Ozturk, M., Takahashi, H., Motte, P., Kew, M., Isselbacher, K. J. and Wands, J. R. (1988). Cell-surface changes associated with transformation of human hepatocytes to the malignant phenotype. *Proc Natl Acad Sci U S A* **85**, 3140-4.

- Wilson, D. R. and Finlay, B. B. (1998). Phage display: applications, innovations, and issues in phage and host biology. *Can J Microbiol* **44**, 313-29.
- Wu, A. M. and Yazaki, P. J. (2000). Designer genes: recombinant antibody fragments for biological imaging. *Q J Nucl Med* **44**, 268-83.
- Wu, H., Beuerlein, G., Nie, Y., Smith, H., Lee, B. A., Hensler, M., Huse, W. D. and Watkins, J. D. (1998). Stepwise in vitro affinity maturation of Vitaxin, an alphav beta3-specific humanized mAb. *Proc Natl Acad Sci U S A* **95**, 6037-42.
- Yang, W. P., Green, K., Pinz-Sweeney, S., Briones, A. T., Burton, D. R. and Barbas, C. F., 3rd (1995). CDR walking mutagenesis for the affinity maturation of a potent human anti-HIV-1 antibody into the picomolar range. *J Mol Biol* **254**, 392-403.
- Yazdi, P. T., Wenning, L. A. and Murphy, R. M. (1995). Influence of cellular trafficking on protein synthesis inhibition of immunotoxins directed against the transferrin receptor. *Cancer Res* **55**, 3763-71.
- Yokota, T., Milenic, D. E., Whitlow, M. and Schlom, J. (1992). Rapid tumor penetration of a single-chain Fv and comparison with other immunoglobulin forms. *Cancer Res* **52**, 3402-8.
- Yokota, T., Milenic, D. E., Whitlow, M., Wood, J. F., Hubert, S. L. and Schlom, J. (1993). Microautoradiographic analysis of the normal organ distribution of radioiodinated single-chain Fv and other immunoglobulin forms. *Cancer Res* **53**, 3776-83.
- Yoon, S. K., Mohr, L., O'Riordan, C. R., Lachapelle, A., Armentano, D. and Wands, J. R. (2000). Targeting a recombinant adenovirus vector to HCC cells using a bifunctional Fab-antibody conjugate. *Biochem Biophys Res Commun* **272**, 497-504.
- Zaccolo, M. and Gherardi, E. (1999). The effect of high-frequency random mutagenesis on in vitro protein evolution: a study on TEM-1 beta-lactamase. *J Mol Biol* **285**, 775-83.
- Zaccolo, M., Williams, D. M., Brown, D. M. and Gherardi, E. (1996). An approach to random mutagenesis of DNA using mixtures of triphosphate derivatives of nucleoside analogues. *J Mol Biol* **255**, 589-603.
- Zhao, H., Giver, L., Shao, Z., Affholter, J. A. and Arnold, F. H. (1998). Molecular evolution by staggered extension process (StEP) in vitro recombination. *Nat Biotechnol* **16**, 258-61.

# Curriculum Vitae

**Yik Andy Yeung**

---

## EDUCATION

### **Massachusetts Institute of Technology, Cambridge, MA**

Doctor of Philosophy in Chemical Engineering, 1999 – 2005

Thesis Advisor: Prof. Dane Wittrup

Thesis Title: Antibody Engineering for Cancer Therapy

Minor: Biology

### **Massachusetts Institute of Technology, Cambridge, MA**

Master of Science in Chemical Engineering Practice, 1999 – 2001

### **University of Wisconsin-Madison, Madison, WI**

Bachelor of Science in Chemical Engineering, 1995 – 1999

## PROFESSIONAL EXPERIENCE

### **Massachusetts Institute of Technology, Cambridge, MA**

Research Assistant, January 2000 – May 2005

- Advisor: Prof. Dane Wittrup
- Develop screening strategies for yeast surface display using magnetic beads
- Clone and construct antibody fragments from hybridoma mRNA using molecular biology techniques
- Isolate novel antibodies against soluble tumor antigen using FACS and magnetic beads
- Engineer and select antibody mutants for improved affinity and stability using yeast surface display
- Purify soluble antibody fragments secreted from yeasts using affinity chromatography and FPLC
- Evaluate the binding of antibody fragments against tumor cell lines using FACS
- Perform microscopy work to determine the internalization of antibody into tumor cells
- Perform biological function assay of antibodies and antibody-toxin conjugates on tumor cells
- Convert antibody fragments (scFv) into IgG format
- Purify IgG secreted from transformed COS cells using affinity chromatography

### **GE Plastics, Mount Vernon, IN & Cargill Inc., Minneapolis, MN**

Master Degree Intern, February 2001 – May 2001

- Design programs to forecast product prices
- Design and evaluate manufacturing processes for new products
- Evaluate the integration among different departments on the product manufacturing

### **University of Wisconsin-Madison, Madison, WI**

Research Assistant, September 1998 – May 1999

- Advisors: Prof. Paul Nealey and Prof. John Yin
- Optimize the lithography process on coverslips
- Deposit gold on coverslips using chemical vapor deposition (CVD)

### **University of Wisconsin-Madison, Madison, WI**

Research Assistant, September 1997 – August 1998

- Advisor: Prof. Douglas Cameron
- Optimize fermentation conditions of genetically engineered yeasts to produce of 1,2-propanediol
- Determine product yield using HPLC
- Perform biological assay on genetically knocked-out yeast mutants

## **AWARDS AND ACTIVITIES**

- Treasurer, Biotechnology Process Engineering Center (BPEC) Student Leadership Council, MIT
- Bleyer Scholarship, Chemical Engineering Dept., UW-Madison
- Rohn Scholarship, Chemical Engineering Dept., UW-Madison
- Donald Othmer Award, American Institute of Chemical Engineering, UW-Madison
- Member, American Institute of Chemical Engineering
- Member, Golden Key Honor Society

## **PUBLICATIONS**

**Yeung, Y.A.**, Koyrakh, I.A., Finney, A.H., Lebowitz, M.S., Wands, J.R. Wittrup, K.D. Isolation and characterization of human antibodies against human aspartyl (asparaginy)  $\beta$ -hydroxylase. In preparation.

Swers, J.S.\*, **Yeung, Y.A.\***, Wittrup, K.D. Integrated Mimicry of B Cell Antibody Mutagenesis by PCR and Homologous Recombination in Yeast. Submitted. \*Equal contribution

**Yeung, Y.A.**, Kellogg, B.A., Rosenblum, M.D., Cheung, L.H., Wands, J.R., Wittrup, K.D. A Single-chain Fv for Delivery of Cytotoxic Moieties into Hepatocellular Carcinoma Cells. Submitted.

Mohr, L., **Yeung, A.**, Aloman, C., Wittrup, K.D., Wands, J.R. (2004) Antibody Directed Therapy of Human Hepatocellular Carcinoma. *Gastroenterology*, 127: S225-31.

Colby, D, Kellogg, B.A., Graff, C., **Yeung, Y. A.**, Swers, J., Wittrup, K. D. (2004) Engineering Antibody Affinity by Yeast Surface Display. *Methods in Enzymology*, v.388: 348-358.

Feldhaus, M. J., Siegel, R. W., Opresko, L. K., Coleman, J. R., Feldhaus, J. M., **Yeung, Y. A.**, Cochran, J. R., Heinzelman, P., Colby, D., Swers, J., Graff, C., Wiley, H. S., and Wittrup, K. D. (2003) Flow-cytometric isolation of human antibodies from a nonimmune *Saccharomyces cerevisiae* surface display library. *Nature Biotechnology*, 21: 163–170.

**Yeung, Y. A.** and Wittrup, K. D. (2002) Quantitative screening of yeast surface-displayed polypeptide libraries by magnetic bead capture. *Biotechnology Progress*, 18: 212–220.